https://researchcommons.waikato.ac.nz/

Research Commons at the University of Waikato

Copyright Statement:

The digital copy of this thesis is protected by the Copyright Act 1994 (New Zealand).

The thesis may be consulted by you, provided you comply with the provisions of the Act and the following conditions of use:

- Any use you make of these documents or images must be for research or private study purposes only, and you may not make them available to any other person.
- Authors control the copyright of their thesis. You will recognise the author's right to be identified as the author of the thesis, and due acknowledgement will be made to the author where appropriate.
- You will obtain the author's permission before publishing any material from the thesis.

Comparative Study of Novel Cold-Formed Steel Sections for Pedestrian Bridges Under Varying Structural Configurations

Shridhar Mangelkar

A thesis submitted in fulfillment of the requirements

for the degree of Master of Engineering

Main supervisor: Dr Zhiyuan (Arthur) Fang

Co-supervisors: Mahmood Khodadadi and Prof James Lim

School of Engineering

The University of Waikato

New Zealand

THE UNIVERSITY OF
WAIKATO
Te Whare Wānanga o Waikato

2025

ABSTRACT

The use of Cold-Formed Steel (CFS) in bridge engineering has received considerable interest due to its favorable properties, including a lightweight structure, a high strength-to-weight ratio and affordability. As an innovative alternative to traditional materials such as hot-formed steel, timber, and reinforced concrete, CFS shows significant potential in pedestrian bridge construction. The research investigates the performance of CFS pedestrian bridges, with the aim of advancing lightweight, prefabricated, and environmentally sustainable infrastructure in New Zealand.

The research primarily focuses on evaluating the feasibility of using CFS for pedestrian bridges by investigating deflection behavior, stress distribution and overall structural performance under standard loading conditions via finite element analysis (FEA). In total, Six types of bridge models --Flat Pratt Truss, Box Truss, Tub Girder, Flat Foot, Box Bridge, and the Modular Panel Bridge-- were thoroughly analyzed under a 5 kPa load. The mesh sensitivity study was conducted to ensure that the simulation results were independent of mesh size, achieving numerical convergence without excessive computational cost, and the simulation procedure is validated by comparing with experimental data sourced from an existing Glass Fiber Reinforced Polymer (GFRP) pedestrian truss bridge. In this study, six Cold-Formed Steel (CFS) pedestrian bridge models were investigated under identical 5 kPa loading, a span/200 deflection criterion as defined by the SNZ-HB-8630:2004 code, consistent boundary conditions, and a yield stress limit of 550 MPa, but with varying spans and geometries. (1) For the Flat Pratt Truss bridge spanning 6 meters, the effect of span on deflection and stress was investigated, revealing a maximum deflection of 0.8 mm and a maximum stress of 77.14 MPa, both well within allowable limits; however, the extremely low stress utilization indicates material overconsumption. (2) For the Modular Panel bridge spanning 7.2 meters, the influence of modular assembly on load distribution was examined, resulting in a higher deflection of

65.88 mm and stress levels reaching 639.4 MPa, exceeding the yield strength. (3) For the Box Truss bridge spanning 6.7 meters, the impact of closed-section geometry on stiffness was studied, demonstrating minimal deflection of 20.3 mm and uniformly distributed stress around 535 MPa. (4) For the Tub Girder bridge spanning 15 meters, the effect of large span on flexural performance was analyzed, identifying significant midspan deflection of 37.5 mm with stresses exceeding the yield strength. (5) For the Flat Foot bridge spanning 30 meters, the influence of extreme span on structural integrity was evaluated, showing excessive deflection of 58.92 mm, though still within the serviceability limits, while the maximum stress of 582.4 MPa surpassed the material yield strength. (6) For the Box Bridge spanning 10 meters, the effect of simple box-section design on structural efficiency was assessed, resulting in a deflection of 13.9 mm and stresses exceeding 550 MPa, demonstrating full material utilization. Among all, the Box Truss bridge was found to offer the most favorable balance between satisfying the deflection serviceability limit and achieving a more uniform stress distribution.

Keywords: Cold-formed steel (CFS), Pedestrian bridges, Truss bridge design, Finite element analysis (FEA), Structural performance, Deflection and stress analysis, Box section geometry, Modular bridge systems.

PREFACE

This thesis is submitted to the University of Waikato, New Zealand, in partial fulfilment of the requirements for a master's degree in civil engineering. The work presented here has not been submitted for any degree or diploma at any other institution. To the best of my knowledge, this thesis contains no material previously published or written by others, except where proper citation is provided.

ACKNOWLEDGEMENTS

First and foremost, I would like to express my deepest gratitude to my main supervisor, Dr. Zhiyuan (Arthur) Fang, and my co-supervisors, Mahmood Khodadadi, Professor James B.P. Lim, for their unwavering support throughout my research journey. Their guidance and invaluable contributions were instrumental in the successful completion of my thesis, and they have greatly shaped my growth as an independent researcher.

I am particularly grateful to Mahmood Khodadadi for his insightful feedback and assistance with the modelling challenges, which were crucial throughout the process. I also extend my heartfelt thanks to Harsh Birwadkar for his constant encouragement and support, which played a significant role in my progress. I also sincerely appreciate my well-wishers in New Zealand, whose encouragement has been vital in shaping this thesis.

My deepest gratitude goes to my best friends in New Zealand Shubham Tiwari, Ahmed Sayadi, Clement Rossetto and my wife, Shradha Mangelkar for their unwavering support throughout the year. I also want to thank my family in India, whose love and encouragement have been a constant source of strength.

I would like to express my sincere gratitude to Formsteel NZ for supplying the structural section data essential to this research. I also gratefully acknowledge the technical support provided by Maria and Simon during the development of the CFS pedestrian bridge model.

Lastly, special thanks to the University of Waikato, School of Engineering, for providing the necessary computing resources and research assistance.

NOTATION

Cold-Formed Steel	CFS
Density	ρ
Back-To-Back	BTB
American Iron and Steel Institute	AISI
Australian and New Zealand Standards	AS/NZS
Finite element	FE
Finite element analysis	FEA
Finite element modelling	FEM
Direct Strength Method	DSM
Tensile strength	ft
Compressive strength	fc
Hot Rolled Steel	HRS
Cross-section	C/S
Young's modulus	*E*
Stress	σ
Strain	ε
Deflection	Δ
Span length of the bridge	L
Megapascal	MPa
Thickness	t

Kilo-Newton	kN
Millimetres	mm
Metre	m
Angle	ϕ
Yield stress	f_y
Translational displacement along global X, Y, Z axes respectively	U1, U2, U3
Rotational degrees of freedom about X, Y, Z axes respectively	UR1, UR2, UR3
Von Mises stress	S_{Mises}
Applied load	P
Reference point	RP
Force	F
Cross-sectional area	A
Screw spacing	s
Diameter	d
Self-Tapping Screws	STS
Formsteel section	FS

TABLE OF CONTENTS

LIST OF FIGURES

LIST OF TABLES

Chapter 1 – Introduction

1.1 Background

During the Medieval and Renaissance eras, stone, masonry, and timber were the common materials utilized in bridge construction due to them being readily available and appreciated for their strength. However, with the Industrial Revolution, bridge construction saw a great innovation in adopting cast iron, which had a stronger and more effective structure design [1]. Another great innovation in bridge design was using a truss system, which was originally designed by Leonardo da Vinci and Andrea Palladio in the 15th and 16th centuries. While these designs were theoretical during those eras, a practical application of a truss system took place in the 18th century, with a majority using wood due to it being easy to work with and easy to produce rods and joints [2]. For example, Australia contains almost 53,000 bridges, about 42,000 of which have been built using timber [3][4]. Such statistics as these refer directly to Australia, but they serve as a benchmark to illustrate the common use of traditional materials in bridge design, and with it, common problems in repair and maintenance. The high maintenance costs, combined with limitations such as a dwindling supply of suitable hardwood, have made it increasingly difficult to replace ageing timber bridges. This highlights a worldwide imperative for the innovation and production of durable, robust, and sustainable materials for bridge design.

The history of bridge engineering can be divided into two dominant eras. The Arch Era, which spans roughly from 2000 BC to the late 18th century, is marked by the architectural achievements of the Romans, who employed the stone arch as a basic element in bridge design. After this period, the Contemporary Era began in the mid-19th century, with the advent of steel as a commercially viable structural material. The outstanding properties of steel, particularly its ability to resist both tensile and compressive loads, allowed for the design and construction

of a range of innovative forms, such as truss bridges, girder bridges, cable-stayed bridges, suspension bridges, and high-span arch bridges [5]. As bridge engineering has progressed, there has been a dramatic trend in recent years towards the use of lightweight, high-strength, and economical materials. Cold-formed steel (CFS) has proven to be a potential candidate to meet the demands of modern infrastructure.

1.2 Bridge classification by structural form

Although bridges can be classified by different methods, the bridge classification according to its structural form is still the common way. This is necessary because the structural form is the most important factor that affects the whole service life of the bridge, including design, construction, repair, and maintenance. Bridges with different structural forms have their load transfer path and suitable range of application. In general, bridges can be classified into beam bridges, rigid-frame bridges, truss bridges, arch bridges, cable stayed bridges, and suspension bridges [5].

1) Truss Bridge

A truss is a structural assembly of connected elements arranged in triangular patterns, and a bridge with a load-carrying superstructure composed of such a truss is called a truss bridge. Truss bridges are one of the oldest types of modern bridge structures refer Figure 1. Truss structures have many advantages, such as a high strength-to-weight ratio, effective use of materials, and the ability to span large distances using members that are relatively light in weight. To simplify calculations, it is generally assumed that trusses have pinned connections between adjacent truss members. As a result, truss members, such as chords, verticals and diagonals are subjected to primarily either tensile or compressive forces. In modern structural engineering related to truss bridges, the standard practice is to work with gusset plate connections, requiring the consideration of bending moments and shears to properly model the

structural response. This consideration can be efficiently carried out through finite element analysis software. However, based on design methodology, the standard assumption of the pinned connection has been widely accepted solely because of safety considerations and the need to simplify the structural design as well as the analytical techniques. Since axial loads largely determine the stress condition in trusses, using the assumption leads to minute discrepancies found in actual bridges and their model equivalents [5].

Despite their advantages, truss bridges also have their challenges. The construction process often requires a high level of precision in assembling numerous interconnected members, where even small connection defects or misalignments can lead to structural weaknesses. Furthermore, maintenance and inspection of these bridges can become increasingly complex because of the large number of joints and members to be assessed. Also, while truss bridges exhibit very high efficiency under axial loading, they can be susceptible to buckling or fatigue under extreme loading conditions if they are not properly designed and maintained.

Figure 1 The Tokyo Gate Bridge. (Photo by Lin.) [5].

2) Beam Bridges

Beam bridges are simple and inexpensive and are supported between piers or abutments. Beam bridges (or Girder Bridges) are the most popular and economically viable structures. To define, a beam bridge is supported at either end by piers (or abutments), such as a log laid across a creek. In other words, the weight of the beam and external load are held up by the beam itself, with internal forces including bending moment and shear force. A positive bending moment tends to compress the upper fibers of a beam and while the lower fibers are in tension. It is essentially much more complex than a cable in tension alone or an arch in compression largely. It can therefore only be made from materials that work well in tension as well as compression. It is obvious that plain concrete and stone are not good beam materials because they are without contradiction weak under tension but very strong under compression. Ancient beam bridges were mainly constructed of wood, while modern beam bridges may be built from iron, steel or concrete using prestressing. Two continuous girder bridges that made of steel and concrete are shown in Figure2, 3 the slab bridges refer to spans without support below the deck, Beam Bridges represents bridges with only longitudinal support below the deck and Girder Bridges refer to bridges with both longitudinal and transverse structural members under the deck [5].

Figure 2 Lagan bridge (concrete continuous girder bridge), Belfast [5].

Figure 3 Queen Elizabeth II Bridge (steel continuous girder bridge), Belfast [5].

3) Rigid-Frame Bridges

The Rigid-Frame Bridge, also known as the Rahmen Bridge, consists of a superstructure supported on vertical or slanted monolithic legs (columns), wherein superstructure and substructure are rigidly connected to act as one entity and are economical for medium spans of moderate length. Rigid-frame bridges came into being in Germany during the early years of the 20th century. Rigid-frame bridges are superstructure-substructure integral structures with the superstructure considered as a girder. Integral bridge types include braced rigid-frame bridges, V-leg rigid-frame bridges, and viaducts in urban places. Rigid connections between superstructure and substructure transfer bending moment, axial forces, and shear forces. This form of bridge design with rigid frames provides definite structural advantages but tends to be complicated to design and build. Moments at the center of deck rigid frame bridge are smaller than those in a simply supported deck and thus a shallower cross-section can be adopted at mid-span. Other advantages include reduced space for approaches and a lack of detailing for the area where the deck bears the abutments (Portland Cement Association, 1936).

However, as with any statically indeterminate structure, the design and analysis become more complex than that of simply supported or continuous bridges. Continuous Prepressed Rigid Frame Chongqing Shibanpo double line Bridge is an outstanding representation of such design with its world record 330 m main span in such category through spanning (86.5+(4x138) +330+132.5) m across the Yangzi River as illustrated in Figure 4 (Qin et al., 2013). The Toyosu Bridge in Tokyo is attractive too as illustrated in Figure 5.

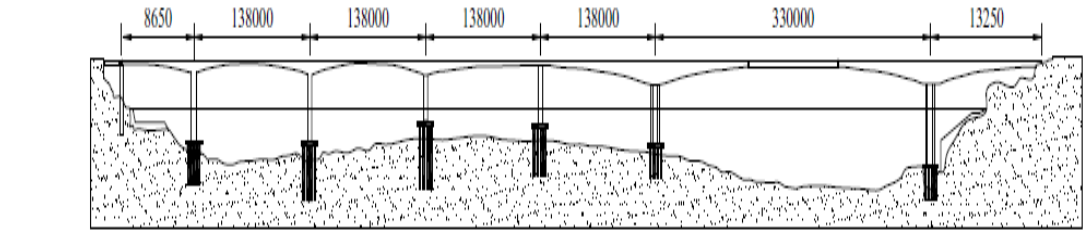

Figure 4 The Shibanpo Bridge in Chongqing, China. (A) Layout of the bridge [5].

Figure 5 The Toyosu Bridge in Tokyo, Japan. (Photo by Zheng) [5].

4) Arch Bridges

An arch bridge is a bridge shaped as an upward convex curved arch to sustain the vertical loads. A simple arch bridge works by transferring its weight and other loads partially into a horizontal thrust restrained by the strong abutments at either side. The arch rib needs to carry bending moment, shear force, and axial force in real service conditions. A viaduct (a long bridge) may be made from a series of arches although other more economical structures are typically used today. The current world's largest arch bridge is the Chaotianmen Bridge over the Yangtze River in Chongqing (China) with a span length of 552 m, as shown in Figure 6 [5].

Figure 6 The Chaotianmen Bridge, Chongqing, China [5].

5) Suspension Bridges

The traditional representation of a typical suspension bridge is that of a continuous girder. It is suspended by suspension cables passing through the main towers and is supported by a saddle structure such as big anchorages that hold the cables. All essential structural members and other elements typical in suspension bridges, including tower, hanger, main girder and the anchorage, are also shown in Figure 7. Main forces at play in a suspension bridge; these are tension in the cables and compression in the towers. The deck, which is usually a truss or a box girder, is then tied by vertical suspenders also in tension to the hangers, which in turn are connected to the suspension cables. Cable supported deck structures weight are transferred by cables to towers, which transfer weight to anchorages at both ends of the bridge, then finally to the ground. The suspension cables will take a curve shape arch-like. However, as opposed to the arch, the suspension cable can support only the tensile forces while the arch transmits through compressive forces. An additional reason is that the cable will "never buckle" and makes very high use possible of the high strength steel materials. Thus, suspension bridges can carry longer main spans than any other types of bridges, practical up to a region of about 2 km and even beyond as shown in Figure 8.

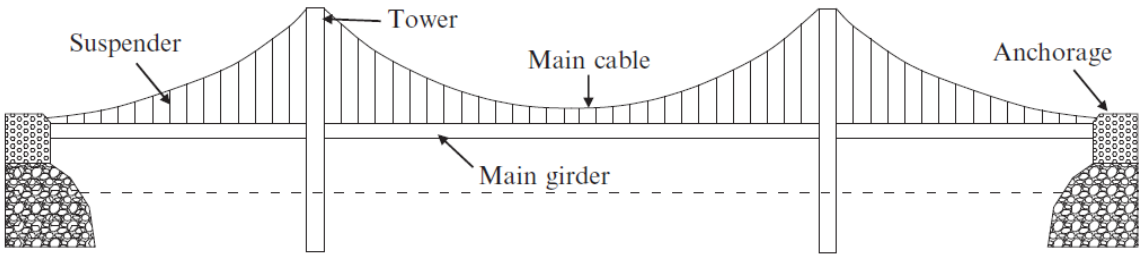

Figure 7 Image of the suspension bridge [5].

Figure 8 Akashi Kaikyō Bridge in Japan [5].

1.3 Selection of bridge types

Selection of the bridge superstructures is closely related to the use of construction materials. Based on the materials used for superstructure construction, the modern bridges can be roughly divided into concrete bridges and steel bridges, with different structural forms. Benefit by the high strength to weight ratio, steel construction requires less material than other traditional technologies and contributes to reducing a bridge's environmental impact. The steel bridges are generally built in large spans such as arch bridges, truss bridges, cable-stayed bridges, and suspensions bridges. Especially for large span bridges, as the dead weight governs the load carry capacity of bridges, the bridge superstructures are built in steel but not concrete. Concrete is a brittle material, like stone, good in compression but weak in tension, so it is vulnerable to crack under bending or twist. Concrete must be reinforced with steel to improve its ductility, naturally its emergence follows the development of steel. However, for some structural forms of bridges, concrete will be a perfect material to build, such as the arch bridges

whose members are mainly under compression. Also, concrete bridges are also widely used for short-span bridges due to the relative low cost and less maintenance in service stage. In addition, with the development of the prestressing technique, the prestressed concrete bridges can also be built in medium spans. The availability of the construction materials should be considered in the selection of the bridge superstructures. The mechanical characteristics of each bridge type are the determinant factor for an appropriate span capacity. Based on the discussion above, the simply supported structure is statically determinate and is simplest to design, and generally, is suitable for short-span bridges [5].

For this study, a cold -formed steel truss bridge (CFS) was selected as the ideal superstructure, mainly due to its adequacy for extension lengths, ranging from 6 to 15 meters. This selection aligns with the structural performance requirements of pedestrian bridges, leveraging the high strength to weight ratio of the CFS. The study aims to evaluate the efficiency of CFS truss bridges within this extension range, particularly in their ability to support significant loads, specifically a uniform distributed load of 5 kPa, minimizing the use of the material. This approach ensures that structural design remains light and economical without compromising performance. CFS has gained significant traction in bridge engineering due to its advantageous properties, particularly its high resistance to weight ratio, which allows the construction of lighter structures without reducing the load transportation capacity. This feature also increases the ease of transport and on-site assembly, making CFS a practical choice for prefabricated structures [6]. The ability to manufacture various transverse forms further enhance project flexibility, allowing structural optimization to meet specific performance requirements [7]. In pedestrian bridge applications, CFS demonstrated reliability under static and dynamic loading conditions, validating their adequacy to these structural systems [6]. In addition, CFS pedestrian bridges can be prefabricated, significantly reducing construction time and hand -to -work requirements. The inherent recyclability of the material also aligns with

sustainable construction practices, classifying -the modern "green" construction concepts [7]. Due to advances in protective coating, the resistive nature of CFS to corrosion had improved, hence increasing its service life [8]. The combability of CFS with many architectural designs, beside compatibility with other materials used to construct buildings, set forth the justification for making use of it in various modern bridge designs [7]. Overall, the use of CFS in bridge building is associated with structural efficiency, economic benefits.

Potential Problems of CFS in Bridge Engineering

There are, however, challenges in applying CFS to bridge engineering applications, in addition to its advantages. Among the main issues, local buckling of thin-walled CFS sections under axial stress is the main factor that could compromise structural integrity in [9]. Buckling behavior is, therefore, of great concern when analysing and designing CFS structures to make sure safety and performance are guaranteed by [7]. Further, the connections in CFS structures are potential points that can fail if not well designed, for example, as seen in experimental studies on CFS truss bridges [10]. Design complexity in the connections calls for extensive testing and verification to avoid construction failures [7]. Long-term durability can also be detracted by CFS bridges environmental effects, for example, corrosion, if in corrosive environments [8]. The durability of CFS structures must be ensured through adequate corrosion protection by coatings or material selection [8]. Lacking full design codes and standards for CFS bridge applications may lead to variability in design practice [7]. This gap necessitates that research and development are continuously undertaken to formulate and implement suitable guidelines so that CFS has successful applications in bridge engineering [7]. These are challenges that have to be overcome if CFS is to realize its full potential in bridge construction.

The thesis explores a set of critical problems related to cold-formed steel (CFS) pedestrian bridge design and construction with a view to suggesting new and innovative

solutions to enhance their structural stability. One such highly salient problem that has been explored in depth relates to design optimality, whereby complex geometrical designs in CFS trusses in pedestrian bridges required thorough examination to ensure fulfilment of specified deflection and stress criteria.

Chapter 2 – Literature Review

2.1 Introductory remarks

Cold-formed steel (CFS) is now a vital material in modern infrastructure with attributes such as strength, structural integrity and affordability. The advancement in the use of CFS in bridge and building construction has drawn much attention in studies citing its flexibility, strength and optimization in varying structural configurations [11]. Various studies in the past explored various aspects of CFS from elementary design principles to sophisticated optimization techniques with the aim of enhancing its application in the structural engineering domain.

2.2 Previous studies on cold-formed steel truss structures

In the ongoing quest to develop efficient, lightweight structural systems, CFS truss structures have gained widespread attention due to their flexibility, high strength-to-weight ratio, and economic benefits. Dizdar et al. [12] conducted experimental studies on full-scale floor trusses fabricated from cold-formed lipped channels using four-point bending tests. They discovered notable differences from conventional design expectations, primarily caused by connection flexibility and global bending effects, and consequently suggested refinements to the Direct Strength Method (DSM) for improved accuracy in design predictions. Similarly, Wood and Dawe [13] evaluated ten full-scale CFS roof trusses, identifying local buckling near heel plates on the top chord as the main failure mechanism. Their study highlighted that incorporating enhancements such as gusset plates considerably increased both the ductility and load-bearing capabilities of these trusses.

Building on these findings, Dawe et al. [14] further investigated offset CFS trusses, confirming that top chord buckling remained the predominant mode of failure. Their research

demonstrated that strategic use of stiffeners could significantly strengthen these trusses, thereby validating predictions made through beam-column interaction methods and DSM approaches. Additionally, Reda et al. [15] employed finite element modeling along with demand-to-capacity (D/C) ratios to accurately pinpoint potential failure locations in truss assemblies subjected to gravity loading. Their analyses indicated that Fink trusses provided superior performance for longer spans, reinforcing the notion that overall system efficiency surpasses the performance of individual truss components.

Research has also focused extensively on the performance of connections within CFS structures. Mathieson et al. [16] introduced the innovative Howick Rivet Connector (HRC), which demonstrated significantly improved ductility and strength compared to traditional screw connections through rigorous experimental and numerical studies. Complementing this, Pouladi et al. [17] utilized finite element analyses to explore eaves joints in CFS portal frames, identifying torsion and shear at screw connections as the primary factors contributing to joint failures. They validated their method for accurately predicting joint stiffness using screw-bolt interaction equations.

The seismic performance of CFS truss structures has also been thoroughly evaluated. Zeynalian et al. [18] assessed the lateral behavior of these structures within electric substations under seismic conditions. Their findings showed that using stiffeners and closed-section profiles substantially enhanced lateral stability, prompting recommendations for seismic design parameters such as the R-factor. Additionally, their study underscored significant cost savings compared to conventional structural systems. In a related study, Usefi et al. [19] developed detailed finite element models of hybrid CFS wall panels that integrated both open sections and square hollow section (SHS) trusses. By calibrating these models against experimental data, they examined 20 different SHS configurations, concluding that the truss layout

profoundly impacts energy absorption, ductility, and lateral strength. Specifically, the X-braced configurations (W16, W20) emerged as highly efficient, particularly suited for mid-rise applications. This work highlighted the benefits of using advanced numerical modeling to reduce dependence on costly full-scale testing, offering both economic and practical advantages.

2.3 Previous studies on steel truss pedestrian bridge

Steel truss pedestrian bridges have been a popular choice for their ability to efficiency in spanning long distances, to transfer forces through truss in an economical way, and to be built with delivery and assembly of individual modules. The traditional steel trusses are mostly used in pedestrian bridges and are manufactured from hot-rolled steel. They have been the subjects of many studies to examine their geometrical and dynamic characteristics, optimization and sustainability as well as the durability of the material. A comprehensive study by Josefin Tjernlund [20] on the issue of sustainable steel truss pedestrian bridges and their economic consequences has investigated different truss forms and various deck types. The study drew the conclusion that both the material and the geometry of the structure are important in the cost of the life cycle, corrosion resistance and it is overall the effectiveness of the materials adopted. In the same way, Roeder et al. [21] pointed out the significance of the control of the vibration and the regulation of the displacement in structures of lightweight steel with the purpose of maintaining the comfort of the pedestrian at the highest level, particularly in the case of dynamic loading. First, attempts have been made to make contributions to the area of research via the most recent research into computer simulations and wind experiments carried out by Bambole et al. [22] on foot over-bridges and the use of hollow steel sections to make the bridges. Their research focused on reducing the deflection and maximization of the efficiency of loading under limited pedestrian demand, which is achieved by the FEM and meets IS and AASHTO-serviceability standards. Impact of Configuration on Deflection and

Performance of Floor Joists through Finite Element Modeling outlined a study that proved deflection minimization and load production rationality through FE Modeling and confirming IS and AASHTO standards of service. They also suggested that only a combination of experimental and numerical methods would be able to solve the problems of analyses of the dynamic response and of personnel emergency. Lately, a specific investigation by Congiu [23] on the parametric design and optimization of steel truss arches under simultaneous loads in multiple directions has been carried out by the author. The author used evolutionary methods combined with finite element modeling to determine the optimum shapes and topologies of the trusses, which effectively demonstrate the influence of the geometry on displacement and stress in a local fashion. These works, in general, bear out that a lack of attention to the creeping of the beams, the deflections of the chords, and the vibrations suppression remains to be the most significant difficulties of achieving a long-span durable steel truss pedestrian-bridge.

2.4 Previous studies on CFS pedestrian bridge

R.W. Lautensleger and I.P. Andrade [8] investigated the feasibility of using galvanized cold-formed steel bridges for application on low-volume roads with considerations of durability, structural efficiency and cost-effectiveness. Their study examined conventional design practices, load factor coefficients and structural analysis of the galvanized cold-formed steel bridge. By conducting full-scale flexural tests on prototype box-section girders, they determined stiffness, strength and compared their performance with conventional materials. The study concluded that box-section girders provide improved lateral load distribution compared to standard beams and the use of galvanized coatings enhances durability significantly making cold-formed steel bridges an economical, maintenance-free option especially in developing countries. To understand the failure mechanisms in small CFS truss pedestrian bridges, Mohamad Ibrahim Zaed Ammar [10] and his team made a systematic study of their structural response under various loading conditions. Using FEA, the researchers

detected critical failure modes such as local buckling, joint failure and material yielding. The study findings suggested design reinforcements that could help improve the joint stability and strength, hence demonstrating that joint design optimization and section properties can greatly improve the safety and durability of pedestrian bridges made from CFS.

Contemporary advances in CFS technology were discussed by J.M. Davies [24], highlighting improvements in material properties, design methodology and structural applications. The research emphasized improvements in high-strength steel, corrosion resistance and the fabrication of complicated cross-sections. In addition, the research emphasized the need for upgrading design models to account for local and distortional buckling phenomena, promoting the use of whole-section analysis to enhance overall structural performance. The design and optimization of lightweight pedestrian foot-over bridges using CFS box sections were explored by V. Chandrikka et al. [25] Their study focused on minimizing dead weight while maintaining structural integrity. Using STAAD Pro for structural analysis, they demonstrated that CFS box-section bridges significantly reduce weight without compromising strength and durability. Their findings confirmed that such structures offer an economical, easy-to-build, and safe solution for pedestrian crossings.

Wei-Wen Yu and Roger LaBoube [26] have written a comprehensive manual covering the design principles of cold-formed steel, including material properties, structural behavior and the latest design specifications in North America. Their book covers both theoretical foundations and experimental evidence, emphasizing the imperative need for empirical verification in conjunction with advanced modeling techniques. The work confirms the application of the Direct Strength Method (DSM) for design calculations, showing its effectiveness in enhancing the accuracy of structural analysis of cold-formed steel. In addition, Yecheng Dai et al. [27] conducted research regarding the buckling resistance behavior of cold-

formed steel built-up stiffened box sections. Their research involved comprehensive experimental testing and finite element analysis that sought to anticipate the influence of parameters such as section thickness, column length, and screw spacing on the buckling behavior of such structures. The researchers determined that current design standards, including AISI S100 and AS/NZS 4600, were unnecessarily conservative by approximately 9.3% and thus recommended new Direct Strength Method (DSM) equations with better accuracy. Within the area of dynamic performance analysis, Maoqi Li [28] analyzed long-span steel truss bridges for pedestrians that undergo pedestrian-induced vibrations. Using finite element modeling (FEM) with ANSYS, the study analyzed the vibration frequencies and their implications for pedestrian comfort and bridge structural integrity. The results were that excessive vertical vibrations presented serious safety concerns, and suggestions were made for implementing damping systems and stiffness improvements to mitigate such effects. Emil Jonback and Gabriel Yakoub [29] explored advances in structural optimization, with a focus on using genetic algorithms to improve steel truss girder designs for pedestrian bridges. Their research led to the development of a parametric design model that could automatically alter truss configurations using finite element analysis and optimization techniques. They noted that the use of bent upper chords significantly improved weight efficiency, particularly for longer spans, and identified global buckling as the primary constraint on truss performance.

Cold-formed steel (CFS) bridges have proven effective in low-volume road networks, with ten galvanized CFS bridges built in Ecuador since 1987. The Colorado Bridge (1988) Figure 09 spans 12.8 m, carrying two-lane traffic on a 7.0-m-wide deck supported by 10 box girders made of 4.2 mm thick steel. The Puente Zapallo en Chone (1989) Figure 10, a 26 m single-lane bridge, features a delta truss substructure and seven continuous box girders made from 5.5-mm-thick steel. Research by GangaRao and Zelina [30] suggests AASHTO fatigue and deflection criteria for low-traffic bridges are overly conservative and could be optimized

for better material efficiency. Their study proposes reducing the live-load deflection limit from L/800 to L/360, with L/500 already in use in Ecuador. CFS trusses offer lightweight construction with high load efficiency, enhanced by box, channel, and I-sections. Optimized screw and bolt spacing improve strength, while CFS-timber composites could enhance axial compression but may risk local buckling failures. Given these advantages, CFS has been selected for this study, integrating advanced design techniques and Abaqus simulations.

Figure 9 Colorado Bridge, Ecuador [8].

Figure 10 Zapallo Bridge, Ecuador [7].

Sai Kumar Nalla's [31] study represents a crucial step in evaluating the performance of long-span CFS trusses. His research involved experimental testing of 48ft and 54ft trusses under uniform loading to assess deflection and load-carrying capacity. A finite element model in ABAQUS was developed to simulate these tests with numerical results closely matching experimental data. The study provided insights into optimizing truss configurations to improve load distribution and minimize deflections, making it a key reference for long-span CFS applications. The integration of CFS in modern infrastructure. In modern construction, steel members are generally classified in two main categories: cold-formed steel (CFS) and hot-formed steel. CFS is made at room temperatures by various processes such as rolling, pressing and bending compared with hot-rolled steel, which is made through moulding processes that expose the material at elevated temperatures [24]. Various cross-sectional configurations of

CFS are commonly applied in construction, such as C-sections, I-sections, Z-sections, angles, hat sections, T-sections and tubular sections. Increased use of CFS in construction is owing to their superior durability, ease of manufacture and excellent properties in structural and non-structural applications [11]. One of the most significant applications of CFS is in truss structures, which consist of triangular arrangements of members to distribute loads efficiently. Compared to conventional beams or columns, trusses offer superior weight distribution and structural stability. The use of CFS trusses in bridges and large-span structures has gained popularity due to their adaptability, ease of construction, and optimized material usage. The studies discussed above collectively contribute to the ongoing evolution of CFS technology, offering insights into its improved structural efficiency, durability, and optimization in various applications [8] [24]. The research by Sai Kumar Nalla marks a significant milestone in the advancement of CFS trusses, particularly for long-span applications. By combining experimental testing with numerical simulations, his study sets the groundwork for future innovations in CFS bridge and building design. With the increasing demand for lightweight, cost-effective and sustainable construction materials, CFS remains at the forefront of modern infrastructure solutions, addressing the challenges of contemporary engineering with enhanced performance, design flexibility and structural reliability.

2.5 Types of trusses

2.5.1 King Post Truss

Kingpost trusses Figure-11 are considered one of the most usable trusses in wooden roofing, the two spans come inclined. Dead, live, snow, and wind loads are transmitted to supports and the ridge. The diagonals serve as the struts and the vertical main central element is referred to as the king post. Nail the lower chord to the ridge.

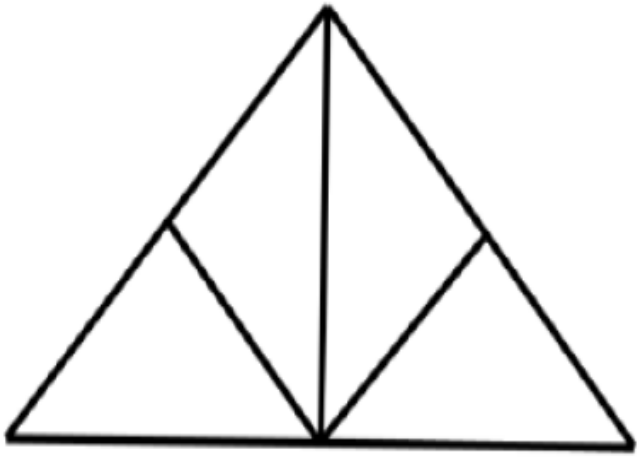

Figure 11King Post Truss [31].

2.5.2 Queen Post Truss

The queen post truss Figure-12 has more vertical members and fewer diagonals than the king post truss. This truss contains two queen post-the two vertical bars instead of one king post. The inclined rafters support loads of their self-weight, wind, snow, and living loads. These then get subdivided between the different members and distributed to the two supports.

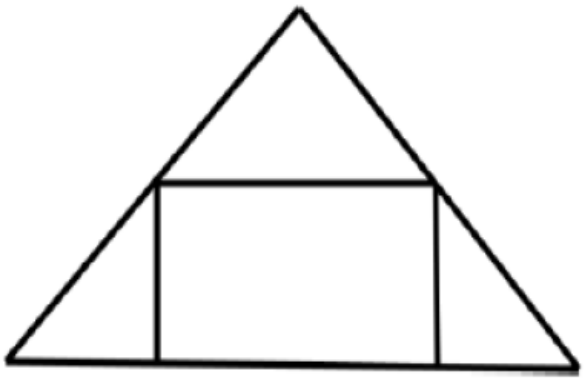

Figure 12 Queen Post Truss [31].

2.5.3 Pratt Truss

One type of truss bridge is the Pratt truss Figure-13, in which the diagonal members slope tapers in towards the middle of the span is one commonly known as Thomas Willis Pratt is one such immensely popular design of truss bridges. Efficiency in carrying a load over long distances and Pratt truss designs are essentially simple to fabricate. Amongst the varied applications that include they are most known in towers, buildings, and bridges.

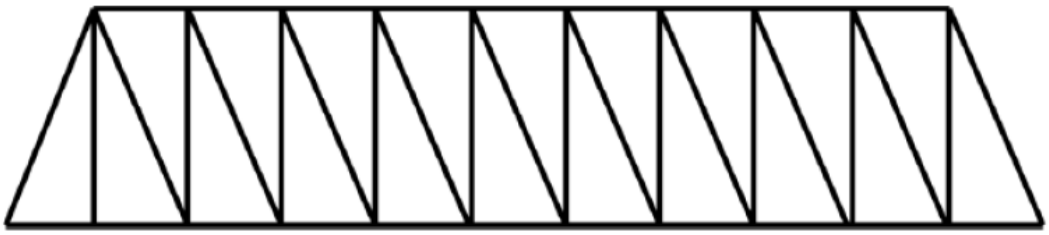

Figure 13 Pratt Truss [31].

2.5.4 Square End Truss

Square-end trusses Figure-14 are normally adopted for span lengths that are normally shorter because their construction is easy, lightweight, and inexpensive. According to Figure, diagonal web members connect the top and bottom chords to form a square shape. We will look into the case of a long-span square-end truss used to form the top chord with five studs and a three-stud bottom chord. Single diagonal stud members placed in opposite directions join the top and bottom chords, while the vertical studs connect both sides of the truss.

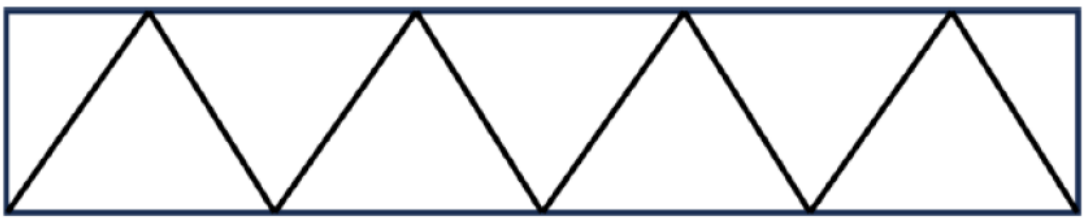

Figure 14 Square End Truss [31].

2.5.5 Truss members acting in tension, compression and truss system

Since truss has relatively consistent strength in both tension and compression Figure15, steel is one of the most commonly used materials in truss construction. However, buckling during compression is a real threat which may reduce the capability of the truss to carry a load. One of the efficient ways to overcome this problem is to use hollow sections, which also offers a resource-effective method for enhancing the truss's load-carrying capability. This can be attributed to their high resistance to lateral-torsional buckling thus increasing the buckling strength of the truss as a whole [32].One additional advantage of using hollow sections over I-sections is that I-sections tend to trap dirt and moisture in their joints, which would have a destabilizing effect on the life of the structure [33]. Another very important design consideration is the positioning of the bridge deck relative to the truss. In the case where the bridge deck lies above the truss, then the system is termed under spanned. If the deck lies between the top and bottom truss chords, then it is referred to as a half-through system; if the deck lies below the truss, then it is termed a through system see Figure-16 [34].

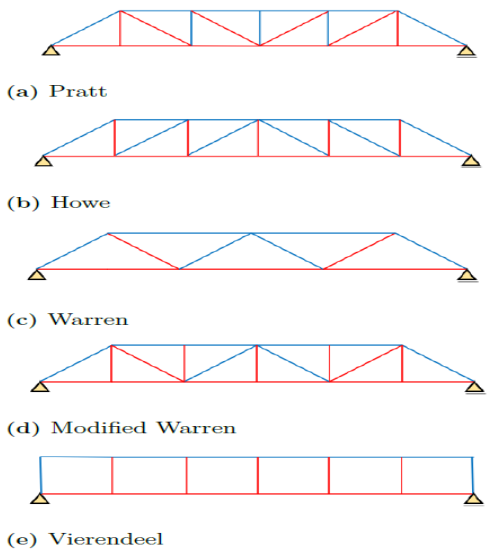

Figure 15 Type of trusses (Red for members in tension, blue for members in compression) [29].

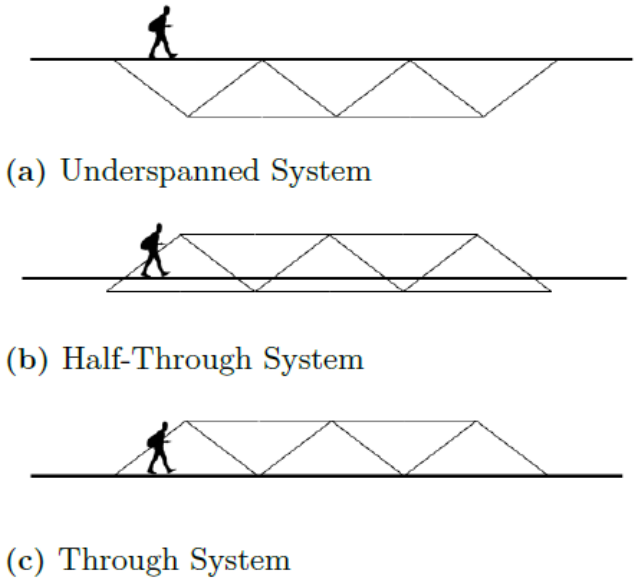

Figure 16 Three types of truss system [29].

Advances in bridge engineering have been characterized by dramatic evolvements of materials and design methodologies that enable the structures to perform efficiently and be more durable and sustainable. Among several alternative materials for such purposes, cold-formed steel is regarded as one of the most promising because of numerous advantageous properties, including a high strength-to-weight ratio, corrosion resistance, and easiness of fabrication. Cold-rolled steel refers to the manufactured steel product that assumes its shape at ambient temperature by rolling or bending, thus receiving consistent and very correct geometrical shapes [35].

Historically, several materials have been used in bridge construction: Timbers, Concretes, and the more traditional hot rolled steel. All these materials have various problems and advantages. Aesthetic and ecological, timber bridges raise some serious questions concerning durability and maintenance [36]. Strong and long-lasting, Concrete bridges are often heavy [37], thus needing extensive supportive systems; the overall cost of building is therefore higher. Hot-rolled steel bridges are renowned for being solid and open, spanning large

distances; however, they are significantly expensive to build and remain extremely labour-intensive to build.

Compared to such conventional materials, cold-formed steel has several competitive advantages: its intrinsic lightweight properties, combined with facility in handling and transportation, could lead to saving time and cost from construction; besides, making it rather resistant to environmental factors, it qualifies for all sorts of climatic conditions while reducing the needs for maintenance considerably [26].

Trusses find their application in supporting bridge construction against gravitational pull from vehicular movement and transmission of these forces into the sidewalks. From the very definition of a bridge, it follows that it is a structure serving to connect different regions to allow passage over an obstacle such as rivers, valleys, and ravines, among others. It is expected that with this setting, the advancement of development projects will be boosted on various fronts.

In truss bridge construction, trusses are designed to carry the gravity loads originating from moving vehicles to the supporting structures of the bridge. Depending on the location of the bridge, depending on the span length truss design may be performed as through type or deck type. While transportation system is attached to truss lower chord in through type the transportation system rests on the truss upper part in the case of a deck bridge. The general structural system supporting the carriage way is designed to transmit the carriage system loads to the nodal points of the vertical bridges. Most of these structures have already reached or exceeded their expected design life span and need replacement or repair. Because of increased traffic needs, incidents of overload, and poor maintenance, a substantial number of steel truss bridges have incurred serious damage, which is affirmed in the work of Lewis et al. in [38]. Accidental overload and impact, force majeure-flood, earthquake, etc.-structural design error,

construction supervision mistake, and not maintaining the structure are a variety of reasons one can note by observing huge numbers of bridge failures. Imam and Chrysanthopoulos in [39] reviewed metallic bridge failure statistics.

Yamaguchi et al., in [40], analysed the causes of post-member failure about the dynamic characteristics of the bridle bridge and recorded that the displacements related to dynamic behaviour can be larger than the displacements obtained by static behaviour; therefore, the dynamic analysis to analyse the behaviour of the truss bridge after a member failure would be proper.

In [41], Manda and Nakamura presented some of the problems in determining the span ratio and the live load distribution affecting structural safety and ductility for such truss bridges. Large deformation elastic plastic method made the collapse process clear. Actual tendencies of the collapse process are quite different by the live load distribution; however, the truss bridge collapsed by plastic buckling or elastic buckling. The study showed that the truss bridge holds an appreciable degree of safety regarding the design live loads, provided it is constructed according to the prevailing design specifications.

While Pinho et al. [42] have looked at performing a pushover analysis in which the structure is subjected to a lateral force of increasing magnitude with a constant distribution until the specified displacement is reached. The pushover analysis performed for the continuous multi-length bridge has been done regarding the standard pushover methods. It is expected that these new single-run methods will give even better results.

Advanced countries have similar needs for replacement. Towards rehabilitation of deteriorating small capacity bridges. GangaRao et al. [30] Recently, applied methodologies related to value engineering analysis to low-volume bridges in the United States, and

concluded. That the successive constants, multiplied by a weighting factor Compared will be the most significant when a low volume is assigned. Bridge: materials cost 23 percent, maintenance aspects 18 percent percentage, durability 16 percentage, operational life 15 percentage, ease of availability 15 percentage, and ease of construction 13%. Applications, analysis and component testing of an all-galvanized Cold-Formed Steel Bridge System for Low-Volume.

Highways in Ecuador and many developing countries are described. In these countries, hot-rolled steel structural Shapes conventionally used in the First World for large-scale building. Members are not domestically fabricated and are too expensive. to import. Hence, cold-formed sections of more Readily available sheet and strip steel is often used as the source elements such as longitudinal girders. Long-term service performances of Apart from this, steel is also galvanized by hot dip galvanizing in many developing countries. Performance data on durability and A review of the literature concerning life cycle cost analysis is presented.

2.6 Problem statement

Several studies have investigated structural performance of hot-rolled steel (HRS) truss bridges, but there have been fewer studies on the use of cold-formed steel (CFS) for bridge construction, especially for pedestrian bridges, and its relative effectiveness for different structural configurations. It should be noted that cold-formed steel has different characteristics relative to HRS, mainly because of its thin-walled profile, higher slenderness ratios, and increased susceptibility to buckling at both local and distortional levels. These characteristics bring high uncertainty to load carrying capacity, deflection control, and general stability under pedestrian live loads. Despite the trend of shifting towards lightweight and modular structures, existing bridge design guidelines, including the New Zealand Bridge Manual, do not include provisions and performance requirements specifically for CFS pedestrian bridges, thus limiting

safe and efficient use. Moreover, difficulties with deflection, sensitivity to local buckling, load transmission through flexible joints, and complex geometric interdependencies make it further difficult to design. Past research has focused mainly upon individual elements or simplified configurations, with results that do not fully address how geometry, span, and configuration affect critical performance characteristics, including deflection, stress distribution, and stiffness.

2.7 Objectives

The objectives of the study are:

- This research aims to develop New Zealand's first Cold-Formed Steel (CFS) pedestrian bridge, offering a sustainable, durable alternative to traditional materials while addressing current design and material gaps.
- To simulate and evaluate the structural behavior of each CFS bridge configuration under a uniform pedestrian live load of 5 kPa, focusing on key performance parameters such as mid-span deflection, stress distribution across members, and compliance with span/200 deflection serviceability limits as per design standards.
- To perform a comparative analysis of different truss geometries and layout arrangements, investigating the influence of span length, load, and geometry on deflection patterns, stress concentrations, and structural stability.
- To assess the extent to which simplified connection modeling (MPC connectors) affects global structural response.
- To establish a performance-based benchmark framework for CFS pedestrian bridge design, providing engineers and researchers with validated design data, modeling approaches, and critical insight into geometry-specific structural behavior.

- Load path uncertainty in complex geometries: In some bridge layouts, such as modular or trusses, load transfer between members is difficult to predict accurately without full-system modeling.

2.8 Implications

This research presents the project and structural evaluation of the First Bridge of Cold Steel Pedestrians (CFS) of New Zealand, demonstrating its potential as a sustainable and efficient alternative to conventional materials. The study explores two viable construction approaches: modular prefabrication, where CFS components are manufactured outside the site for rapid assembly with minimal work and environmental impact and site manufacturing, which allows greater flexibility in adapting to specific project conditions. Although detailed design guidelines and construction techniques have not been developed, this research provides critical information on structural performance, particularly in relation to deflection behavior, stress distribution and standard loading capacity. The study systematically analyses several Truss geometries of Truss, including box trusses, flat Pratt truss and modular panel bridges, to evaluate their feasibility under standard loading conditions. In addition, the research validates the use of finite element analysis (FEA) in the evaluation of the performance of the CFS bridges, establishing the bases for future tests and design standardization. This study contributes to the early-stage development of CFS pedestrian bridges in New Zealand, providing a basis for future optimization studies and formal project provisions.

2.9 Thesis structure

The research project is divided into seven chapters.

- Chapter 1 presents the study's background, classifies different bridges based on their structural forms and describes the selection process for the considered bridge types.

- Chapter 2 presents a comprehensive review of the literature on CFS pedestrian bridges, types of trusses, previous research and identifies the knowledge gap along with the objectives and significance of the study.
- Chapter 3 describes the procedure used to model finite elements, including model elements, material properties, boundary conditions and meshing strategy.
- Chapter 4 focuses on the numerical investigation of the CFS lattice bridge, presenting the development of the FE model, validation and a parametric study on span variations.
- Chapter 5 presents several alternative CFS bridge designs such as tub girders, flat foot bridges and box bridges and compares their performance over various spans.
- Chapter 6 includes comparative study of deflection and stress distribution between different geometries of bridges and their correlation to span and structural form.
- Chapter 7 summarizes the study by giving main findings and recommendations for future research, along with detailed manufacturing drawings placed in the appendix.

2.10 Summary

This chapter provided a background about the research project and its idea development. It presented the objectives of the study, which involve the investigation and proposal of alternative materials that are more durable, sustainable, environmentally friendly, and cost-effective than the currently used traditional materials for road bridges. It then presented the outline and structure of the thesis and provided a summary of each chapter. The following chapter is the literature review, which presents the published research to date on bridges and cold-formed steel (CFS), as well as the factors that affect the use of CFS road bridges. Finally, it identifies the knowledge gap and what has not been done in this area so far.

Chapter 3 – Methodology

3.1 Finite element models for analysis of cold formed steel pedestrian bridges

ABAQUS [43] a general-purpose FE solver is used for numerical analysis. The simulations included both geometric and material nonlinearities which means a suitable solution method needed to be chosen. It is often preferred to avoid dynamic methods to solve static problems because inertial effects can adversely affect the results. A general static step was initially tried for the CFS pedestrian bridge FE models. It was later discovered that the FE truss model could not handle the contact definitions, so it was decided to run all models using ABAQUS/Standard with an implicit dynamic step. A quasi-static dynamic step was utilized in Abaqus Standard to replicate static loading conditions, ensuring computational stability for thin-walled CFS structures, while avoiding inertial effects at the beginning of the analysis.

The FE models were developed as an attempt to better understand the distribution of stresses and to predict the deflection at mid span on Main beam and all of transverse at centre. The key application of the simulations is to assess the feasibility of using the FEM to predict capacities and maximum deflection under 5kpa [44] loading on transverse and material properties not able to be physically tested due to time and resource limitations.

A shell element (S4R and S3R) is generally used to model structures where the thickness is significantly smaller than the other dimensions by about a ratio of 1:10 compared to the global geometry, such as the thin gauge steel used in the CFS pedestrian bridge (Simulia 2012). This element is defined in one plane and the thickness is extruded, usually from the centre of the element outwards. The main advantage of using shell elements to model thin structures is that the computational cost of providing accurate stresses and deformations in the thickness direction are small compared to solid elements.

3.2 Model parts

The sections of CFS truss pedestrian bridge were created as separate parts which were generated in 3D modeling space, deformable shell and later extruded to specific required dimensions for different parts. As interest is largely in deflection of main span beam and transverse, the connection between different parts used as self-tapping screw (STS) was deemed unnecessary due to its added complexity to reduce computational time and resources. The thickness and position of STS were idealised and approximated.

3.3 Material properties

The material properties of the components of CFS pedestrian bridge were modelled as elastic plastic using the isotropic linear elastic material model together with the metal plasticity model available in Abaqus/Standard.

3.4 Contact Interaction

Contact conditions must be properly defined between interacting surfaces when simulating cold-formed bridge components or any other structure with contact interactions in Abaqus. The cold-formed bridge simulation presented here develops a detailed explanation of the contact interaction used, which involves key considerations: finite sliding, surface-to-surface contact formulation, enforcement methods and the setting for “Penalty” was used in the tangential direction, and the friction coefficient was taken as 0.2. The same coefficient was used in [45] for CFS truss.

There are many physical contacts in the simulated structure. In the standard static analysis, ABAQUS provides surface to surface contact with the option of either finite-sliding formulation or small-sliding formulation. The finite-sliding formulation allows any arbitrary motion of the surfaces. The small-sliding formulation allows two bodies containing contacting

surfaces to undergo large motions, but the contacting surfaces perform relatively small sliding movement to each other and arbitrary rotation of the bodies is permitted[46]. Since the sliding movements involved in CFS truss pedestrian bridge is to analyse large deformation in connections where components might slide over each other and nonlinear sliding path, the finite sliding option was chosen in the study. When applying surface to surface contact in ABAQUS, assignment of the master surface and the slave surface refer Figure 17, should be carried out with great care. In principle, the master surface on the body should be the strong material. Furthermore, in this study, the simulation results were found not to be sensitive to the surface friction coefficient used and a nominal value of 0.2 was acceptable [47].

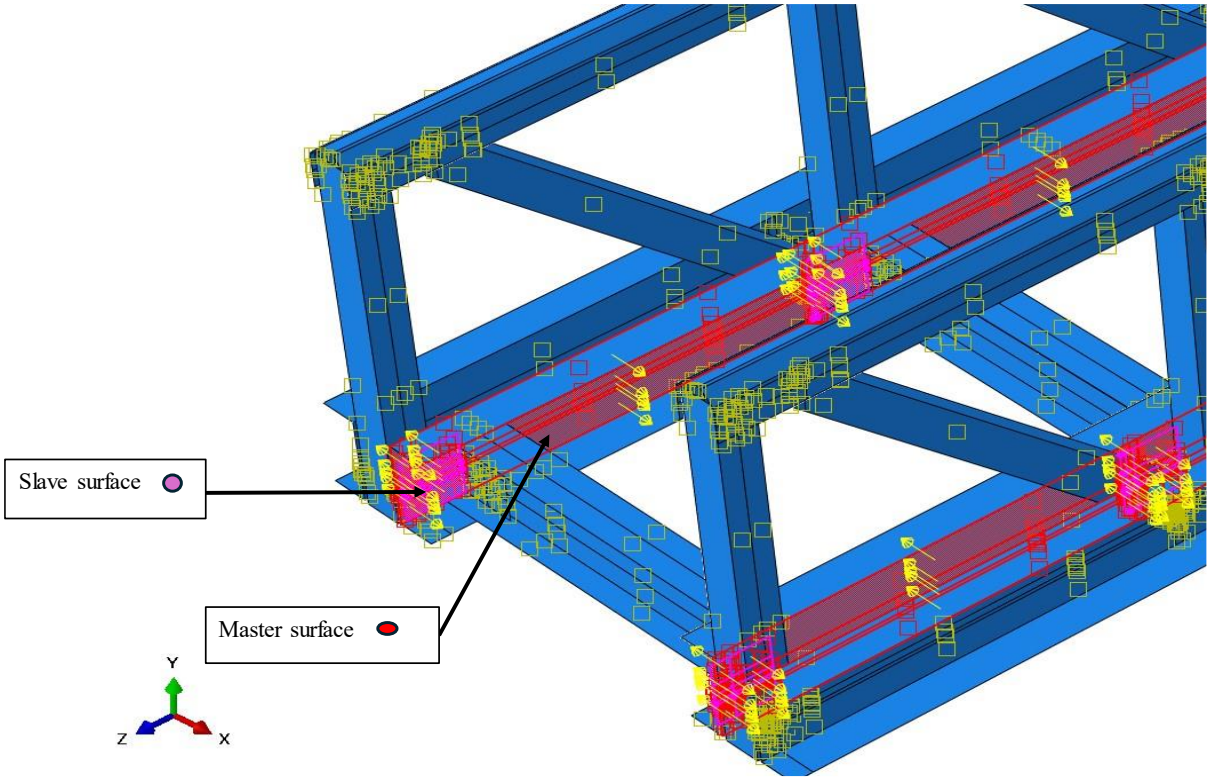

Figure 17 shows the interaction of master surface and slave surface.

3.5 Connector modelling

The level of detail attained in the present work represents a good compromise to study the bridge response and stress transfer among the different elements, simplifying the interactions at the level of the bolt connections, which were not modelled. The first and simplest approach to model the connectors was using BEAM multi-point constraints (MPCs) Figure 18,19,20. This method aligns well with the logic of the current study, as MPC constraints effectively couple the degrees of freedom of fastening points on both surfaces, ensuring realistic stress transfer while minimizing model complexity.

MPC constraints eliminate the degrees of freedom of a particular node, in this case by coupling the degrees of freedom of the fastening points on both surfaces. They have been used in the past to model the behaviour of screw connectors in CFS built-up specimens[48], [49]. This approach has the advantage of reducing the size of the model. However, it does not allow any output to be obtained from the connectors (e.g. the connector shear forces), and since the constraints are imposed by eliminating the degrees of freedom of one of the fastening nodes, it cannot be used to model more complex connector behaviour such as slip or bearing deformations of the connected plates. Nonetheless, for the scope of this work, the use of MPCs is deemed appropriate, providing a suitable compromise for accurately representing the structural behavior while maintaining computational efficiency.

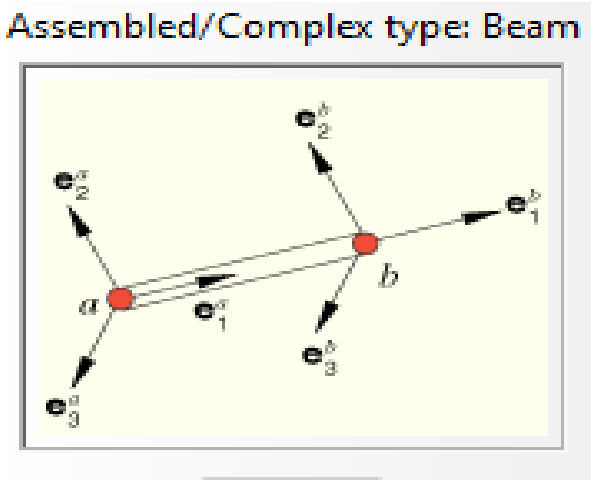

Figure 18 shows the Beam Connector [43].

The above Figure 18 from Abaqus represents the orientation and connectivity of a beam element between two nodes, a and b, in the context of beam mechanics. In addition, the Figure highlights the local coordinate systems for the beam at these two distinct nodes. Figure 18 is explained in detail:

1. Nodes a and b

- These are the end points of the beam element. The beam connects from node a to node b.

2. Local coordinate axes $e_1^a, e_2^a, e_3^a \; and \; e_1^b, e_2^b, e_3^b$ Each node is associated with its own local coordinate system. The axes are defined as follows:

- $e_1^a \; and \; e_1^b$ These are oriented along the longitudinal axis of the beam that connects nodes and b.
- e_2^a, e_3^a and e_2^b, e_3^b perpendicular to the beam's axis and define the beam's orientation in space.
- The orientation of these axes has an influence on the torsional, bending, and shear rigidity of the beam.

3. Beam direction

- The direction of the arrow on the line connecting nodes a and b indicates the beam element orientation. This usually follows the node numbering order (from a to b).

4. Significance of the Diagram

- It provides a clearer picture of the orientation forces, moments, and constraints applied on the beam element. If this is indicative of a section of your cold-formed steel truss bridge, maintaining the correct orientation of these beams within the global framework is essential for precise structural analysis.

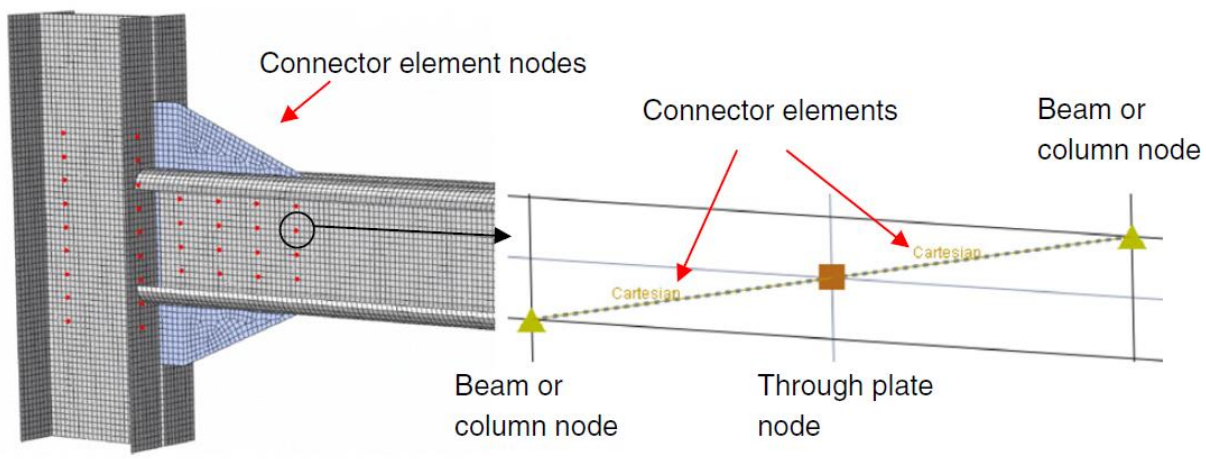

Figure 19 shows FE model of beam connector elements [50].

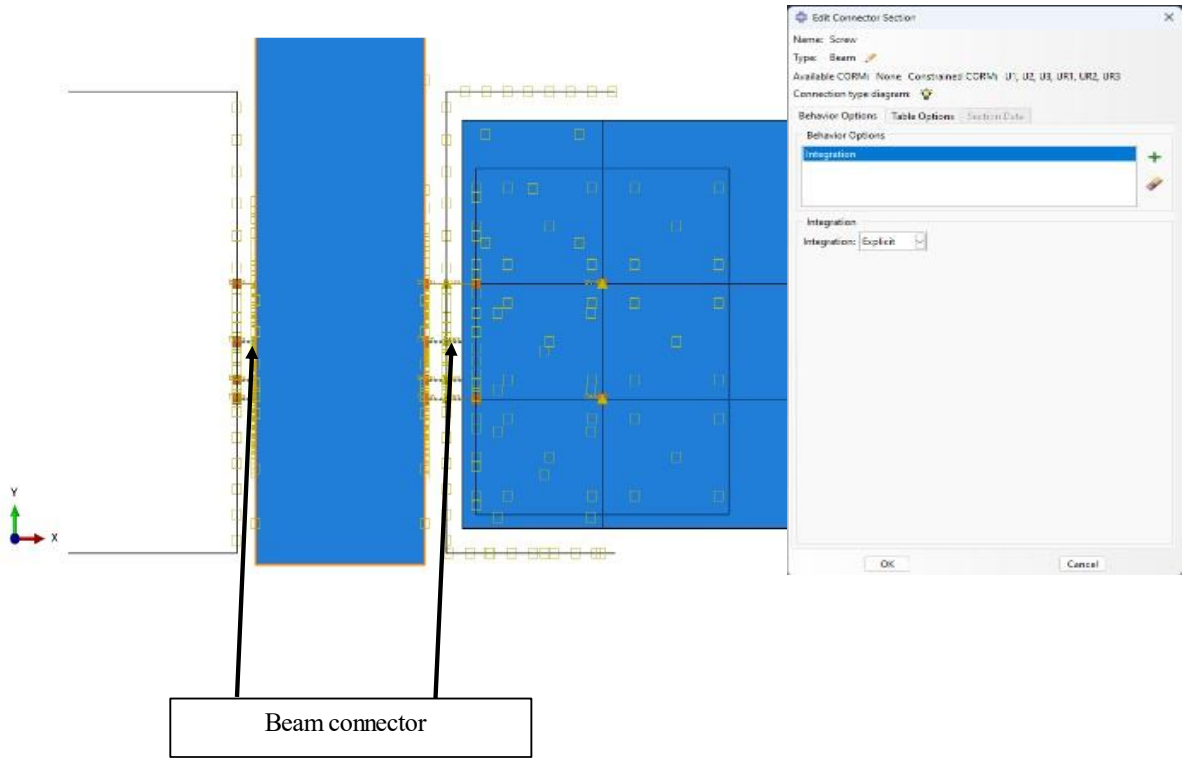

Figure 20 shows FE model of beam connector elements to assembly parts.

3.6 Load and boundary conditions

In the analysis, the CFS bridge under uniformly distributed load is studied. The load applied on the transverse beams as a pressure load with magnitude of 5kpa refer Figures 18,19.

The boundary condition for the configuration given in this CFS truss bridge structure shown in Figure22, analysed in Abaqus, includes partly restrained supports, which are important for the realistic simulation of the structural responses under an applied load. The imposed boundary conditions are against translational displacements along the global X and Y axes, U1 and U2, respectively, and against rotational displacements about the Y-axis and Z-axis, UR2 and UR3, respectively. By doing so, it shall prevent in-plane displacements and rotations and, hence, maintain the truss structural integrity within the X-Y plane with no possibility of geometric instability cases such as lateral torsional buckling or huge distortions under load. On the contrary, the translational freedom along the Z-axis due to U3 and the rotational one about the

X-axis due to UR1 indicates that the aim of the design is toward a hinge-like functionality or sliding support which offers a form of torsional flexibility or vertical displacement. This kind of boundary condition becomes very relevant when simulating a CFS truss bridge because members are thin walled, requiring careful management of the support conditions to effectively capture their realistic load distribution and buckling responses. By duplicating highly realistic boundary constraints, the Abaqus model will further enhance the structural analysis by allowing deep understanding of how the truss responds to complex interactions of loads refer Figure 21.

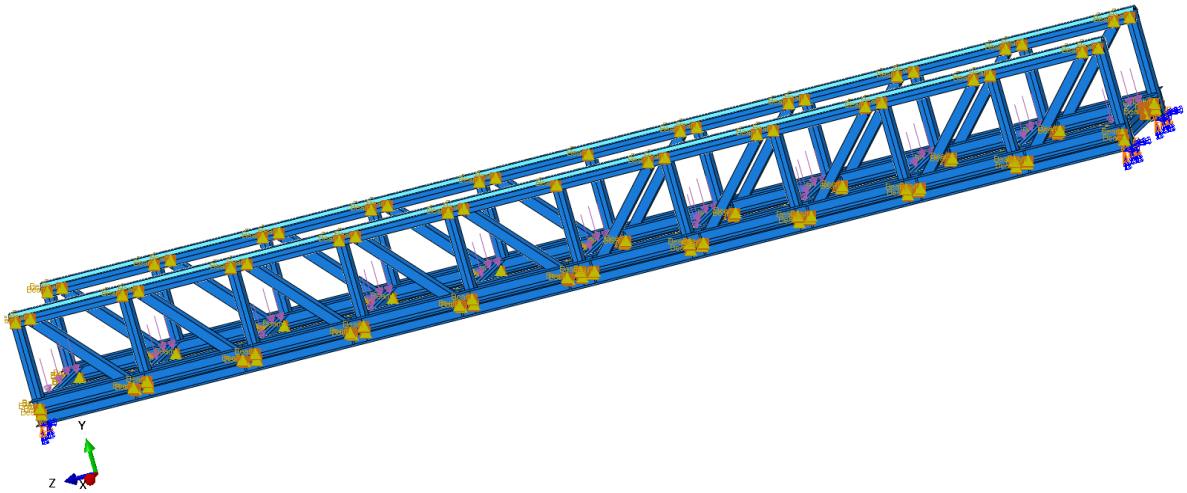

Figure 21shows the Load applied on transverse beam.

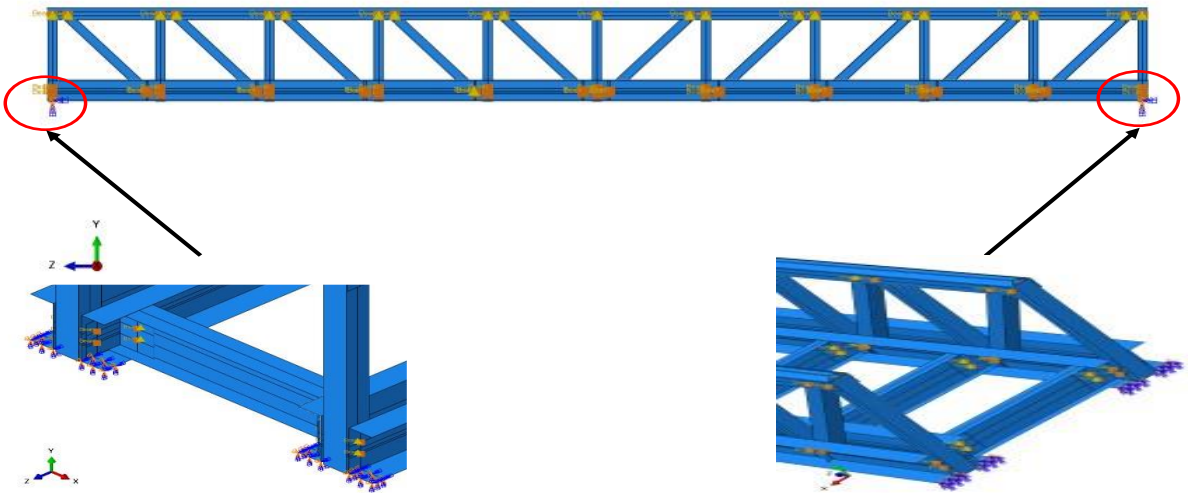

Figure 22 shows the applied boundary conditions at the bottom of Main span section on both ends.

3.7 FE Meshing

The two element types chosen for the mesh analysis were the conventional shell elements S3R and S4R, available in Abaqus/Standard. These are general-purpose quadrilateral linear elements that have been widely used by other researchers to model the non-linear behaviour of cold-formed steel members [49], [51], [52]. These elements can be used to model thick and thin shell problems. They account for the transverse shear deformations present in thick shell elements. However, as the thickness of the shell decreases and the transverse shear deformations in the element become negligible, the elements follow discrete Kirchoff theory, where plain sections normal to the mid-surface of the shell remain straight and normal throughout the deformation of the mid-surface. The elements account for thickness changes because of in-plane deformations, and they are not affected by transverse shear locking. These elements use finite membrane strain formulation, allowing for arbitrarily large deformations and rotations. Therefore, they are suitable for non-linear geometric analysis. S4 is a fully integrated shell element with three translational and three rotational degrees of freedom at each node. It has four integration points and does not have hourglass modes in either the membrane or bending response of the element. However, due to its number of integration points, this element is computationally more expensive, especially for large problems, than its counterpart S4R element with reduced integration points. S4R elements only use a single integration point to formulate the element stiffness. They can provide accurate results, although they are prone to hourglassing modes. However, in the problems under consideration hourglassing modes were not found to be an issue.

A mesh sensitivity analysis was meticulously conducted to identify the optimal mesh size for the structure under investigation. The results of this analysis, as shown in the Figure 23, highlight the relationship between mesh size and deflection. Mesh sizes ranging from 10mm to 50mm were analyzed, with the corresponding deflections measured to ensure

accuracy in the structural simulation. The deflection values show a slight decrease as the mesh size increases, stabilizing at approximately 0.80mm for larger mesh sizes. This stabilization indicates that further refinement of the mesh beyond a certain point does not significantly impact the accuracy of the results.

Based on these findings, a 20mm x 20mm mesh size was selected as the optimal choice. This decision was justified by the balance it provides between accuracy and computational efficiency. The deflection at this mesh size is consistent with the results obtained for finer meshes, such as 10mm x 10mm, while significantly reducing computational time and resource demands. This approach ensures a reliable and efficient analysis, supported by the results of the sensitivity study, forming a robust foundation for the structural evaluation.

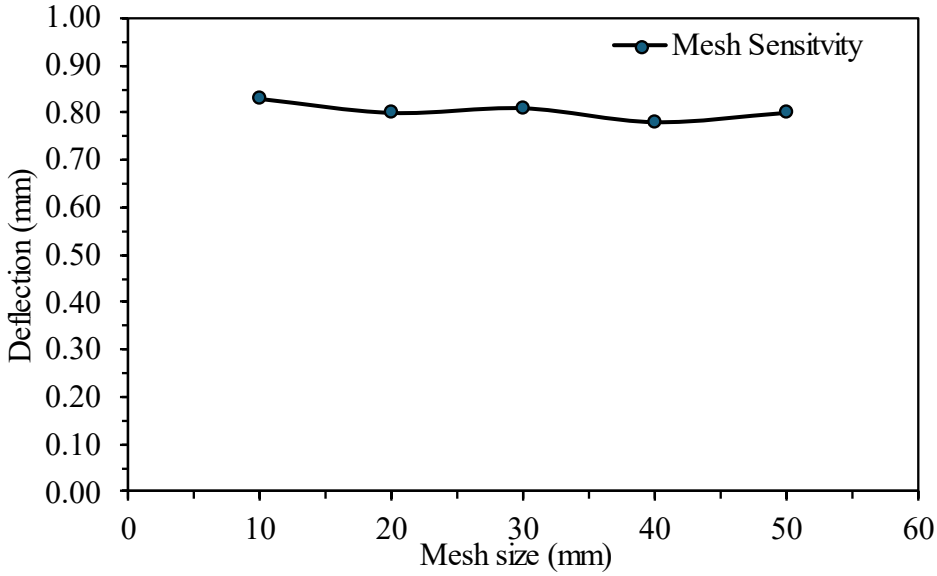

Figure 23 Graph for mesh sensitivity analysis.

Chapter 4 – Structural analysis of CFS truss bridge

This chapter presents a detailed numerical analysis of the structural performance of Cold-Formed Steel (CFS) pedestrian bridges by using Finite Element Analysis (FEA). This study utilizes Abaqus software to develop validated FEA model that simulate the performance of various CFS bridge configurations under standardized loading conditions. The investigation focuses on evaluating key parameters such as deflection behavior and stress distribution. A previously validated GFRP bridge model is used as a baseline, with CFS material properties introduced to assess performance. The outcomes of this numerical analysis serve to establish a foundational understanding of CFS bridges for pedestrian applications.

4.1 Experiments from literatures

Several experimental studies have investigated the structural performance of cold-formed steel (CFS) pedestrian bridges under both static and dynamic loads. Awaludin et al [6] constructed a 7 m span CFS Warren truss footbridge 1.2 m wide, 0.8 m deep with a steel deck and subjected it to static load tests and dynamic excitation. Under design loading, the bridge exhibited small deflections 8.1 mm with combined dead and live load and a high fundamental frequency of 7–8.5 Hz, decreasing slightly under live load. The high stiffness meant the natural frequency exceeded typical pedestrian walking frequencies, avoiding resonance. Measured accelerations due to normal walking and running were modest (peak ~0.11g), indicating that the bridge remained comfortable for users. Notably, after sustained sinusoidal loading at its natural frequency for an hour, no reduction in natural frequency was observed, suggesting no appreciable stiffness degradation or fatigue damage. These results demonstrate that CFS truss bridges can meet serviceability criteria, with deflections within limits and adequate dynamic performance under pedestrian loading.

Dynamic performance and vibration serviceability have also been a focus of recent studies. Xu et al [53] performed static and dynamic testing on a long-span multi-span CFS footbridge in China, including load tests, natural frequency measurement, and pedestrian comfort evaluations. Their data showed that the as-built CFS bridge had a vertical natural frequency well above the range of walking-induced frequencies, thus inherently avoiding resonance. However, under dense crowd loading, the structure experienced relatively high accelerations, leading to discomfort according to human perception criteria. The researchers modified the bridge adding stiffness or damping to improve comfort and subsequent tests confirmed that the upgrades effectively reduced acceleration response to acceptable levels. This finding highlight that while CFS pedestrian bridges can be very stiff for their weight, serviceability under dynamic crowd loads may govern design – requiring attention to vibration control even if strength and deflection criteria are satisfied.

Experimental studies have also shed light on typical failure modes of CFS bridge structures. Because CFS members are thin-walled, local buckling and connection failures tend to govern ultimate behavior. Ammar et al [10] tested two small-scale 4.8 m span CFS truss bridge specimens to investigate failure mechanisms. One truss used conventional screw-fastened gusset-plate connections specimen B1, while the other incorporated screws with adhesive bonding and thicker gussets specimen B2. Under two-point bending to failure, the specimen with only screws reached 3420 kg load before the gusset plate buckled and several screws sheared a connection failure mode. This indicates that strengthening CFS connections via adhesives or stiffened gussets can significantly increase load capacity and relocate the weak link from the joints to the members.

Similarly, Nalla's [31] full-scale tests on 15–16 m long CFS trusses originally designed as roof trusses reported that connection points were the critical failure zones. The dominant

observed failure mode was fracture at the web-to-chord connections, rather than failure of the members themselves. Such results consistently underscore that bolted or screwed connections and gusset details are often the vulnerability in CFS truss systems, governing the ultimate strength and collapse mode.

Compared to these experimental works, the present research takes a broader, simulation-based approach to explore multiple bridge configurations. Whereas most literature studies focus on a single bridge prototype or truss type, few have systematically examined a wide range of CFS pedestrian bridge geometries under consistent loading for comparison. In this thesis, detailed finite element models (developed in Abaqus) are used to analyze various CFS bridge forms – including a flat Pratt truss, a box truss, a trough-style tub girder, a panel bridge, and a box-girder/truss hybrid – all subjected to standardized pedestrian load conditions. By evaluating deflection behavior and stress distribution across multiple geometries, the work extends the knowledge base beyond what individual experimental case studies have covered. Indeed, there is a noted lack of studies examining numerous CFS bridge layouts in parallel. The FEM results in this research help fill that gap, identifying which configurations provide the best structural performance and why, under identical load criteria. In essence, the numerical experiments complement and expand upon the findings from literature by generalizing them to a wider design space.

4.2 Development of FE model

The finite element model (FEM) was developed starting with the analysis of the pedestrian truss bridge, which consisted of Glass Fiber Reinforced Polymer (GFRP) profiles. The main aim was the confirmation of the accuracy of the finite element model before the same technique would be used with the Cold-Formed Steel (CFS). The GFRP bridge was typical with a span of 6 meters, width of 0.75 meters and maximum height of 0.53 meters. In this study,

structured meshing with quadrilateral elements was applied to the CFS sections to ensure high-quality finite element discretization. the Quad element shape and Structured meshing technique were selected to generate a regular and uniform mesh across the geometry. Standard deformable shell elements were employed, specifically the S4R type, which are four-node quadrilateral elements with reduced integration, capable of accurately capturing both membrane and bending behaviors. The meshing with a size of 20 mm was selected after mesh sensitivity study to ensure the best balance of precision and computational cost. Shell elements were used to model the thin-walled parts, while the material model used was of the linear elastic type, based on the parameters experimentally confirmed by Rimkus [54], Young's Modulus (E) of 31.3 GPa, and Poisson's Ratio (ν) of 0.23 [54].

Boundary conditions were adopted to replicate realistic support conditions, with one end pinned and the other roller support. The uniformly distributed load (UDL) of 5 kPa [55], equivalent to the total force of 13.3 kN was uniformly distributed across the bridge deck. Abaqus simulation accurately simulated the linear structural behavior under the conditions of service-level loads, which were all within the elastic range and avoided the complications involved in plastic or nonlinear behavior. This setup allowed for accurate predictions of load-deformation behavior and stress distribution across the structure.

4.3 FE validation

The experimental work focused on the structural response of a GFRP pedestrian truss bridge model under static loading conditions. A wooden deck served to ensure equal load distribution and deflections at different locations on the bridge model were measured to evaluate the structural response. For accurate measurement, the bridge rested on four pads, with the chosen floor beams having pinned and roller supports below them. Steel bricks, with a weight range of 20-25 kg, were placed on the model to create a uniformly distributed load of 5

kPa, reaching a total force of 13.3 KN in four phases of loads. Linear variable displacement transducers (LVDTs) were placed along the length at strategic locations to measure deflections. The results showed a deflection value of maximum 6.635 mm at the middle, which was below the acceptable value of 12 mm, thus proving the stiffness of the structure to be good enough. Comparative numerical analysis through SolidWorks supported the findings, showing the error range varying from 0.3% to 10.5%. The findings confirm the usability of GFRP profiles as pedestrian bridges; more research must be conducted to evaluate their dynamic response and long-term durability.

Pedestrian truss bridge model is made of GFRP profiles sections. The length of considered structure was 6 m, width – 0.75 m, height – 0.53 m. The mesh and element type of the model consisted of a uniform 20 mm element size, as shown in the simulation images. This choice ensured an effective simulation of the structural behavior while maintaining computational efficiency, balancing accuracy and processing time. Regarding material properties, the GFRP profiles were assigned a modulus of elasticity (E) of 31.3 GPa, a value validated through experimental testing [54]. The linear elastic model was used to represent the GFRP material because it accurately captures its behavior under service-level loads, where the response remains predominantly elastic, allowing for efficient and reliable simulation of structural performance without introducing the complexity of nonlinear modelling. The material was modeled with a linear elastic behavior, allowing accurate representation of its initial response under loading, ensuring realistic deformation and stress distribution.

Table 1 Mechanical and physical characteristics of GFRP material taken from [54].

Characteristic	**Value**
Density, ρ	1.8 g/cm3
Tensile strength, *ft*	240 MPa
Compressive strength, *fc*	240 MPa
Modulus of elasticity (experimental), *E*	31.3 GPa
Poisson coefficient, *v*	0.23

The stress-strain response obtained from the simulation corresponds to the behavior of a material defined with linear elastic properties in Abaqus [43]. According to the Abaqus User Manual (Section 17.2.2, Version 6.6), the linear elastic behavior assumes that stress is linearly proportional to strain, consistent with Hooke's Law. In the simulation, the material property module was specified using the elastic keyword refer Figure 24, which defines isotropic elasticity through two independent parameters: the Young's Modulus (E) and Poisson's Ratio (ν) as shown in table 1. This input enforces a linearly elastic, reversible response under small strain assumptions. The resulting stress-strain graph displays a straight-line relationship, confirming that the material exhibits no permanent deformation, no plastic yielding refer Figure 25, 26 and maintains constant stiffness throughout the loading. The linear trend of the stress-strain plot and absence of any deviation or nonlinearity thus confirm that the analysis remained entirely within the elastic regime and the simulation output faithfully represents the material's idealized elastic behavior as defined in Abaqus manual.

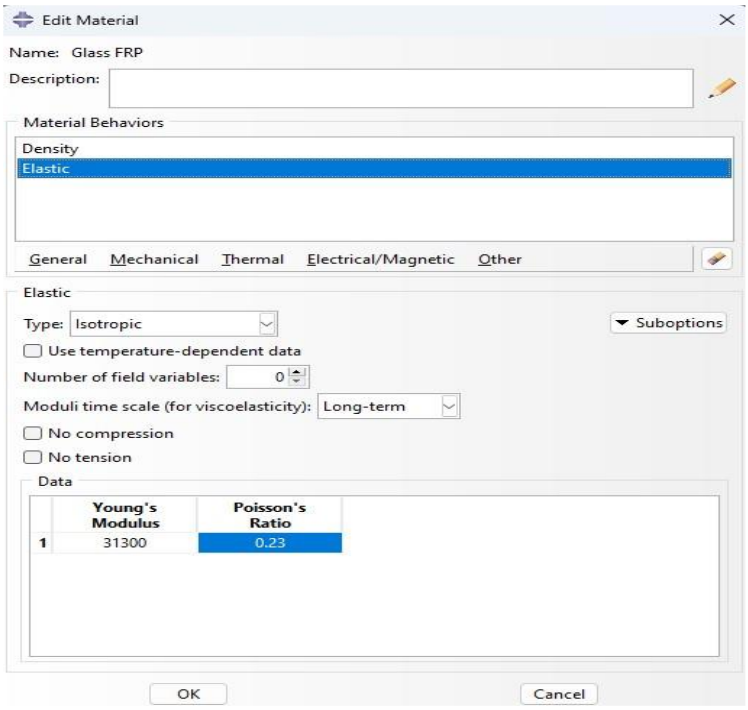

Figure 24 Defining of linear elastic material properties for GFRP in Abaqus CAE using isotropic elasticity [54].

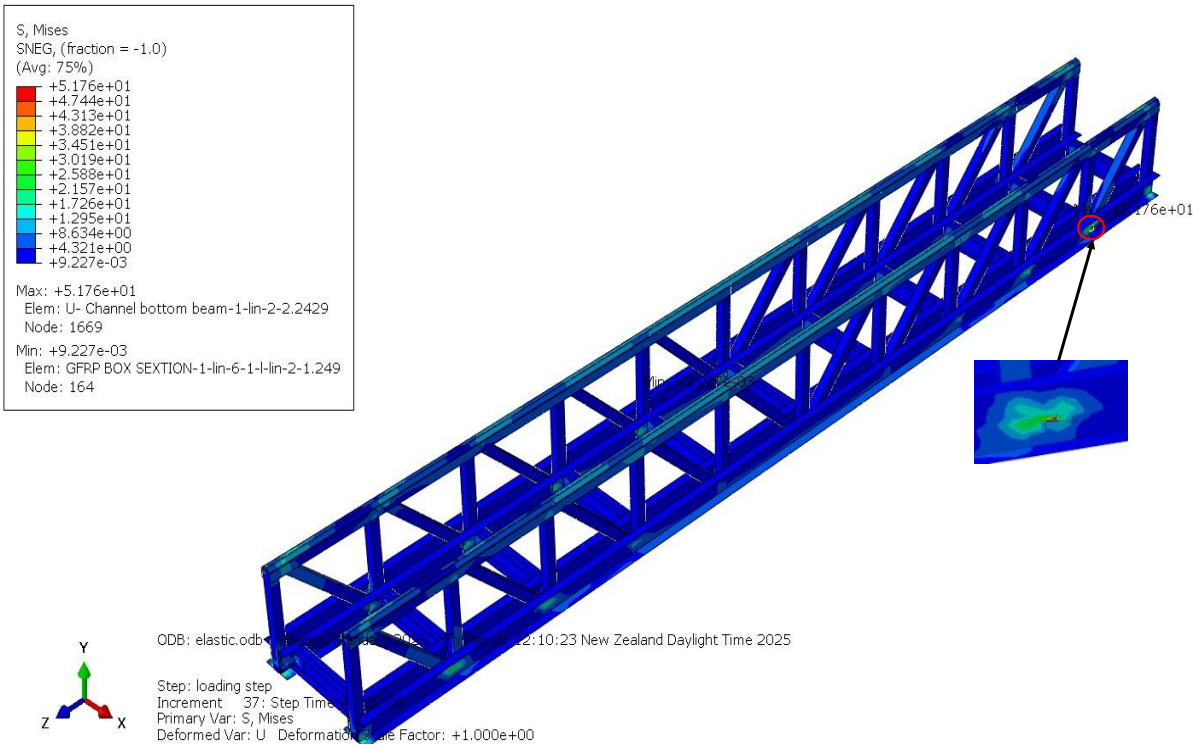

Figure 25 S Mises output from Abaqus CAE using linear elastic material model.

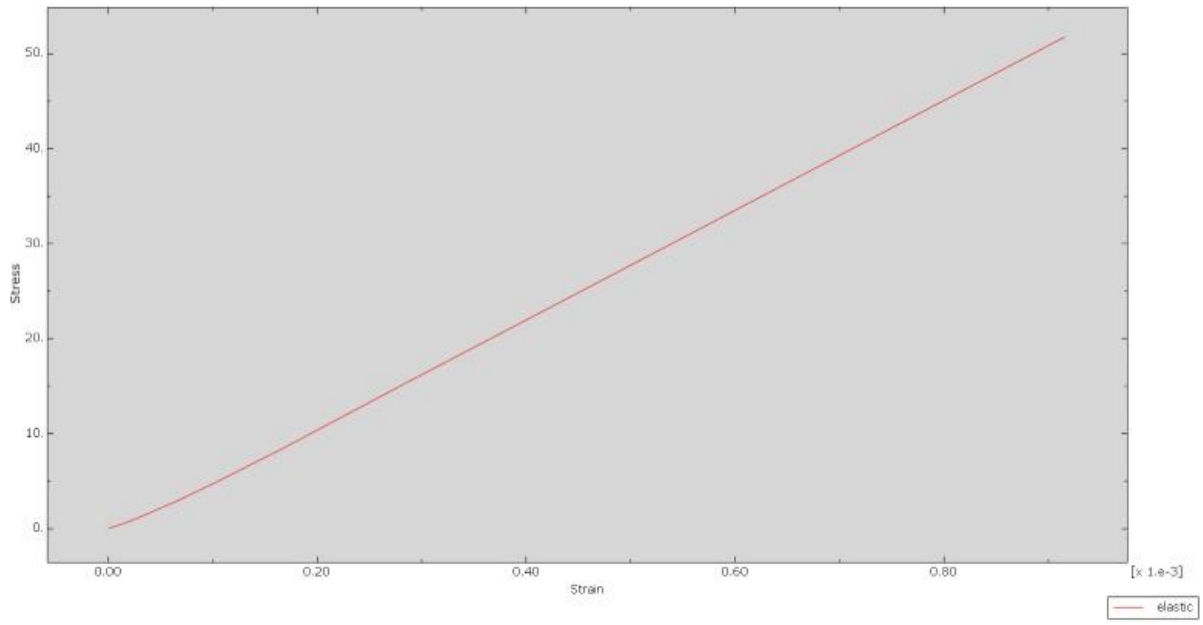

Figure 26 Stress–strain curve for GFRP material obtained from Abaqus simulation confirming proportional elastic behavior.

Result comparison for the fourth stage loading deflection values is captured in the following table 2.

Table 2 shows comparison of Validation results.

Metric	**Experimental (Δexp) mm**	**Numerical (ΔFEM) mm**	**Difference (%)**
Maximum Deflection at Mid-Span	-6.371	-5.748	9.78

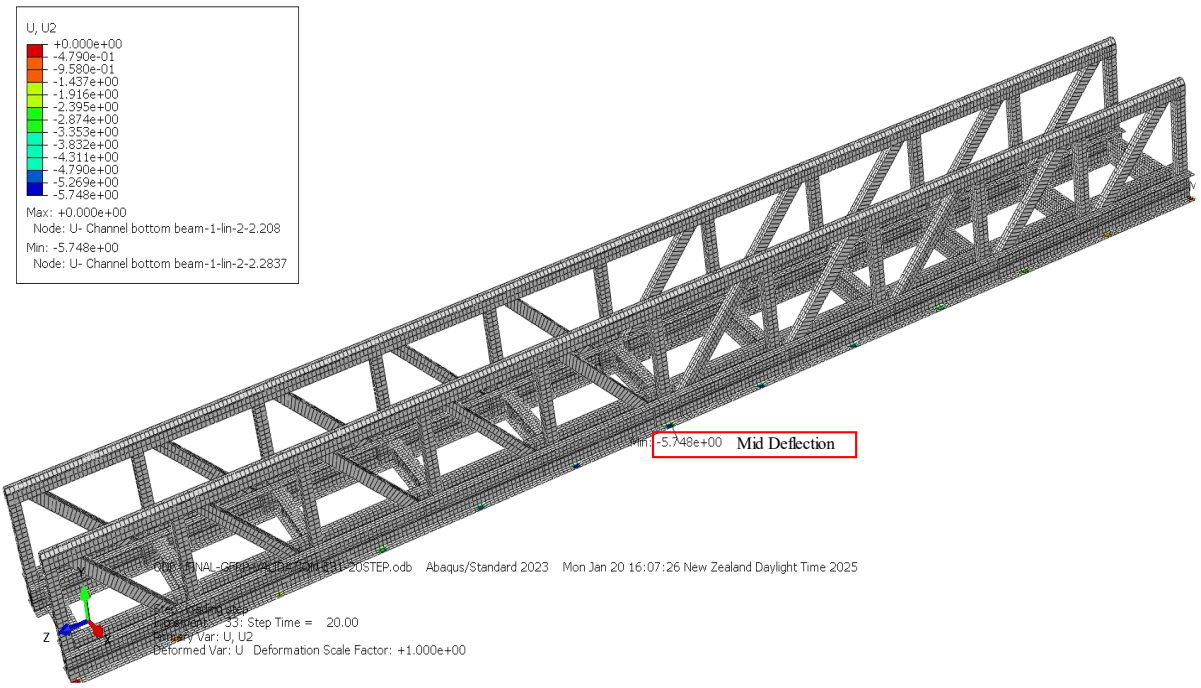

Figure 27 Mid span Deflection for validating model [54].

The simulation in Abaqus foresees a maximum deflection value of −5.748 mm, 9.78% less than in experimental testing. While this difference is higher than the ideal range, it is within an acceptable limit for numerical modeling of complicated GFRP truss bridge structures, in which differences can occur due to uncertainties associated with material properties, boundary conditions and simplifications in the computational model. This difference is common in finite element analysis since these methods are based on assumptions that do not always account for the complicated behaviors in actual conditions. However, the observed difference is sufficient to confirm the accuracy and reliability of the numerical method used for structural analysis.

Key Observations

The Abaqus output indicates a relatively stiffer behavior when compared with experimental values, possibly due to such factors as: linear elastic behavior for GFRP, even when the actual behavior can include minor nonlinear behavior. Despite the discrepancy, the results confirm overall effectiveness and durability of GFRP truss bridge prototype under

pedestrian loads. The deformational behavior exhibited in Abaqus output (refer to Figure 27) confirms to the predicted distribution and configuration of loads and deformations in a range of loading cases as shown in Figure 28.

The decision to apply cold-formed steel (CFS) to the same Abaqus model originally validated for GFRP is based on the fundamental principles of structural mechanics and finite element modeling. Since the model has already been verified for GFRP, its geometry, boundary conditions, and loading conditions remain valid irrespective of the material change. The substitution of CFS was done purely to observe how the structure would behave with a different material, without conducting a direct comparative analysis. This approach is reasonable because FEA models are fundamentally material-independent, meaning that the same setup can be used with different material properties, geometric changes are introduced. Although the original experimental tests were conducted on GFRP, applying cold-formed steel to the validated model allows for an exploratory study of the structural response under a different material system. Steel is a commonly used material in structural applications, and using the same model provides insight into its load-deformation characteristics in the same structural configuration.

Since CFS exhibits higher stiffness and ductility than GFRP, its structural behavior can be expected to differ, particularly in terms of deflections and stress distribution. However, the decision to apply CFS was not for the purpose of direct comparison but rather to assess how the existing model, already validated for GFRP, would react to a material with different mechanical properties. This approach is a standard practice in engineering simulations, where a validated model is often repurposed for material investigations without requiring a completely new setup.

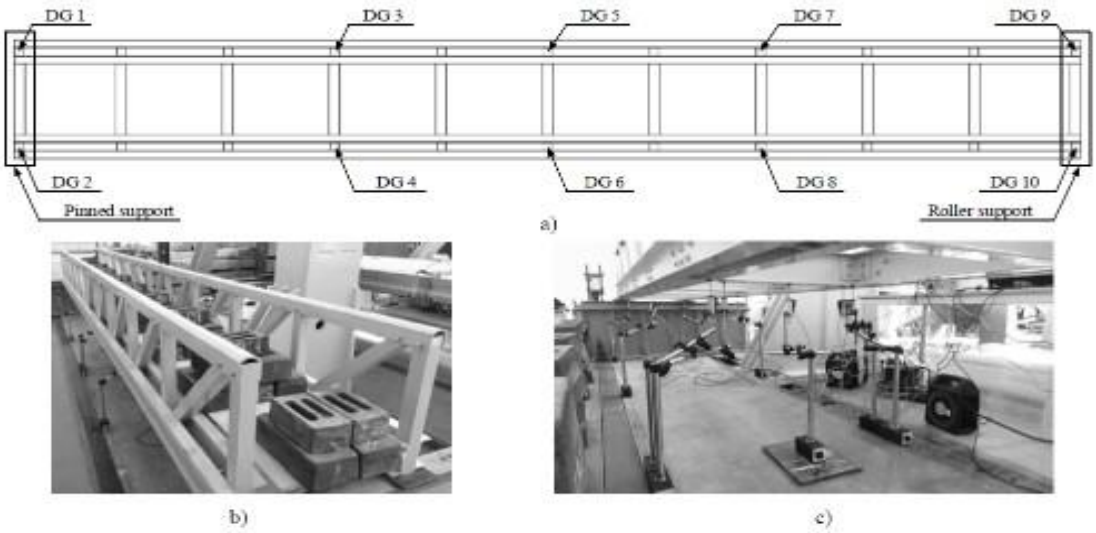

Fig. 2. Arrangement of the displacement gauges (a) and (c); load distribution on a wooden bridge deck (b).

Table 2. Total weight on each floor beam and order of the loading stages.

Floor beam (FB)	1	2	3	4	5	6	7	8	9	10	11
Loading I, kg	70.9	132.9	131.8	-	-	-	-	-	-	-	-
Loading II, kg	70.9	132.9	131.8	132.6	131.0	130.9	-	-	-	-	-
Loading III, kg	70.9	132.9	131.8	132.6	131.0	130.9	131.0	132.5	-	-	-
Loading IV, kg	70.9	132.9	131.8	132.6	131.0	130.9	131.0	132.5	131.8	133.0	71.0

Loading stage	Maximal deflection Δ, mm					$\Delta_{Th}, E_{obs,avg}/\Delta_{Exp}$	$\Delta_{Th}, E_{nom,k}/\Delta_{Exp}$
	Δ_{Exp}	$\Delta_{Th}, E_{obs,min}$	$\Delta_{Th}, E_{obs,avg}$	$\Delta_{Th}, E_{obs,max}$	$\Delta_{Th}, E_{nom,k}$		
I	-0.794	-0.875	-0.832	-0.794	-1.080	1.048	1.360
II	-3.407	-3.958	-3.765	-3.590	-4.882	1.105	1.433
III	-5.322	-5.822	-5.538	-5.281	-7.182	1.041	1.349
IV	-6.371	-6.680	-6.354	-6.058	-8.239	0.997	1.293

Figure 28 shows the Maximum deflection (highlighted) for fourth loading stage [54].

4.4 Parametric study

4.4.1 Effects of a 6-Meter Span on Deflection and Stress in a Flat Pratt Truss Cold-Formed Steel Pedestrian Bridge

Introduction

Figure 29, 30 shows the design and geometry of the truss bridge model. The geometry of the bridge specimen was selected regarding lightweight truss design recommendations for short span pedestrian bridges [23]. The prototype was designed according to serviceability requirements and assembled using structural components as listed in Table 3. The dimensions of the structure were: length – 6 m, width – 0.75 m, and height – 0.53 m. The behavior of the pedestrian bridge was simulated using Abaqus CAE software [43]. The geometry, support conditions, and loading configurations of the numerical model were directly adopted from the experimental bridge prototype reported by Rimkus et al. [54]. In the simulation, Cold-Formed Steel (CFS) sections, characterized by a Young's modulus of 200 GPa and a yield stress of 550 MPa, were employed to replace the original Glass Fiber Reinforced Polymer (GFRP) profiles in order to evaluate the mid-span deflection behavior and the overall structural response.

Figure 29 shows pedestrian bridge for Parramatta City Council NSW [56].

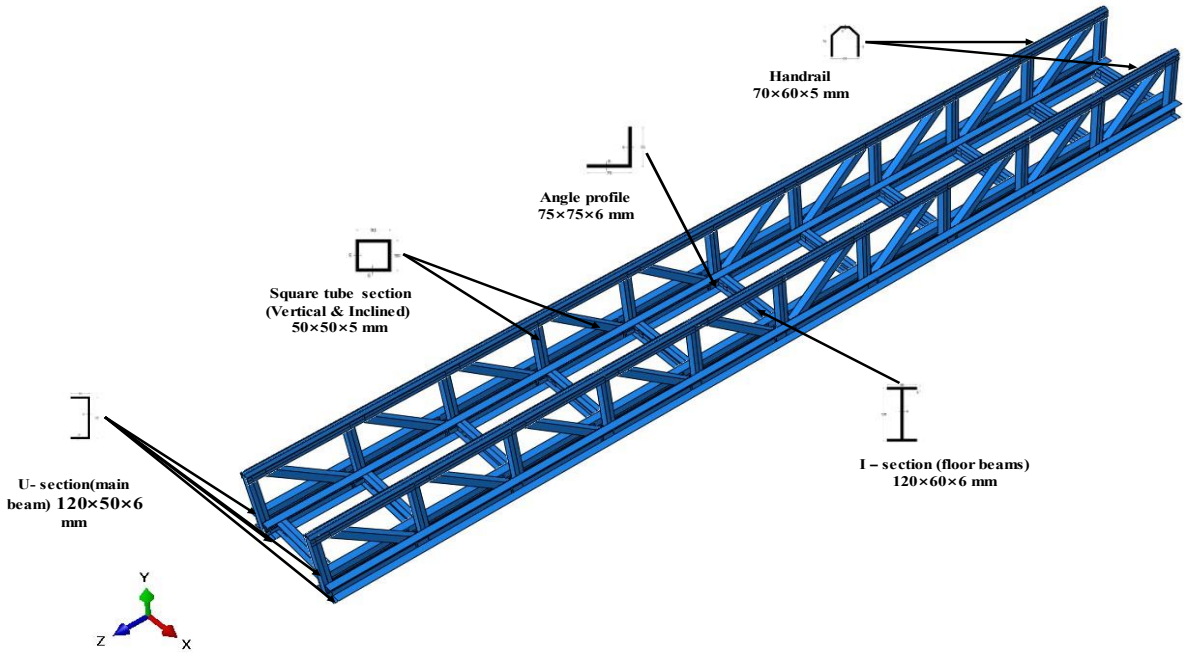

Figure 30 shows the design and geometry of the truss bridge model [54].

Model parts

The models were constructed based on the measured cross-sectional dimensions of the components from GFRP bridge [54]. The CFS pedestrian bridge parts were created in 3D modeling space, deformable shell and later extruded to specific required dimensions for different parts. The parts used in pedestrian bridge are mentioned in table-3 with dimensions and follows with Figure - 31.

Table 3 shows type of parts used in pratt truss bridge with length and thickness in mm [54].

Part	**Length (mm)**	**Thickness (mm)**
I- section	515.9	6
U- section	6000	6
Square tube section vertical	530	5
Square tube section inclined	670	5
Handrail	6000	5

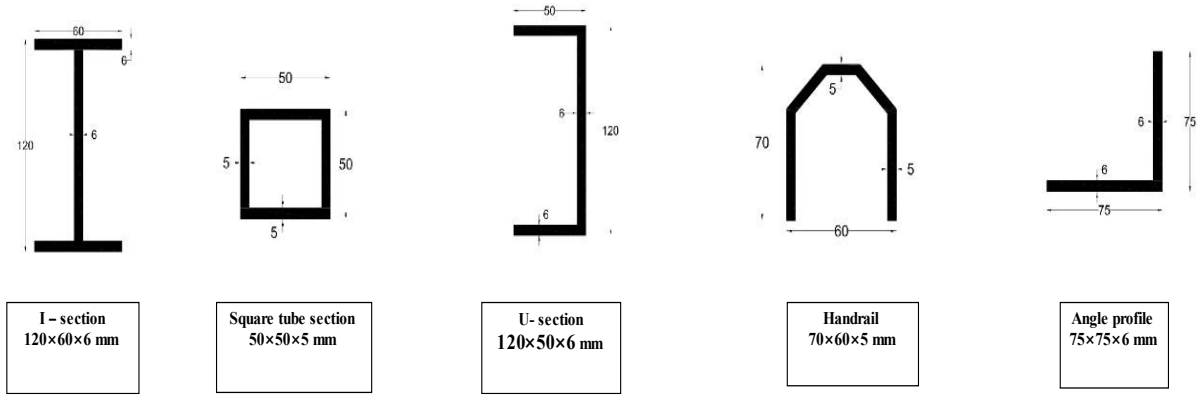

Figure 31 shows geometry and dimensions used for CFS pedestrian bridge [54].

Material properties

Material properties for the finite element (FE) models were obtained from the coupon tensile tests of section L-G420, specifically coupon F-5, conducted by Gong-Wen Li et al. [57]. The tests were performed at room temperature following the GB/T 228.1–2010 standard. The yield stress was reported as 478 MPa, and the elastic behavior was characterized using a Young's modulus of 206 GPa and a Poisson's ratio of 0.3.

Assembly

The design, geometry and dimensions of the Short Span Flat Pratt Truss CFS Pedestrian Bridge was composed according to serviceability requirements and assembled using structural components of 5 shapes: 120×60×6 mm I-profile, 120×50×6 mm U-profile, 50×50×5 mm square tube, 75×75×6 mm angle profile and 70×60×5 mm handrail. The bottom chord beam was realized by two U-profiles coupled by square tube. The connection between the CFS

profiles was made by pinned connections. Floor beam (FB) scheme and cross section are presented in Figure 32 respectively.

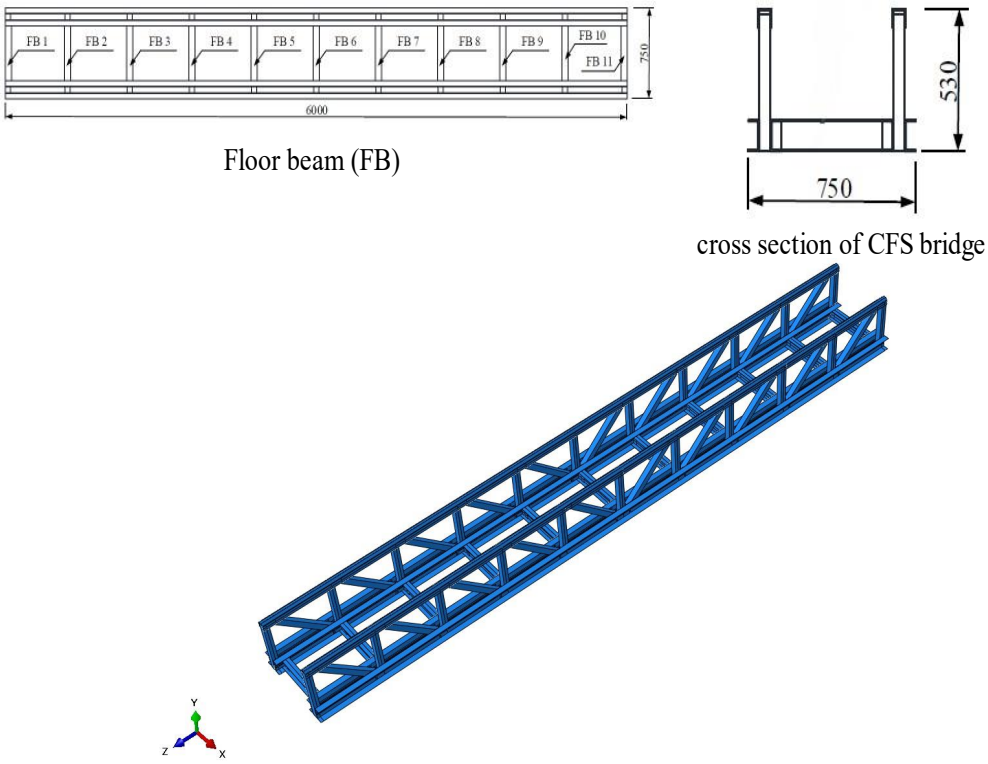

Figure 32 shows FE model of Abaqus Simulation in Assembly.

Meshing

A total of 6 individual parts were modelled and assembled as CFS truss pedestrian bridge in Abaqus. In addition, the parts were partitioned through datum plane to reduce the geometry complexity and perform a smoother mesh. The structured meshing technique was adopted as shown in Figure 33. Each partition of part has been assigned with different mesh size. A mesh that's too coarse can lead to inaccurate results, while a mesh that's too fine can make the simulation computationally expensive and time-consuming. A finer mesh generally

leads to more accurate results but at the cost of increased computational time. A balance must be struck based on the project study requirements. As our main aim of the study is to identify the deflection of bottom chord i.e. main span of CFS bridge the structured meshing with 20mm size was chosen.

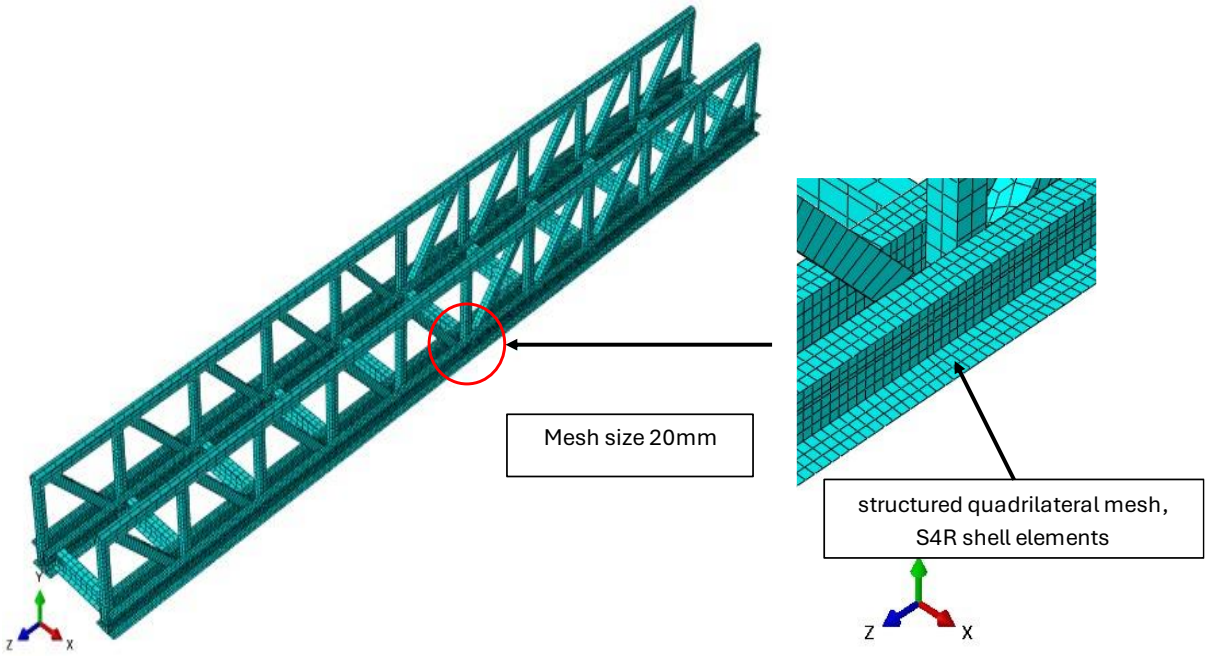

Figure 33 shows FE model Meshing.

Results and Discussion

Deflection Analysis

The results of Abaqus simulation are the represent the deflection and stress distribution response of the cold-formed steel truss bridge under the action of uniformly distributed load at 5kPa [55] onto the top surface of transverse beams for the CFS. Figure 18 represents the deflection of the entire bridge, showing final deflection at the mid-span, where bending effects are most significant. The deflection measured remains within the span /200 permissible limit

30mm, according to the SNZ-HB-8630:2004 [58] design requirements. The main span bottom chord, which experiences predominant tensile forces, shows a steady small deflection pattern, indicating sufficient axial rigidity in vertical members to prevent stretching and failure of the truss structure. Additionally Figure 34 illustrates the transverse beams under a load of 5 kPa, with deflection results displaying a regular load distribution; all maximum deformations remain within allowable limits. Therefore, the transverse beams can carry the applied load and transfer it to the major truss members with minimal deformations. Overall, the analysis confirms that the design of the cold-formed steel truss bridge is lightweight and economical while ensuring structural adequacy for the specified loading.

Figure 35 (Graph) represents the result of this setup, the deflection shown in graph displays a symmetrical distribution of vertical displacement along the bridge span, which is characteristic of beams or truss members under uniformly distributed loading. The deflection values are nearly zero at the fixed ends (0 mm and 6000 mm) due to the applied boundary conditions, while the maximum downward deflection of approximately -0.8 mm occurs at mid-span (around 3000 mm), where bending moments are the highest.

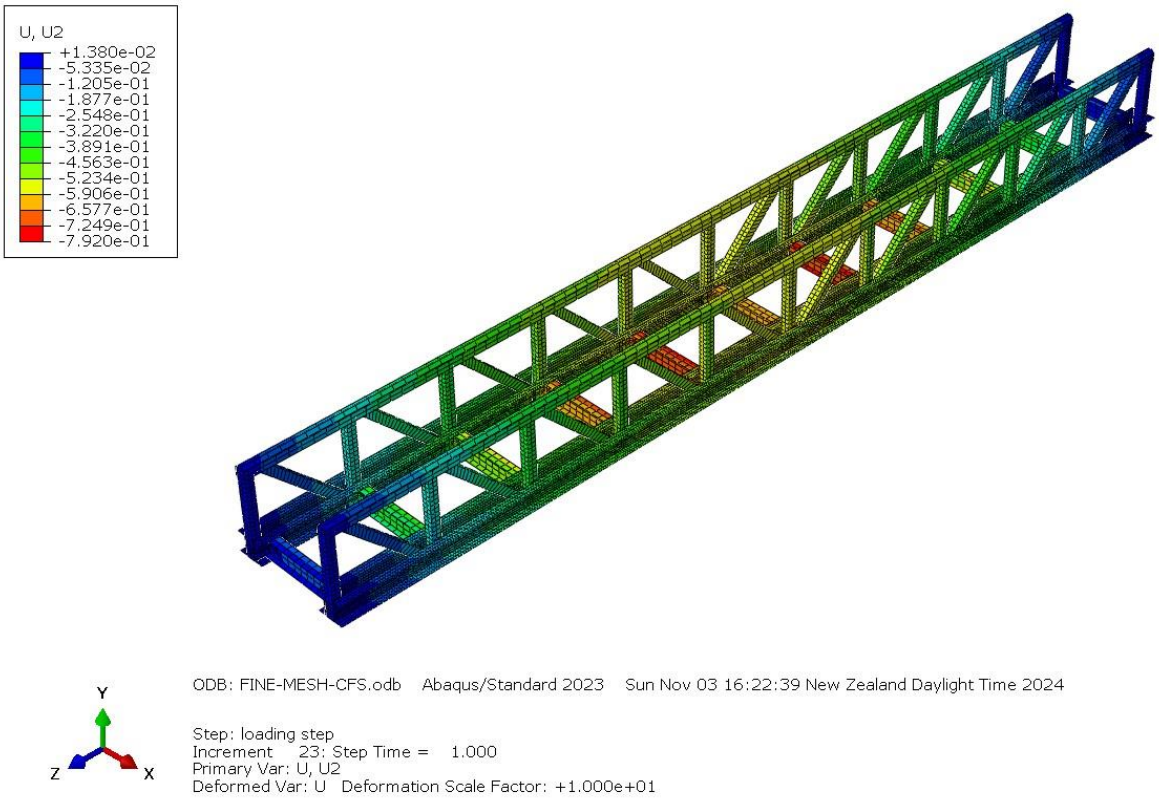

Figure 34 shows final deflection of bridge.

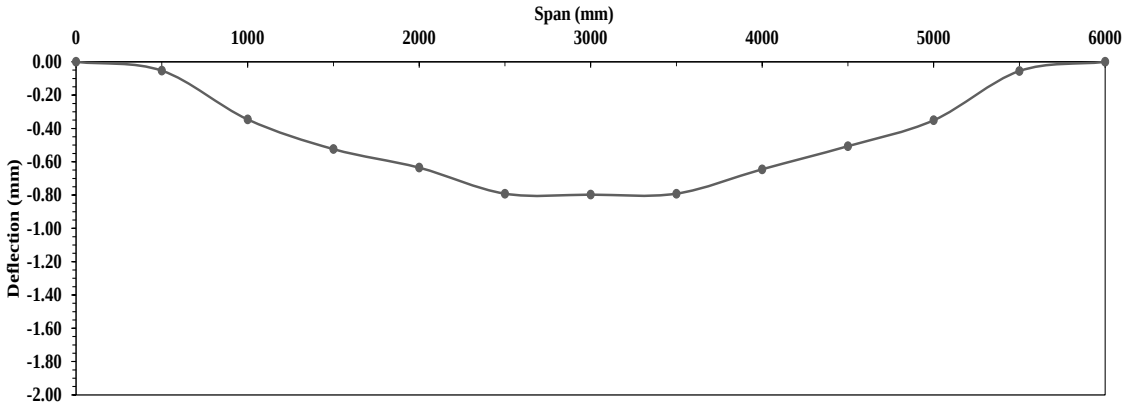

Figure 35 shows symmetrical distribution of vertical displacement along the bridge span.

Stress distribution analysis

The finite element analysis (FEA) of the cold-formed steel pedestrian bridge was conducted in Abaqus to evaluate stress distribution under simulated loading conditions. The material, characterized by a yield stress of 478 MPa was modeled with detailed truss members

and L-angle connectors. Results from the Von Mises stress analysis indicate a maximum stress of 77.14 Mpa refer Figures 36,37, observed at a critical L-angle connection and Figure 38 shows the high stress concentration around connector region. Localized analysis reveals significant stress intensification at the L-angle connector, with maximum stress 77.14 Mpa near the load transfer region (bolts). The stress concentrations are attributed to geometric discontinuities and load-bearing effects, necessitating careful design optimization to mitigate fatigue risks. Despite these concentrations, all stress values remain well below the material's yield limit, providing a safety factor of approximately 6.2. This study demonstrates the structural integrity of the design while emphasizing the importance of connection detailing for long-term performance. Further validation through physical testing and optimization of connector design is recommended to ensure resilience under cyclic loading. We need to optimize the material thickness or layout.

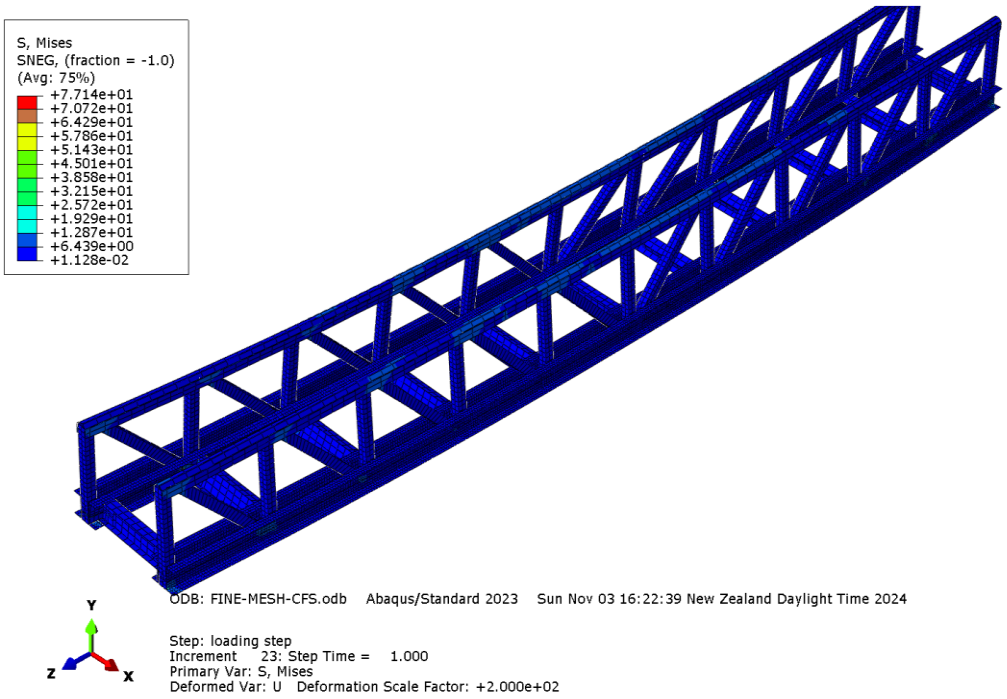

Figure 36 shows Results from the Von Mises stress analysis of bridge.

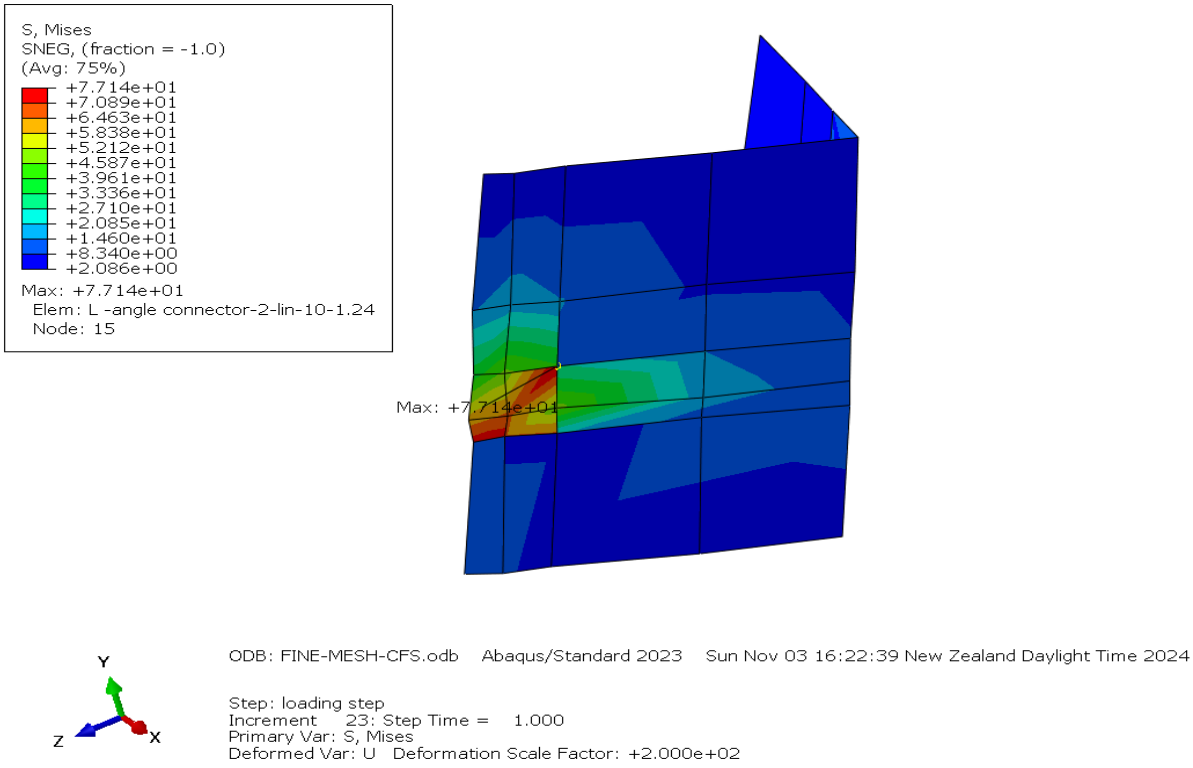

Figure 37 shows Results for the maximum Von Mises stress at clamps near connectors.

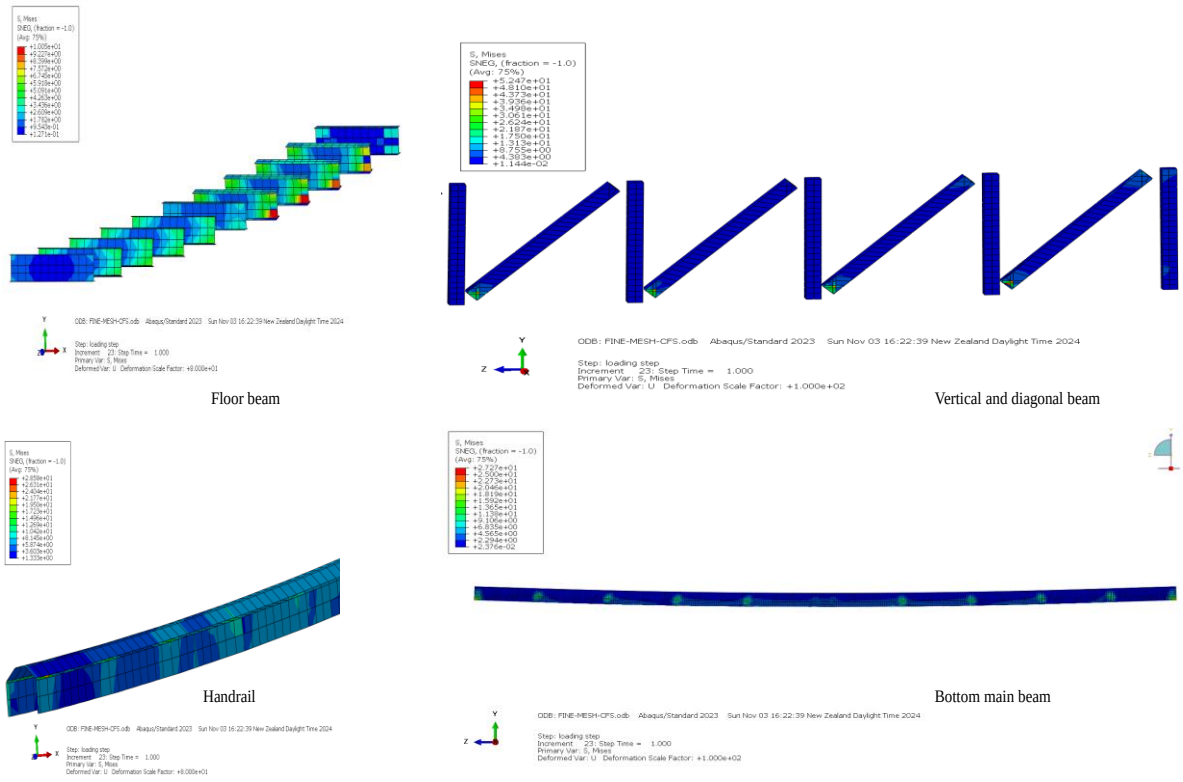

Figure 38 shows the connector region where high stress concentration was observed in different parts of assembly.

4.4.2 Effects of a 7.2 - Meter Span on Deflection and Stress in a Panel Truss Cold-Formed Steel Pedestrian Bridge

Introduction

Modular bridges are prefabricated, portable truss bridges that were first developed during World War II [59] . They were designed by British engineer Sir Donald Bailey to help Allied forces quickly and efficiently transport troops, vehicles, and supplies over rivers. They are employed in a variety of applications, including military operations, disaster relief efforts, and remote areas where access to traditional construction materials and equipment is limited. Modular bridges continue to be an important technology for the construction of both permanent and temporary bridges (temporary crossings while long-term structures are being built). They are also utilized as a quick replacement for bridges that have been destroyed by earthquakes, floods, or storms. For example, they were used to replace a bridge that collapsed in Merritt, British Colombia due to a flood in 2021 and the bridge that divides Lafitte, Louisiana, and Jean Lafitte Salinas which was damaged in the aftermath of Hurricane Ida in 2021 [59]. The modular bridge construction relies on the concept of the assembly of a series of modular shear panels connected using clamps through bolts at the top and bottom chords of two successive panels. The inherited free-rotation connections of the through bolts assembly conform to the regular truss analysis of the bridges assuming pinned connection between members. The design of modular bridges is strongly conditioned by a set of parameters, namely geometric requirements (span, number of lanes, width of the deck), assembly (topographical conditions and accessibility of the margins), transport, connections, and modularity, among others. The deck width is standard and depends on the number of lanes: 1 lane normal width - 3.15 m; 1 lane extra width - 4.20 m; 2-lanes - 7.35 m. Since modular bridges had their backgrounds in the military area, the main guidelines to design are also military. The Trilateral Design and Test Code for Military Bridging [60] developed by the US, UK and Ger many, provides

recommendations on the various parameters that should be considered in the design of temporary bridges. This review of modular bridge concepts has been incredibly helpful in considering the design of modular bridges using cold-formed steel (CFS) sections. The use of modular CFS sections could offer innovative solutions for quick assembly, easy transportation, and effective adaptation to diverse topographical and logistical conditions. Moving forward, a key focus will be on evaluating deflection and stress distribution within CFS sections to ensure structural integrity and optimal performance in modular bridge applications.

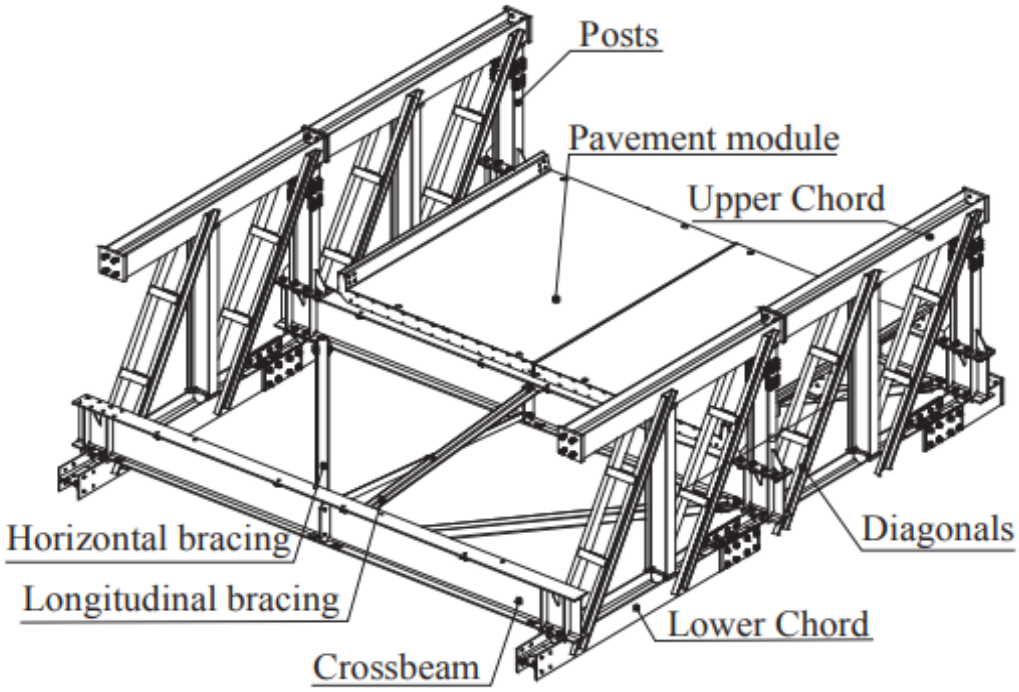

Figure 39 shows cross-sections of modular bridge [59].

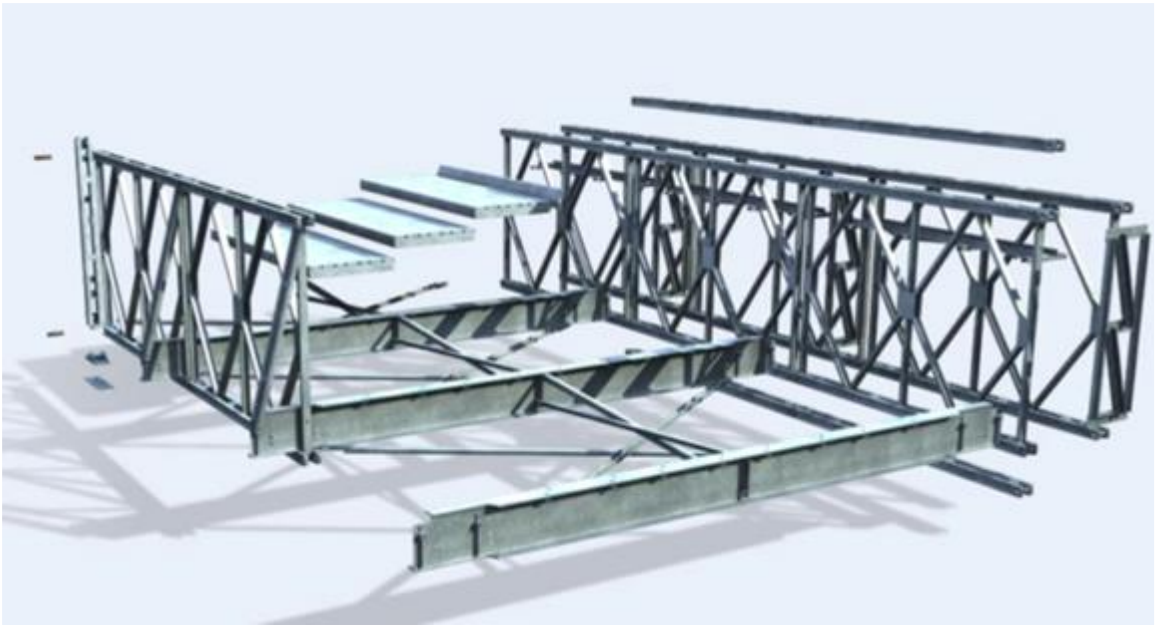

Figure 40 shows Bailey Bridge Model by Mabey (Mabey Bridge, 2019) [60].

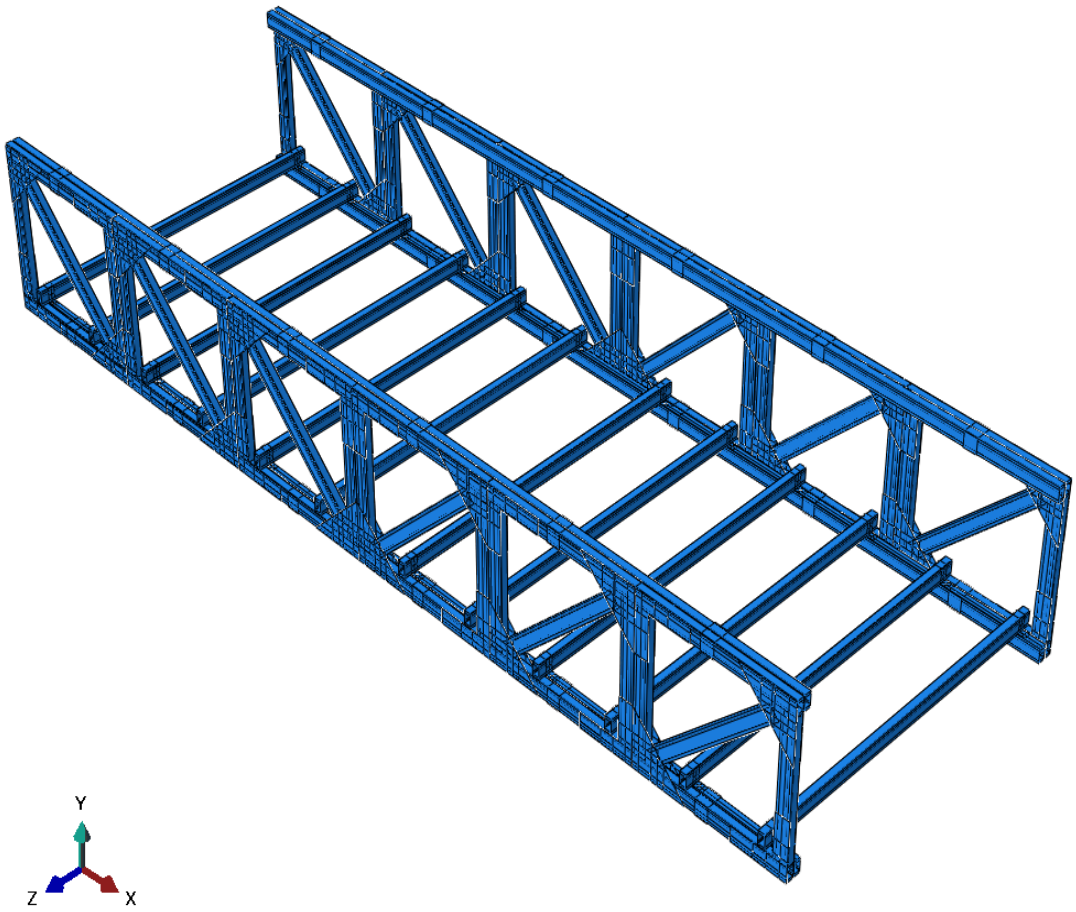

Figure 41 shows the design and geometry of the modular panel truss bridge model.

Figure 41 shows the model of Modular panel truss bridge and its configuration in terms of its geometry. The theory in Bailey bridge, utilized in most cases in terms of its application in both military and emergency rescue scenarios, was developed specifically with a focus towards its modularity, quick installation, and efficiency in terms of its structure. Its use of such philosophies in its realization grants ease in assembling and adaptability in field settings. An in-depth discussion of individual items utilized in its bridge model can be seen in Table 4, with a discussion of its use of materials and dimensions in terms of its cross-sectional shape. Overall dimensions for its bridge model include a 7.2-meter long, 2.5-meter wide, and 1.2-meter-high configuration, modelled for computational analysis.

Model Parts

The modular bridge parts were created in 3D modeling space, deformable shell and later extruded to specific required dimensions for different parts. The parts used in pedestrian bridge are mentioned in table - 4 with dimensions and follows with Figure-42.

Table 4 shows type of parts used with length and thickness in mm.

Part	**Section application**		**Length (mm)**	**Thickness (mm)**
FS-90195N	Horizontal	Panel Assembly	1200	1.95
FS-90195N	vertical		1000	1.95
FS-90195N	Inclined		1250	1.95
FS-90195N	Main Span	Top and Bottom chord Main span	7200	1.95
FS-90195N	Transverse		2500	1.95

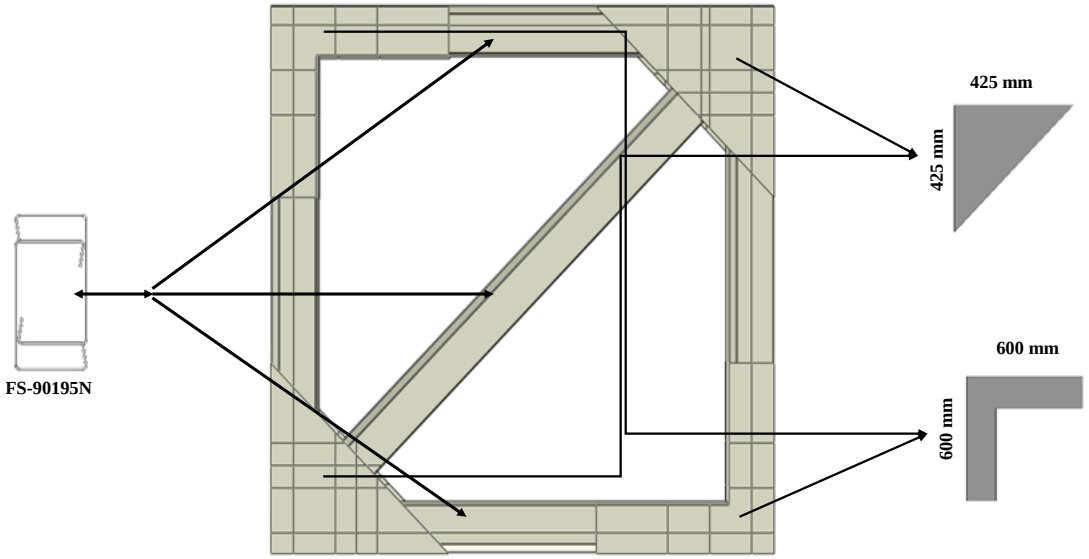

Figure 42 shows Panel components.

Material properties

The data used in the FE models corresponded to the 'static' values of the material properties obtained from the coupon test conducted by Yecheng Dai [61] for section 500N and coupon number 1.95mm- mean with the yield stress of 639.4 MPa and the elastic behaviour was defined using a Poisson's ratio of 0.3 and with a Young's modulus (E) of 203 Gpa.

Assembly

This bridge is a modular truss structure composed of several connected structural members with plates forming each panel. It consists of two lateral trusses with vertical, diagonal, and horizontal members; therefore, it is classified as a Pratt truss, which is very effective in terms of load distribution. The bottom cord of the CFS pedestrian bridge here is created by a nested section with additional square clamps to give it better stability. The transverse floor beams are connected by U- clamps with both bottom main span beam and panels, while distributing the applied load across the structure. Top main span

beams on upper chord of panels act as handrails and provide safety for users. This modularity also allows for prefabrication, easy on site assembling while maintaining the integrity and functionality of structure refer Figure 43.

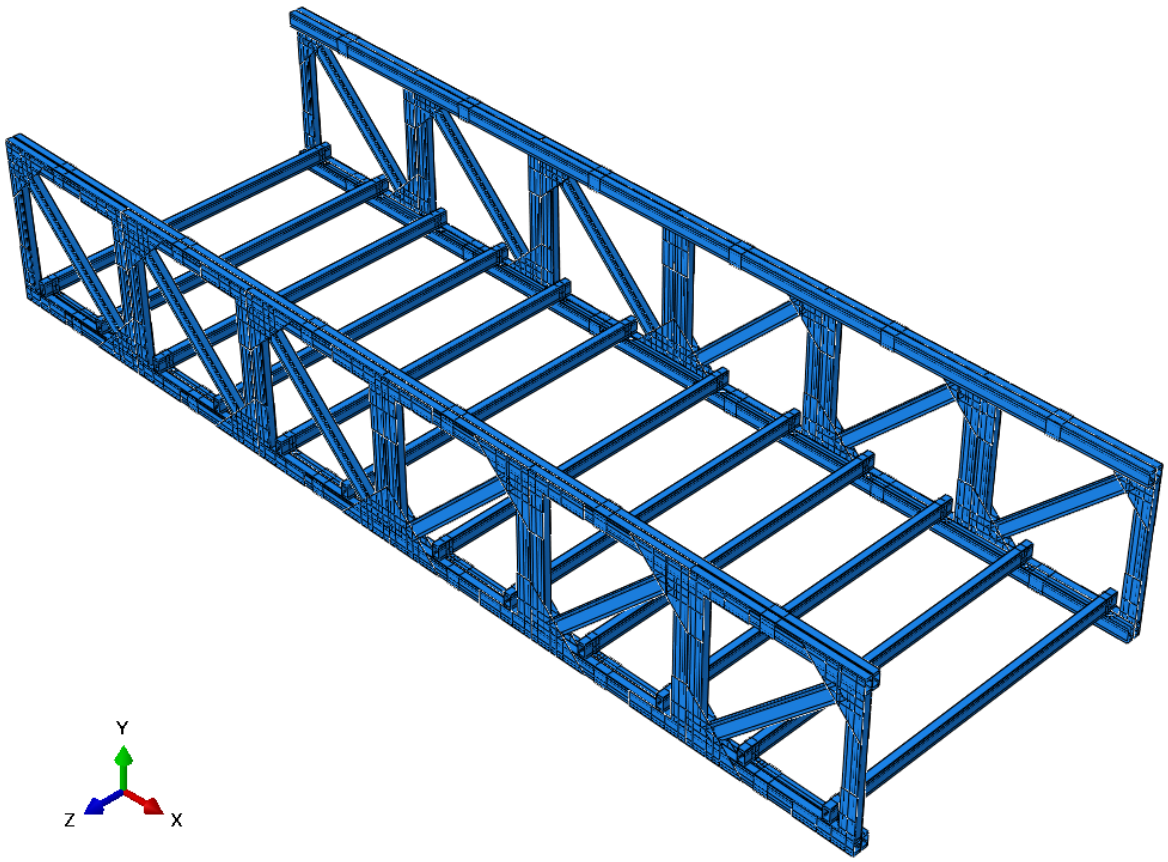

Figure 43 shows Assembly of modular bridge.

Meshing

The structured meshing was adapted where a systematic approach has been followed and well-defined grid pattern for finite element analysis is realized refer Figure 44. Its various components were divided by datum planes to simplify these intricate geometries and to assist the process more efficiently. A 20mm mesh size was used for assembly balancing the trade-off between computational efficiency and accuracy of results. A fine mesh allows to capture stress

concentration and deflection behavior in important areas. The meshing process further allowed the consistency and quality of elements in the front bench to minimize simulation errors.

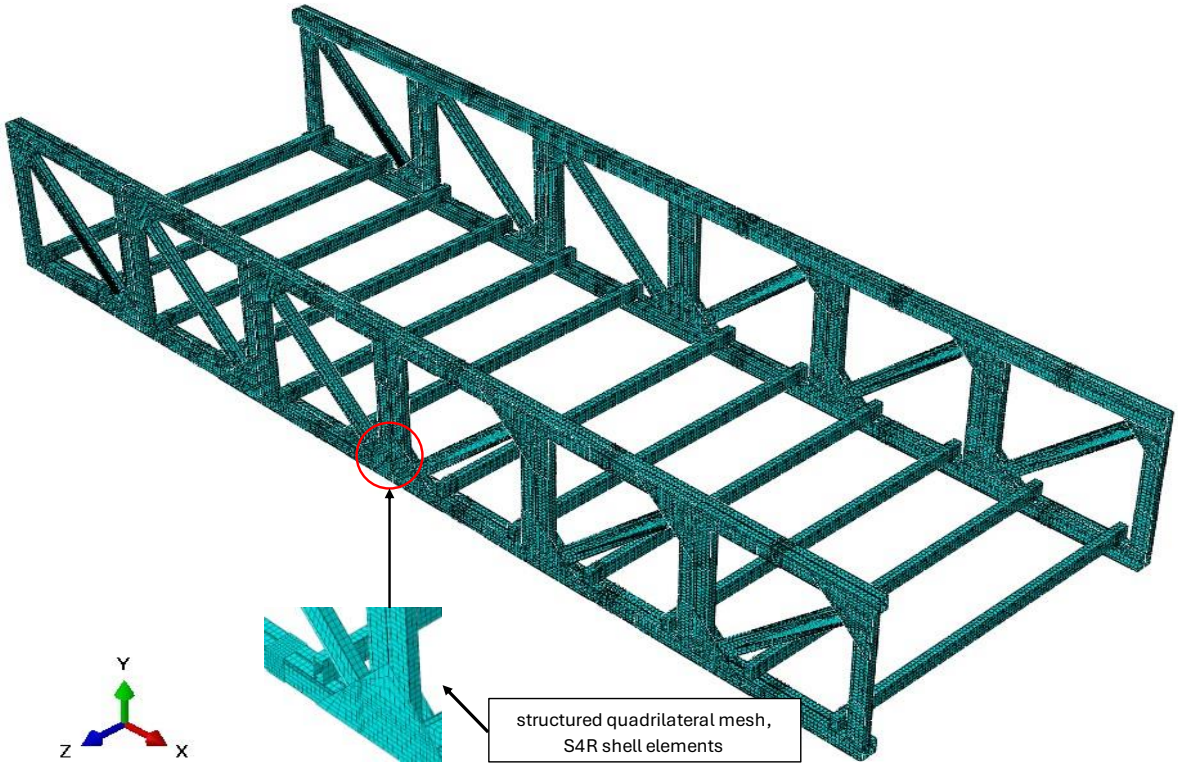

Figure 44 shows structural meshing of assembly.

Results and discussion

Deflection Analysis

The deflection analysis shown in Figure 45 represents the deformation under a uniformly distributed load of 5 kPa applied to the top surface of the transverse beams. The bridge has a span of 7200 mm and a width of 2500 mm. According to the deflection limit criteria of span/200, the maximum allowable deflection for this structure is:

$$\text{Maximum allowable deflection} = \frac{\text{span}}{200} = \frac{7200}{200} = 36\text{mm}.$$

From the deformation results in the Figure 45, the maximum deflection observed is approximately 65.88 refer Figure 45, 46 at mid transverse beams, which exceeds the allowable limit of 36 mm.

Recommendations for Mitigating Excess Deflection:

To address excess deflection in the modular bridge, several measures can be implemented to enhance its structural performance. Increasing the cross-sectional area of the transverse and longitudinal members by using thicker or larger CFS sections will improve stiffness. Critical members, especially the transverse beams, can be reinforced with stiffening elements such as doubler plates to minimize deformation. Utilizing a higher grade of steel will enhance resistance to deformation. By adopting these provisions, may be deflection can be reduced to comply with allowable limits, ensuring the structural integrity and serviceability of the CFS pedestrian bridge under the applied loading conditions.

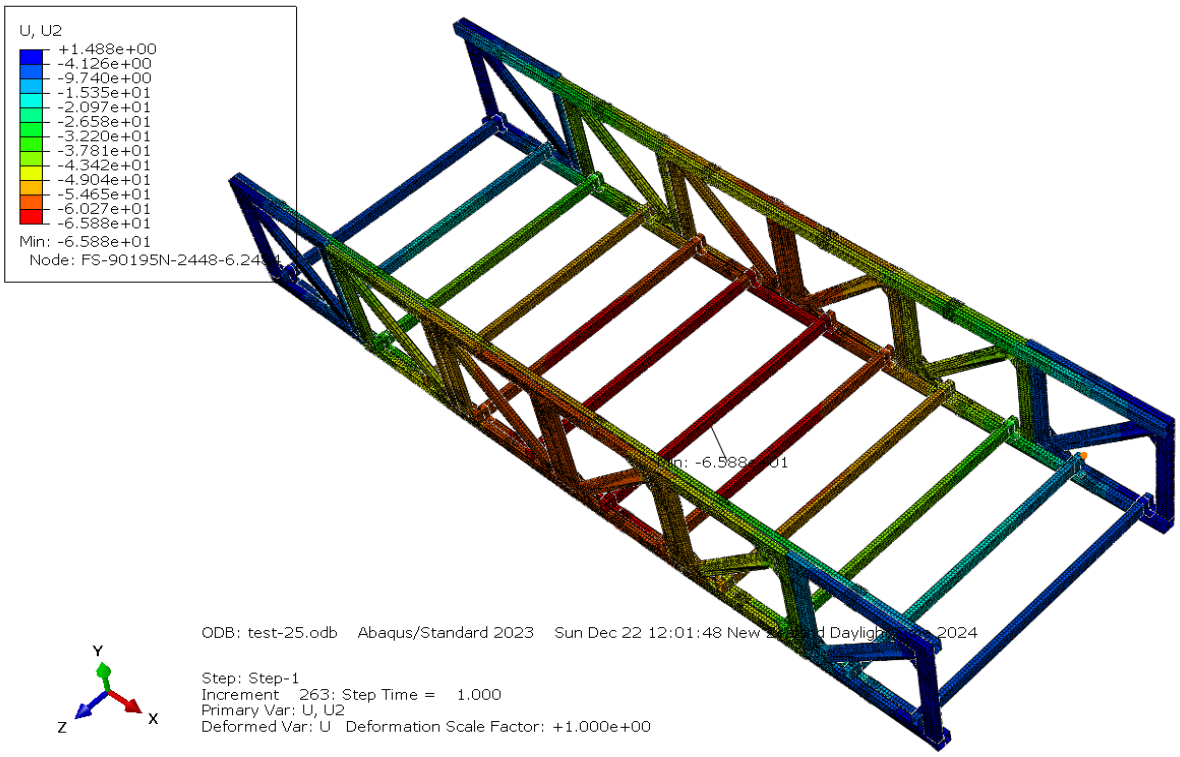

Figure 45 shows final deflection of modular panel bridge.

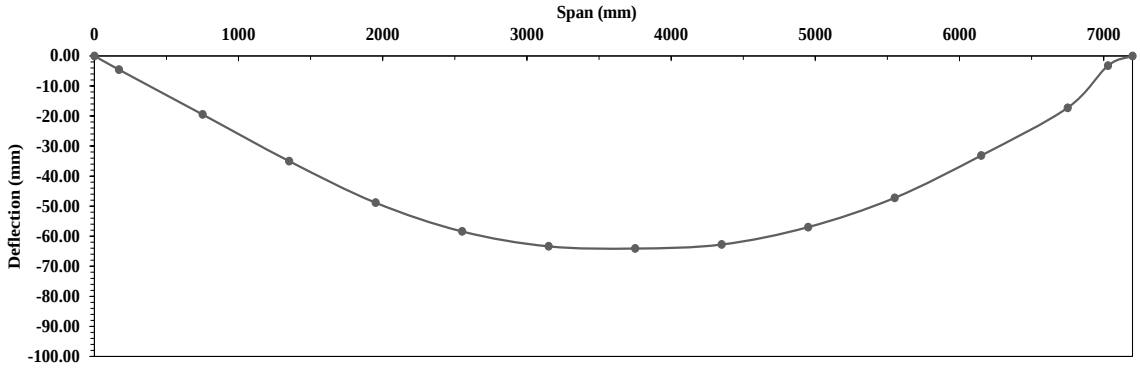

Figure 46 shows symmetrical distribution of vertical displacement along the bridge span of modular bridge.

Stress distribution

The following is the stress distribution analysis corresponding to the CFS modular pedestrian bridge for the specified loading conditions; the yield stress of the material is 639.4MPa. It can be seen from the von Mises stress refer Figure 47, contours that the maximum value is 639.4MPa, concentrated in just few elements, which is mainly concentrated around the bottom of both resting ends of bridge and around pin connector of panel plate where load transfer and high stress are expected. Figure 48 shows the high stress concentration around connector region.

Recommendations for Mitigating Excess Stress:

In this study, boundary conditions were applied to simulate the bridge being supported at both ends. The selected support area was 50 mm × 50 mm on each bottom support. This small contact area resulted in high localized stresses, as indicated by the red contours near the supports. To mitigate this, the actual structure could incorporate a larger support area of 300 mm × 50 mm at both ends. Additionally, increasing the thickness of the assembly from 1.95 mm to 3 mm, as well as optimizing the spacing and number of pin connectors through trial runs of the model, can help reduce stress concentrations. These adjustments would significantly

lower critical stress levels, enhancing the structural integrity and functional performance of the bridge.

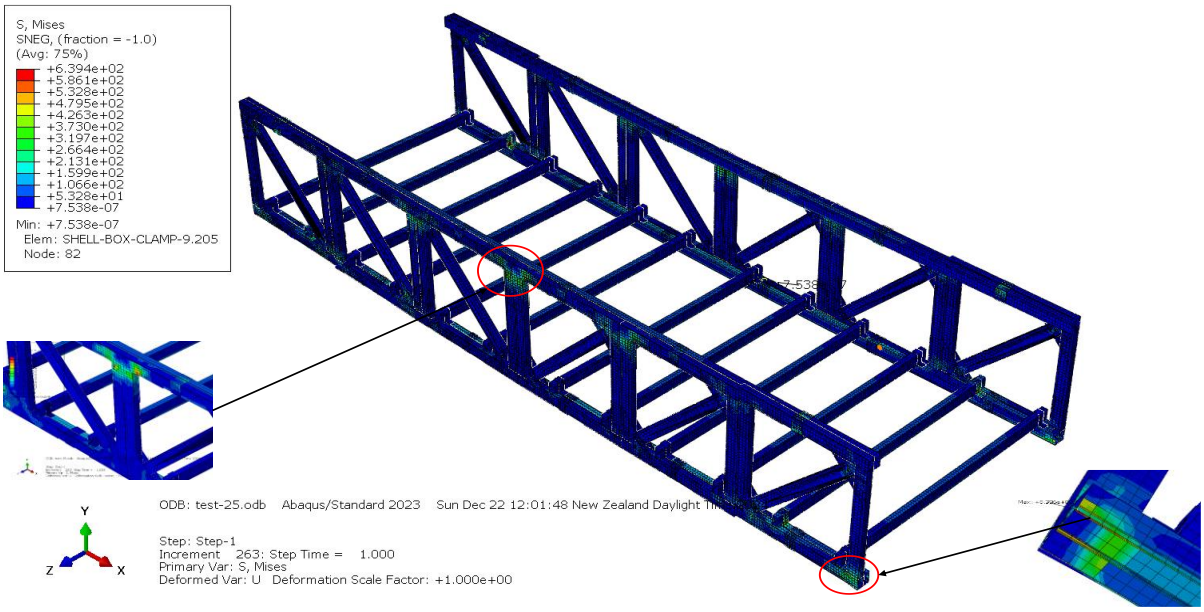

Figure 47 shows Results from the Von Mises stress analysis of modular bridge.

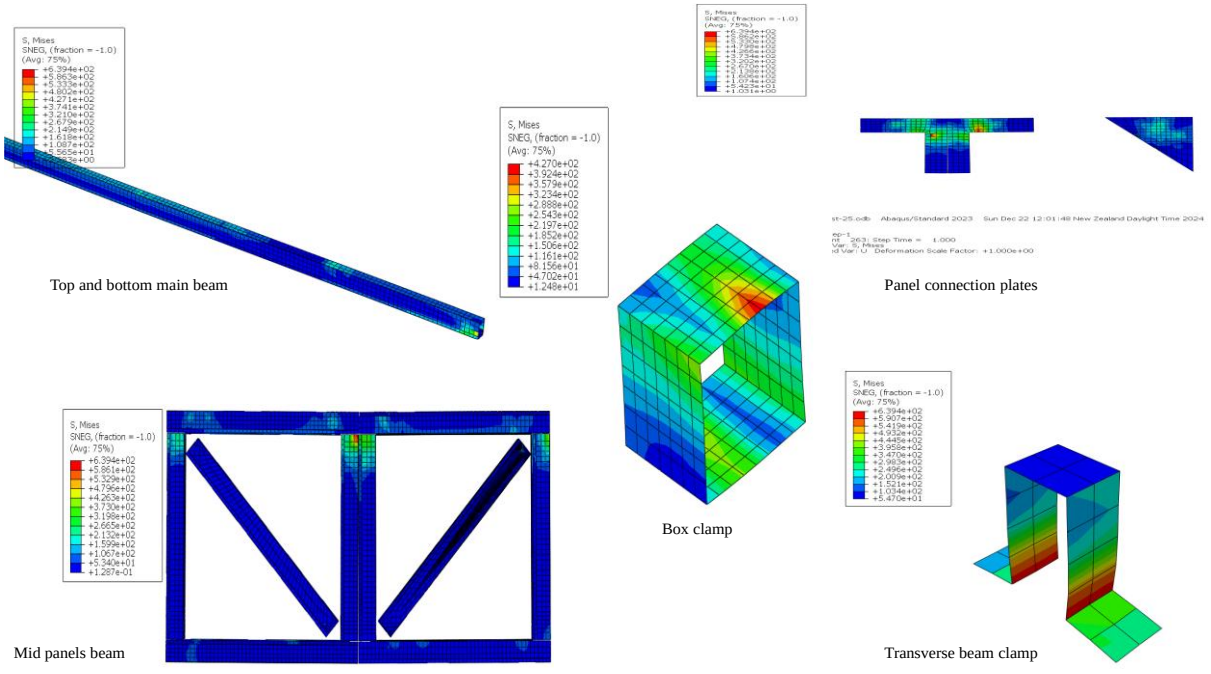

Figure 48 shows the connector region where high stress concentration was observed in different parts of assembly.

4.4.3 Effects of a 6.7 - Meter Span on Deflection and Stress in a Box Truss Cold-Formed Steel Pedestrian Bridge

Introduction

A box warren truss similar as shown in Figure 49, 50 was selected for the bridge design because the design is based on structural efficiency, stability. According to studies, closed section designs such as box trusses provide better torsional stability than open trusses and much less susceptible to local buckling and connection failures [6] and failure mechanisms studies on small span pedestrian truss bridges made of CFS indicate that considerable improvement in structural integrity can be achieved by using built-up box sections since they help mitigate connection failures and local buckling problems[6], [10]. The box truss bridge configuration was selected for the pedestrian bridge as a structure that would ensure better structural and functional efficiency besides minimal materials used and durability over time.

Figure 49 Shows the Box warren truss bridge layout [62].

Figure 50 Shows the Box truss bridge product by Canam Bridges USA [62].

Model parts

The CFS warren box truss bridge parts were created in 3D modeling space, deformable shell and later extruded to specific required dimensions for different parts. The parts used in pedestrian bridge are mentioned in table-5 with dimensions and follows with Figure-51.

Table 5 shows type of parts used with length, thickness in mm and their application.

Part	Section application	Length	Thickness (mm)
FS-270115	Transverse	3000	3
FS-270115	Truss Vertical sections	2500	3
FS-270115	Truss Inclined sections	2700	3
FS-270115N	Main Span	6700	3

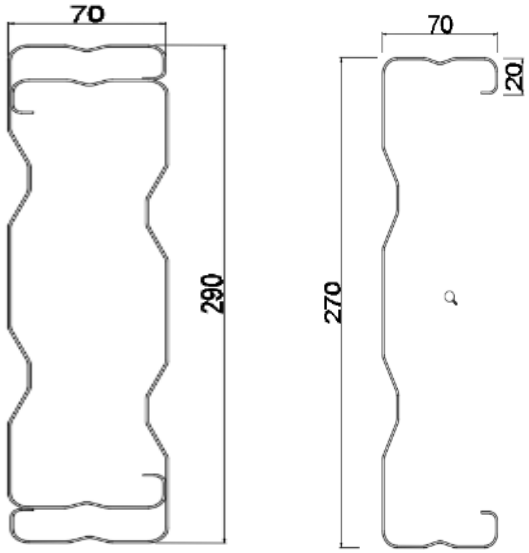

Figure 51 shows geometry and dimensions used for CFS Box truss bridge.

Material properties

The data used in the FE models corresponded to the ‘static’ values of the material properties obtained from consulting the manufacturer and section thickness is 3mm- mean with the yield stress of 550 MPa and the elastic behaviour was defined using a Poisson’s ratio of 0.3 and with a Young’s modulus (E) of 203 Gpa.

Assembly

The assembly of the box truss bridge follows a structured and sequential approach to ensure efficient construction as shown in Figure 52. It utilizes a box truss configuration, where the main structural elements form interconnected triangles to efficiently distribute loads. The through-truss design places the primary truss members above the deck, increasing lateral stability. The truss system incorporates diagonal and vertical post, preventing lateral deflection. The deck is supported by floor beams spanning between the lower chords of the truss, ensuring uniform load transfer. The top chord is the uppermost horizontal structural element that carries compressive forces, preventing the bridge from buckling under loads. The bottom chord is the lower horizontal member, primarily subjected to tensile forces, helping to resist stretching and maintain the overall structural integrity of the truss. Gusset plates and clamps are interconnected using screw connections to secure the joints, ensuring that the truss members remain rigid and stable under load conditions capable of withstanding axial and lateral forces.

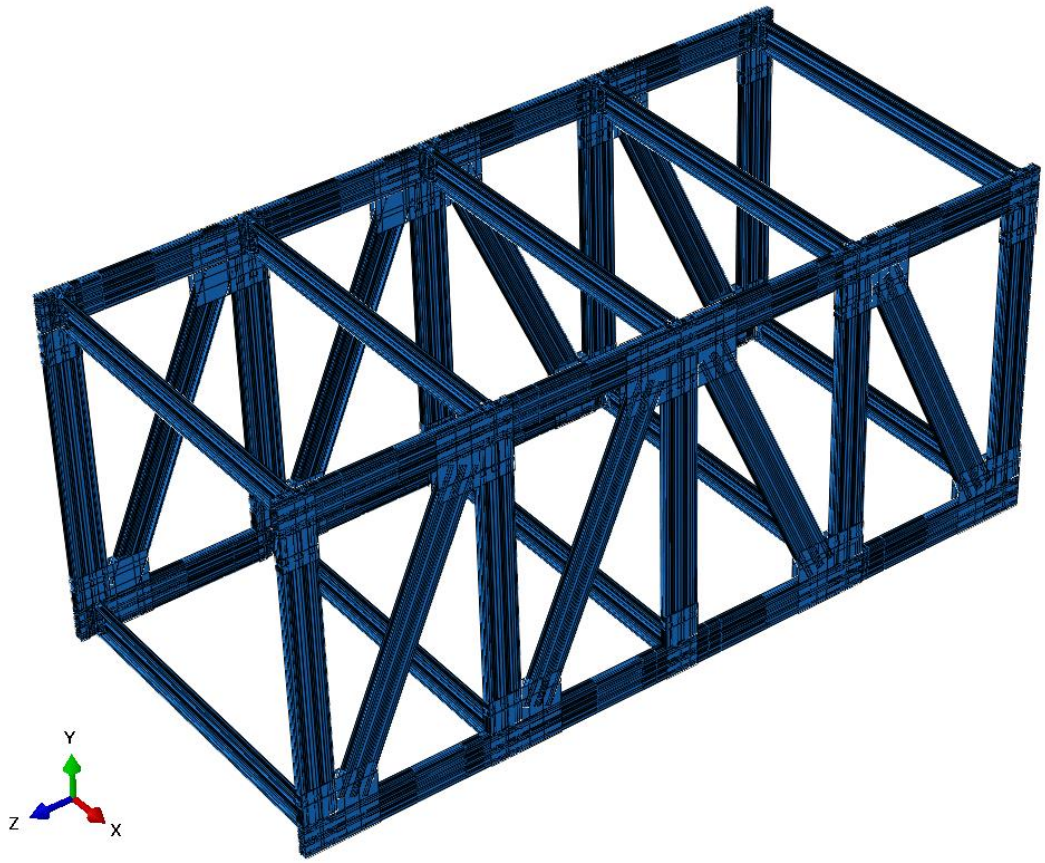

Figure 52 shows the assembly of the CFS box truss bridge model.

Meshing

The meshing technique employed in Abaqus for the cold-formed steel box truss pedestrian bridge entailed the use of structured quadrilateral (Quad) and triangular (Tri) shell elements as shown in Figure 53, which allowed for effective element distribution and improved computational accuracy. The Mesh Controls settings were modified to apply structured meshing, thus minimizing mesh transitions to ensure even stress distribution and improve convergence. A global seed size of around 20 was set to balance computational cost and accuracy, and curvature control was enabled to enhance mesh details in areas with curves and prominent features. In choosing the element types, the model employed shell elements borrowed from the default element library, thus improving computational efficiency in thin-walled structures typical of cold-formed steel sections. To counteract the issues of shear

locking, especially beneficial for elements with high aspect ratios, the reduced integration approach was adopted.

In the applied meshing strategy, quadrilateral shell elements were used mainly in most areas due to their high accuracy and stability; triangular shell elements were used in regions with complicated geometries where structured meshing was not feasible. Linear geometric order was maintained to achieve a balance between computational efficiency and solution accuracy. This ensures that stress concentrations, particularly those that are near joints and load application areas, are well represented, thus improving the credibility of the analytical results on structural evaluation and optimization.

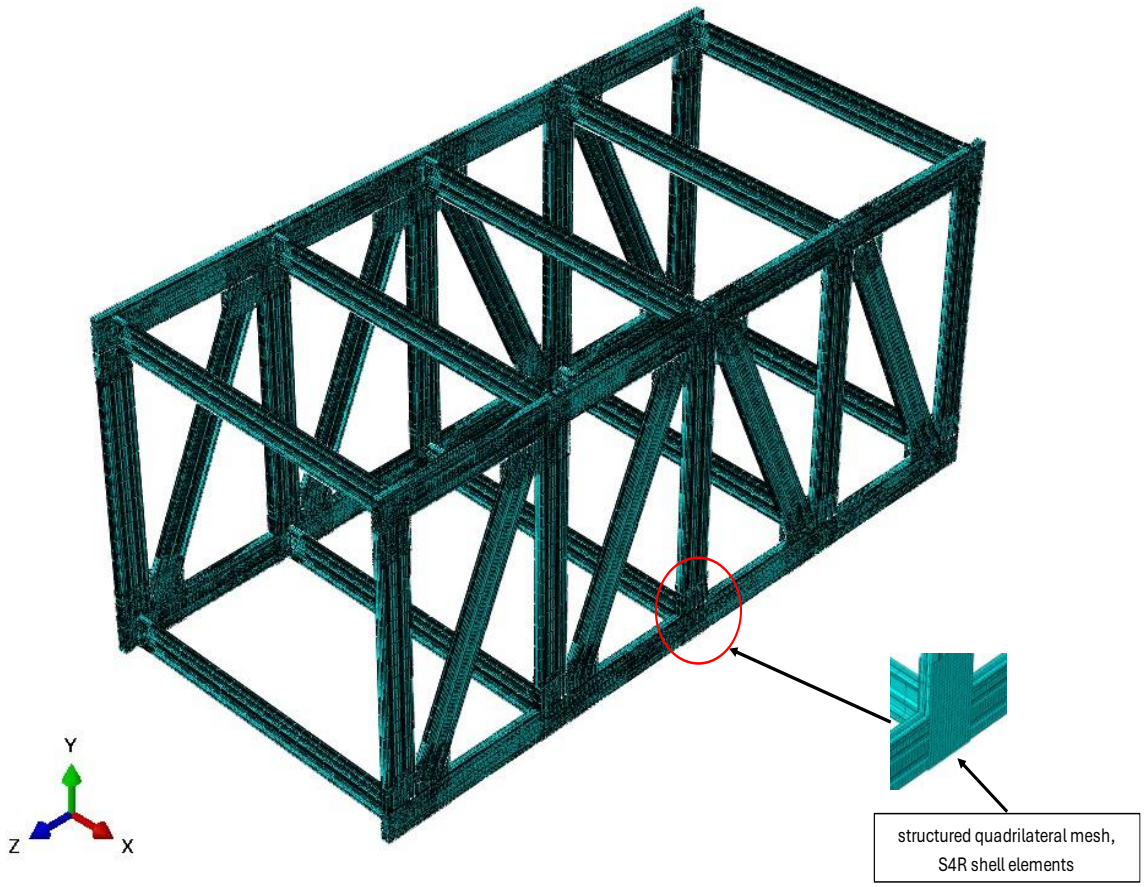

Figure 53 shows structural meshing of box truss bridge assembly.

Results and discussion

Deflection Analysis

The results obtained from the simulation explain the pattern of vertical displacement (U2) across the bridge structure as shown in Figure 54. The maximum deflection observed was -20.30 mm, occurring exactly at the center of the lower transverse member, as expected for the reaction of a simply supported structure under defined loading conditions. Further, the deflection at the bottom chord at the main span attained -2.87 mm, representing a relatively insignificant level of deformation at that point. This observation indicates that the bottom chord resists load well and contributes significantly to the overall stability of the bridge. The pattern of deformation shows a symmetrical deflection pattern, with zero displacement at the fixed ends, thus confirming the correct application of boundary conditions. As expected, the maximum deflection occurs at the bridge center and decreases progressively towards the supports, representing a common response reported in truss and box-section pedestrian bridges when subjected to uniform loading conditions. The measured displacement values fall within the acceptable span/200 criterion [58], thus confirming the structural acceptability for pedestrian use.

The deflection analysis Figure 55,57 and graph 56,58 for transverse beam and main span beam respectively have been included to illustrate the deformation patterns for 5kpa loading condition. The graphical representation provides clear visualization of how bridge structure responds.

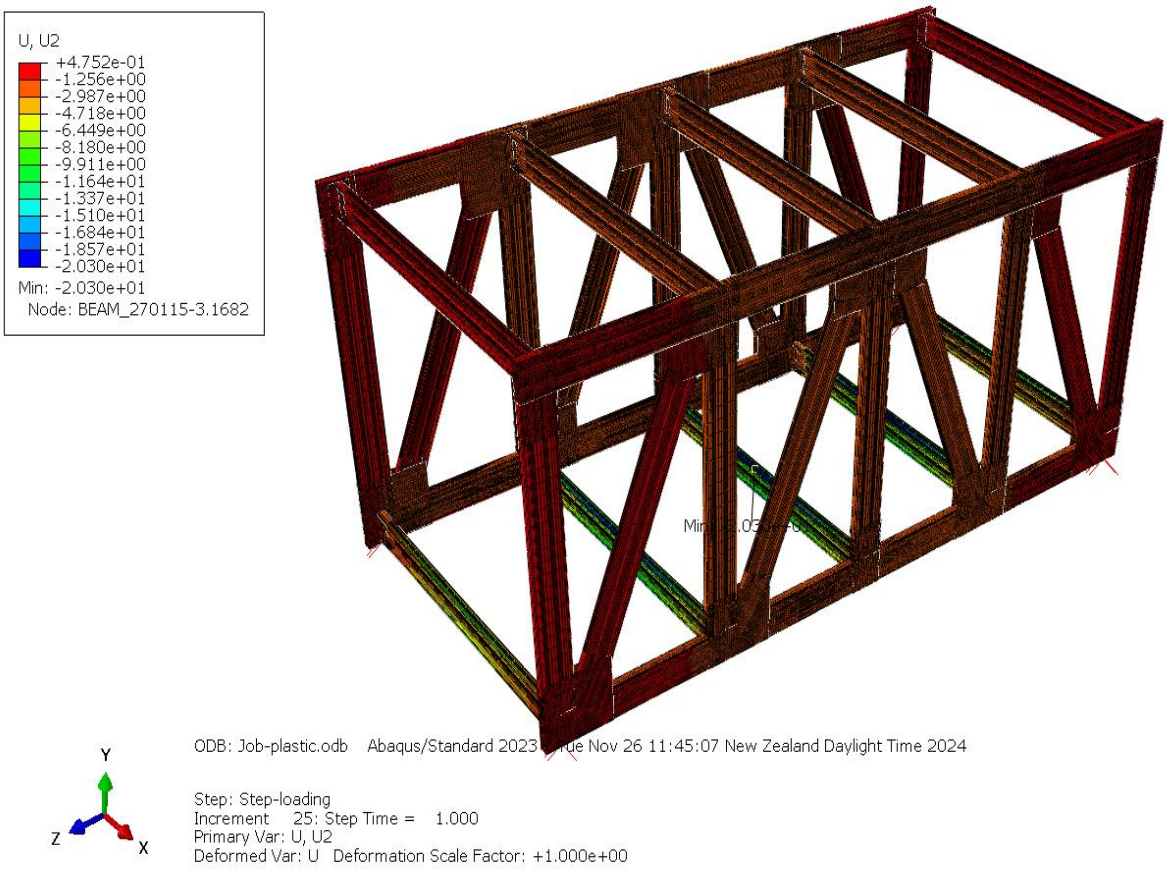

Figure 54 shows final deflection of CFS box truss bridge.

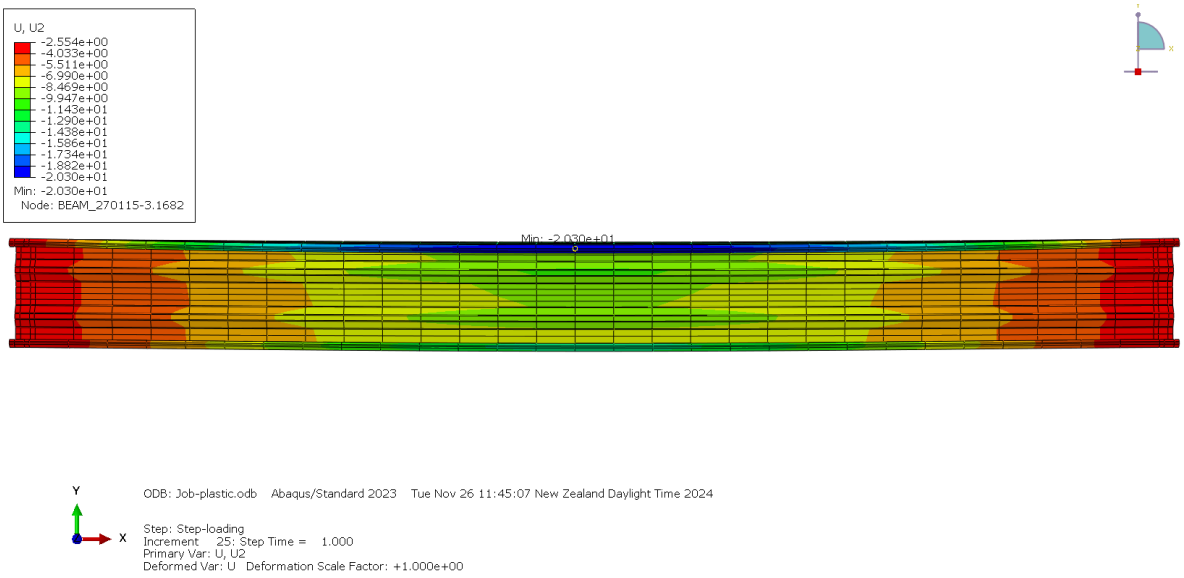

Figure 55 shows final transverse deflection of CFS box truss bridge.

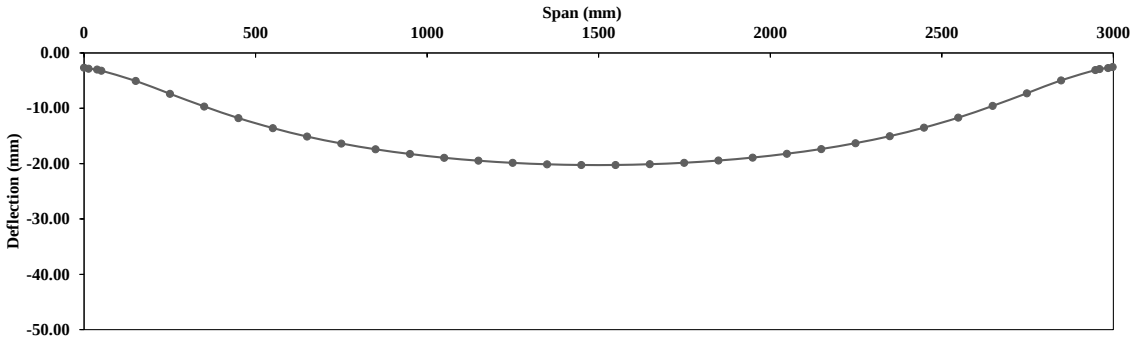

Figure 56 shows symmetrical distribution of vertical displacement along the transverse of box truss bridge.

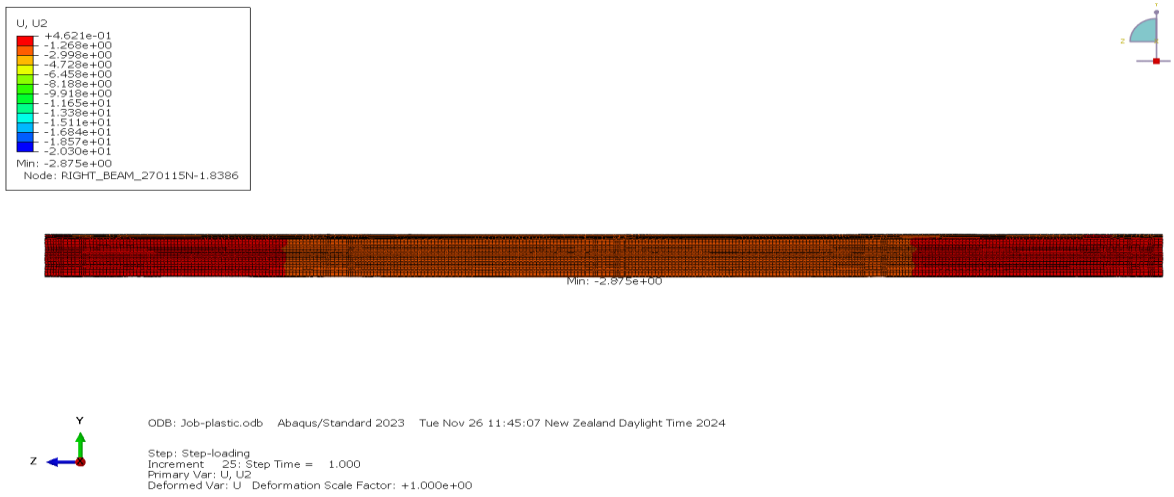

Figure 57 shows final main span beam deflection of CFS box truss bridge.

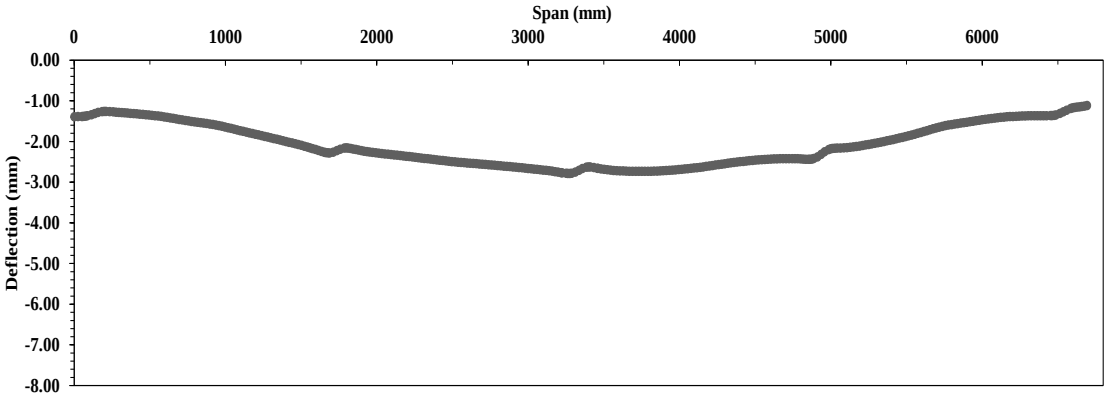

Figure 58 shows symmetrical distribution of vertical displacement along the bottom main beam of box truss bridge.

Stress distribution

The stress distribution analysis, as seen in the simulation results shown in Figure 59 related to the stress distribution of the transverse beam and the main span have been included to explain the load-carrying capacity and critical stress regions of the bridge structure. The von Mises stress contour plot shows areas of stress concentration with maximum and minimum stress as shown in Figure 60, thus providing a view of the structural response to loading conditions. The maximum recorded stress value is 535 MPa, located in the region of the clamps, while the minimum stress reading is 1.041×10^{-2} MPa, indicating an efficient load transfer mechanism across the structure. The stress distribution along the transverse beam supports the fact that the load is efficiently transferred to the main truss members, while the stress distribution across the main span shows expected stress variations, with localized peaks at the points of connection. These plots are of great importance in determining material efficiency, locating potential failure regions, and improving structural design to maximize performance.

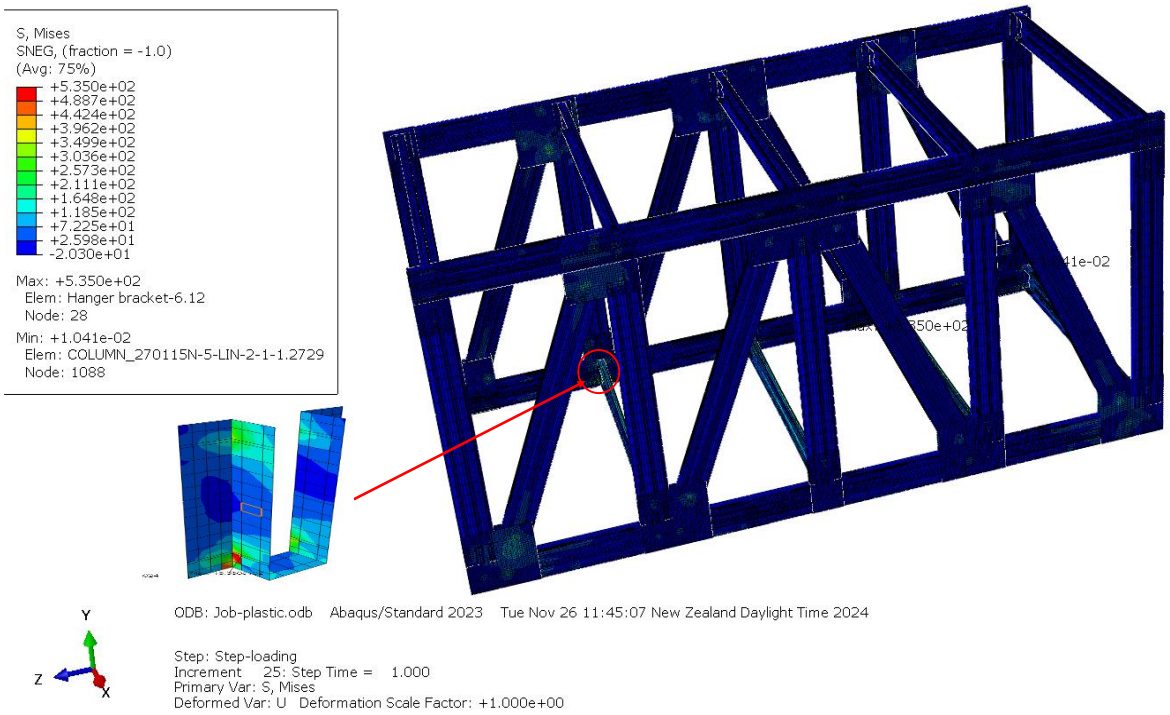

Figure 59 shows Results from the Von Mises stress analysis of CFS box truss bridge.

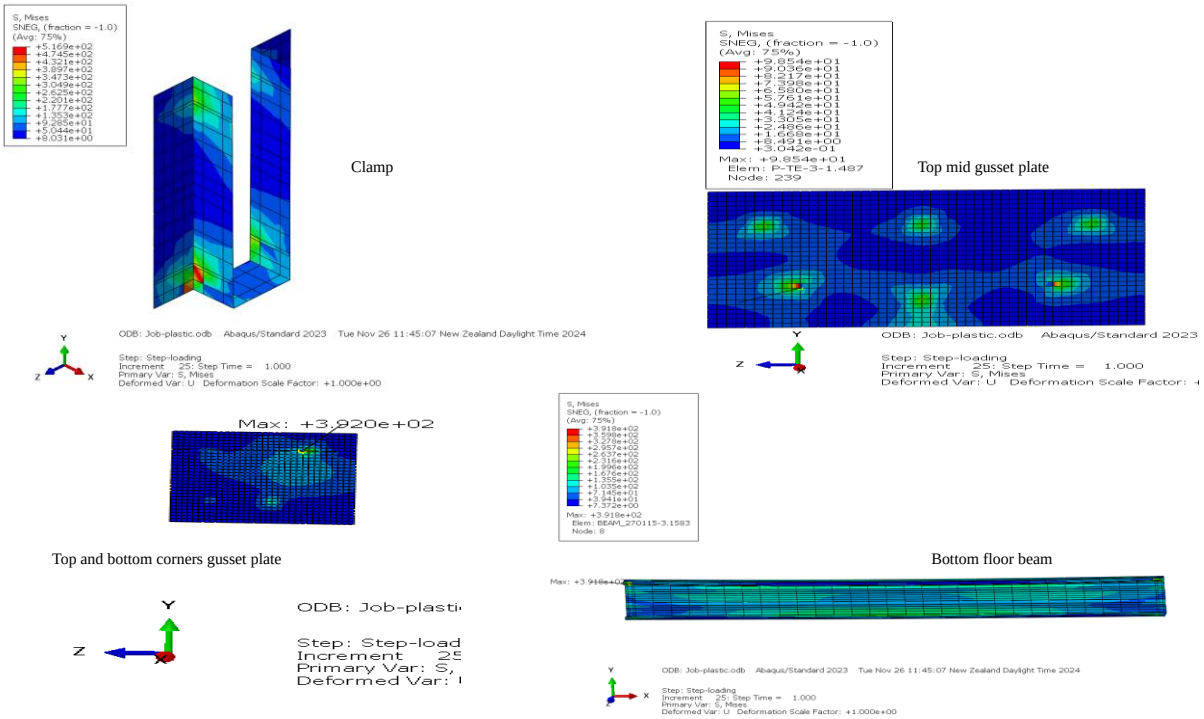

Figure 60 shows the connector region where high stress concentration was observed in different parts of assembly.

Chapter 5 – Alternative CFS bridge design and analysis

5.1 Effects of a 15 -Meter Span on Deflection and Stress in a tub girder Cold-Formed Steel Pedestrian Bridge

Introduction

Figure 61 illustrates a typical twin tub-girder system, labelling its major components. The girder under study in this study is a 15-meter span, 1.2-meter-wide tub girder, which includes a 7.5-meter location for its mid-span support, whose boundary conditions imitate pier-like support. A tub girder is defined as a virtually closed trapezoidal structure consisting of a single cell, made up of an upper and a lower flange, along with two sloping webs that meet—refer to Figure 62. Figure.

The upper flanges have a horizontal box sections system known as the top flange lateral system, while stability in the other direction is attained by using plate diaphragms and cross-frames. In a normal situation, different forms of tub-girders make connections in support points using plate diaphragms, and intermediate points in a span using cross-frames. This arrangement of frames and diaphragms, however, may be modified based on individual requirements. Plate diaphragms can be termed end diaphragms when positioned on abutments and support diaphragms when positioned on intermediate piers. In addition, diaphragms and cross-frames can be termed internal when positioned in the interior of the tub girder and external when positioned for girder connections.

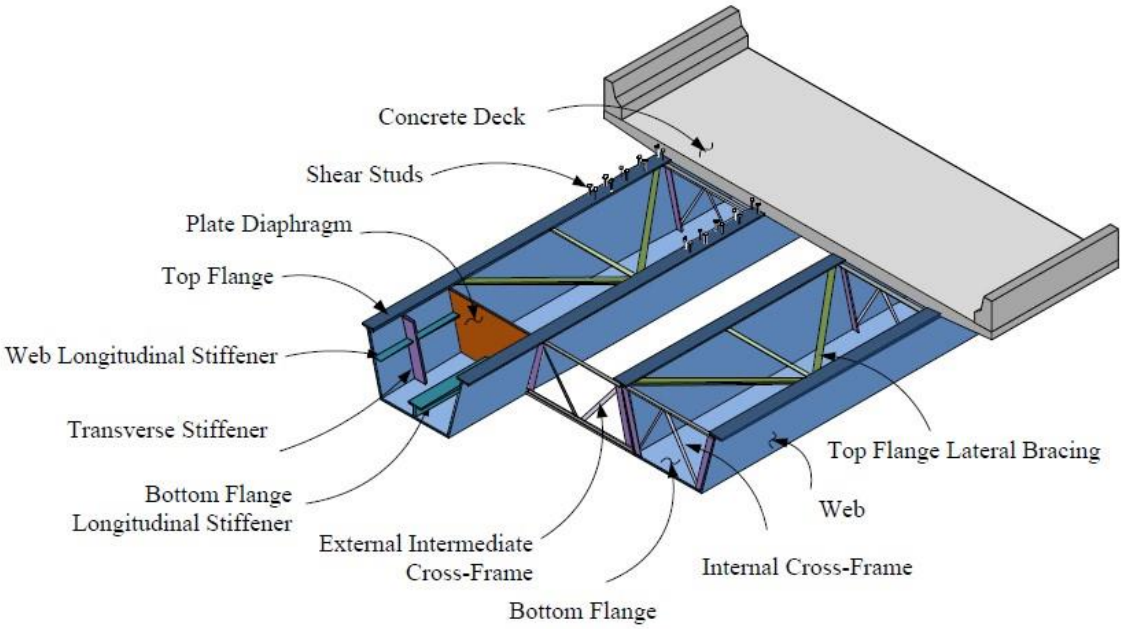

Figure 61 Components of standard tub-girder system [63].

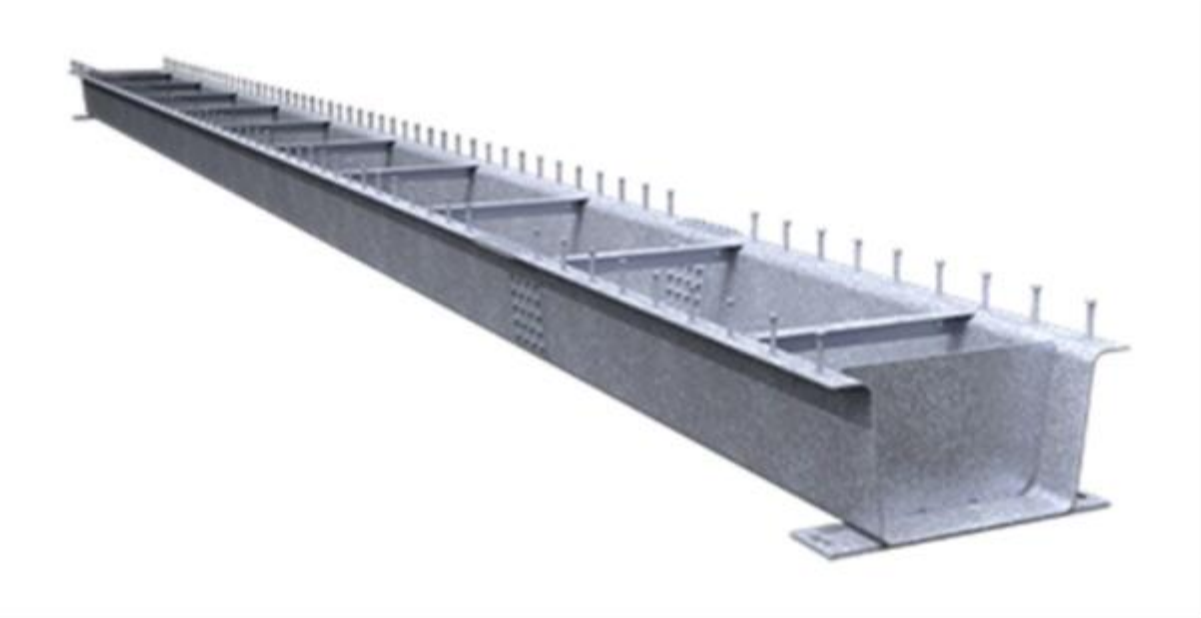

Figure 62 Shows a tub girder prototype by Valmont structures [64].

Figure 63 Shows tub girder bridge under construction in Milwaukee, WI, USA [63].

Model parts

The CFS tub girder bridge parts were created in 3D modeling space, deformable shell and later extruded to specific required dimensions for different parts. The parts used in bridge are mentioned in table-6 with dimensions and follows with Figure-64.

Table 6 shows type of parts used with length, thickness in mm and their application.

Part	**Section application**	**Length (mm)**	**Thickness (mm)**
U-Tub girder	Girder- web, Flange	15000	3
Box section	Top flange lateral (Brace)	1200	3
Top Plate	Deck	15000	3
End-Support plate	Sole Plate	1000	3

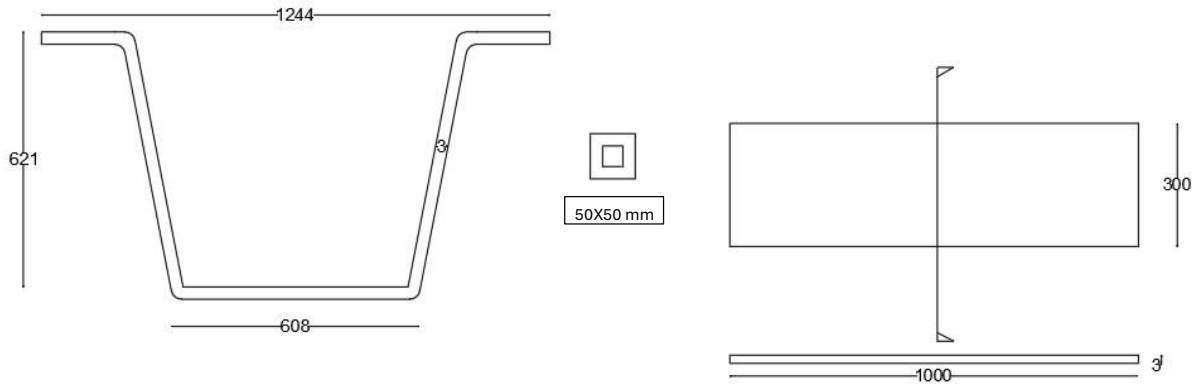

Figure 64 shows geometry and dimensions used for CFS tub girder bridge.

Material properties

The data used in the FE models corresponded to the 'static' values of the material properties obtained from consulting the manufacturer and section thickness is 3mm- mean with the yield stress of 550 MPa and the elastic behaviour was defined using a Poisson's ratio of 0.3 and with a Young's modulus (E) of 203 Gpa.

Assembly

The tub girder is trapezoidal in shape as shown in Figure 65. The girder contains a lower flange, sloping sides, and a pair of upper flanges. The individual span section of these is constructed and subsequently combined using bolting in a process of forming a long span girder. Steel plates first undergo manufacturing, cutting and forming in a process of producing web and flange sections. The girder can have stiffeners in its web for additional stability but not included in current simulation. In its construction, its tub girders can be propped in some points, such as in support in abutments and in mid-span pier support, for a correct spread of loading. The system is secured using a system of a top flange lateral bracing system, which is a horizontal truss system for connecting upper flanges. The internal diaphragms facilitate in loading transfer and strengthen the system. The process of constructing it is a process of

inserting and securing each girder in a subsequent process, followed by adding a system of a bracing and deck component.

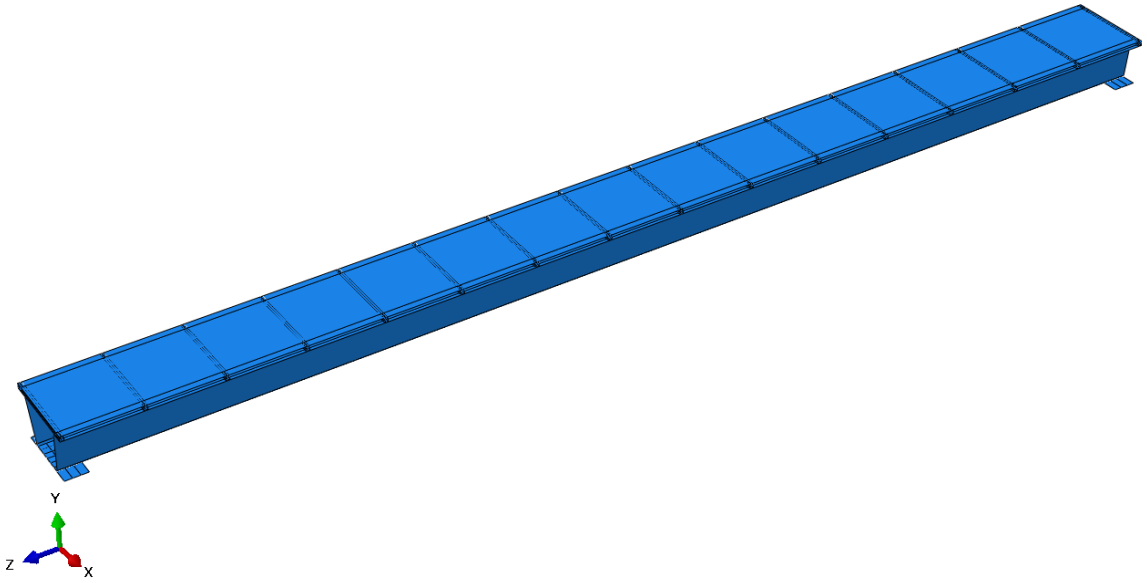

Figure 65shows the assembly of the CFS tib girder bridge model.

Boundary conditions

The boundary conditions (BC) on a tub girder bridge 15 meters in length and 1.2 meters in width describe how supported a girder is and designed to realistically simulate structural support shown in Figure 66. BC-1, at position 0 meters, is a fixed support, meaning it cannot move up (U1, U2, U3) or turn (UR1, UR2, UR3) degrees of freedom are fully restrained. The girder cannot move or rotate at this end acts as rigidly connected support. BC-2, at position 15 meters, is pinned, meaning This allows horizontal movement while preventing vertical displacement and rotation about specific axes. BC-3, at position 7.5 meters, does not allow vertical displacement (U2 = 0) and is a mid-support that does not allow much deflection. All these boundary conditions in combination cause the bridge to behave as much as possible in a realistic manner once it is loaded, stabilizing it as much as necessary as it turns as necessary.

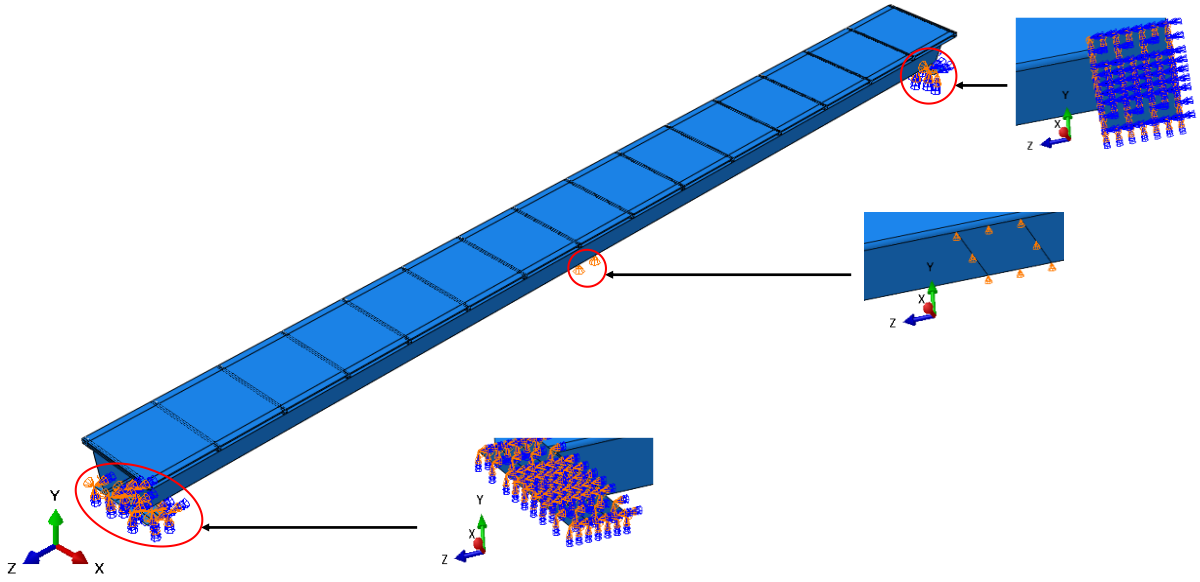

Figure 66 shows the applied boundary conditions at the bottom of Main span section on both ends and midspan.

Meshing

The Element Type belong to shell family are being selected. Shell elements are of two types: the 3-node triangular shell referred to as S3 and the 4-node quadrilateral shell referred to as the reduced-integration version of the S4R. The S4R is usually selected since it is well-suited to problems with a lot of bending dominated problems as well as being computationally efficient to calculate. Triangles (S3) are selected if the quadrilateral elements cannot easily fill the entire area, ensuring complete meshing coverage. The 20mm is the mesh size that is being used. To maintain sufficient resolution for capturing stress variations while keeping the computational cost reasonable. A finer mesh might provide a closer approximation, but a lot of processing is necessary. Conversely, a larger mesh might not provide very realistic results. The 20mm helps to ensure the model can observe where stress is accumulated, notably at areas of significant stress, such as at joints and areas of applied loads.

Using 20mm by 20mm element size as shown in Figure 67 to construct the mesh is the optimal means of illustrating the way stress occurs and the way the bridge made of cold-formed steel will operate. It is also cost-effective with the ability to calculate the structure thoroughly to enhance the bridge design.

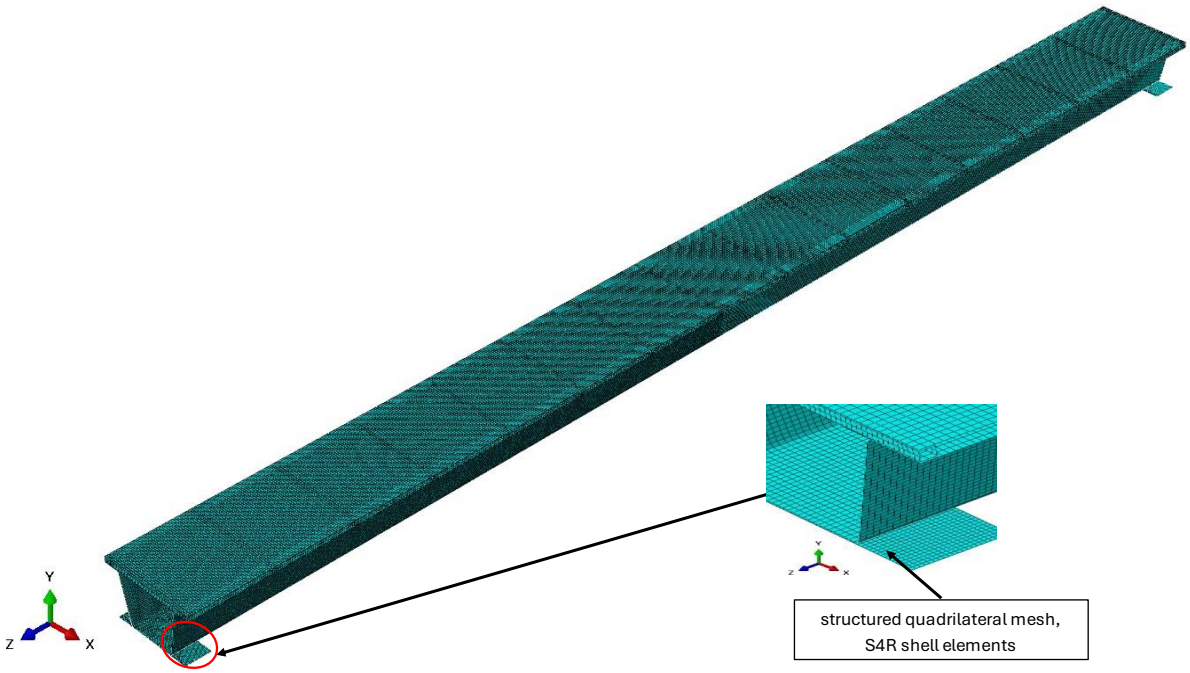

Figure 67 shows structural meshing of tub girder assembly.

Results and discussion

Deflection

The results from the finite element analysis (FEA) shown in the Figure 68, 69 represent the vertical displacement (U2) in a tub girder of span 15 meter long and 1.2-meter-wide bridge structure under 5kpa loading conditions. The structure is subjected to a uniformly distributed loading, essentially replicating pedestrian loading. Additionally, the boundary condition at the 7.5-meter point in the middle gives the structure two effective 7.5-meter-long spans in the overall 15-meter structure. The end points at 0 and 30 are fixed, essentially inhibiting any displacement at 0 and 30.

Deflection at bottom surface of tub girder: The bottom of tub girder surface experiences deflection with the maximum deflection of 10.60mm at span of 1.367 meter and 13.633 meter respectively as shown in Figure 70. Based on the criterion in the span/200 standard relative to the admissible maximum deflection, the admissible in this case is 37.5mm. Since the noted maximum value of deflection is 10.60 mm, thus confirming that the structural integrity of the bridge is satisfactory to the required serviceability standards of deflection control. The recorded deflection value is low enough to ensure user comfort, maintain structural stability, and prevent problems related to excessive deformation. The results confirm that additional reinforcement measures are not required, as the tub girder has sufficient stiffness to withstand the applied loading conditions without causing unacceptable deformation levels.

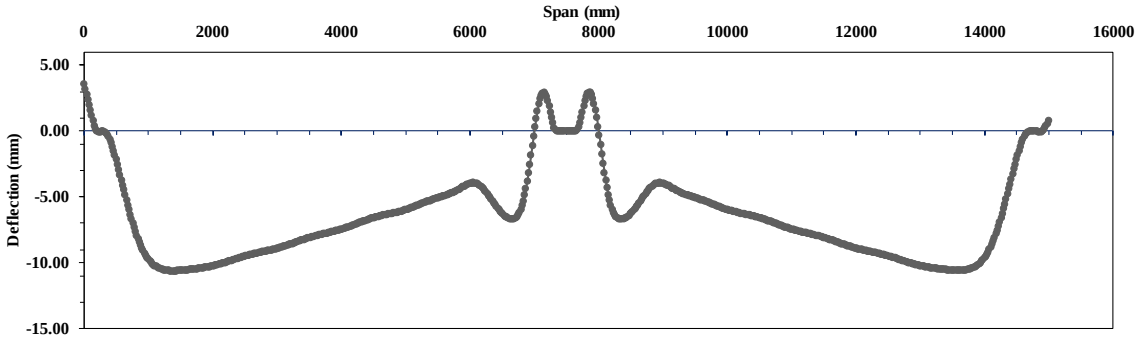

Figure 68 shows symmetrical distribution of vertical displacement along the CFS tub girder.

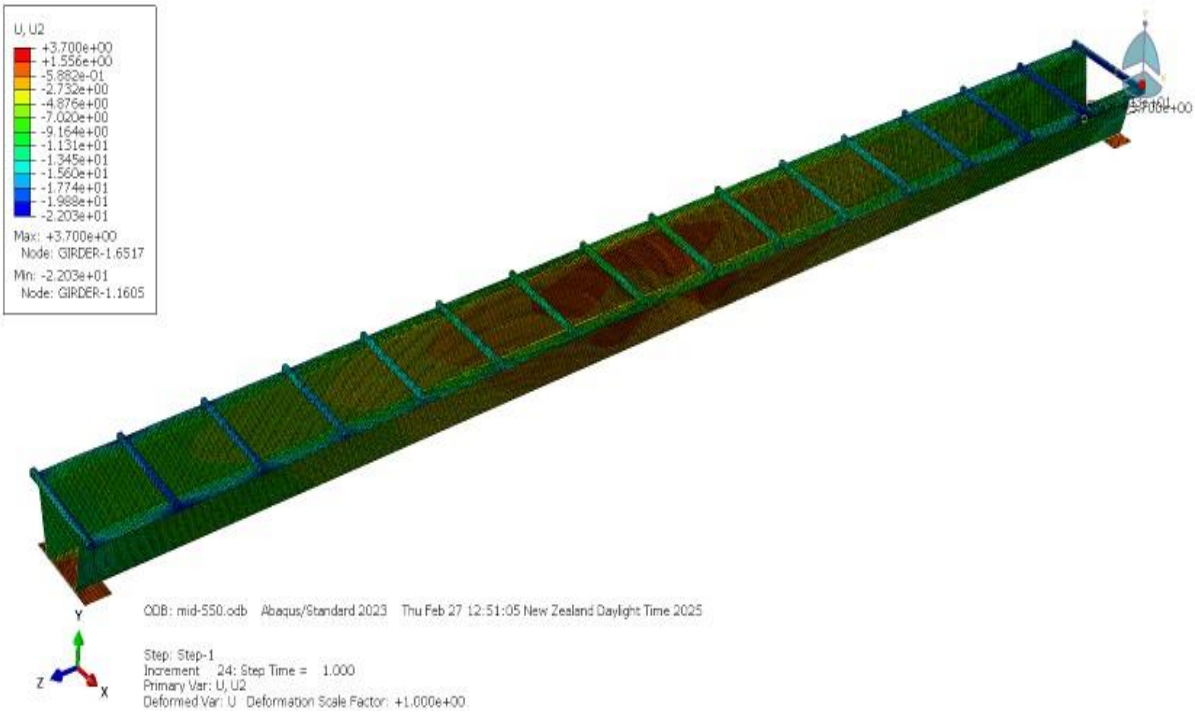

Figure 69 shows final deflection of CFS tub girder.

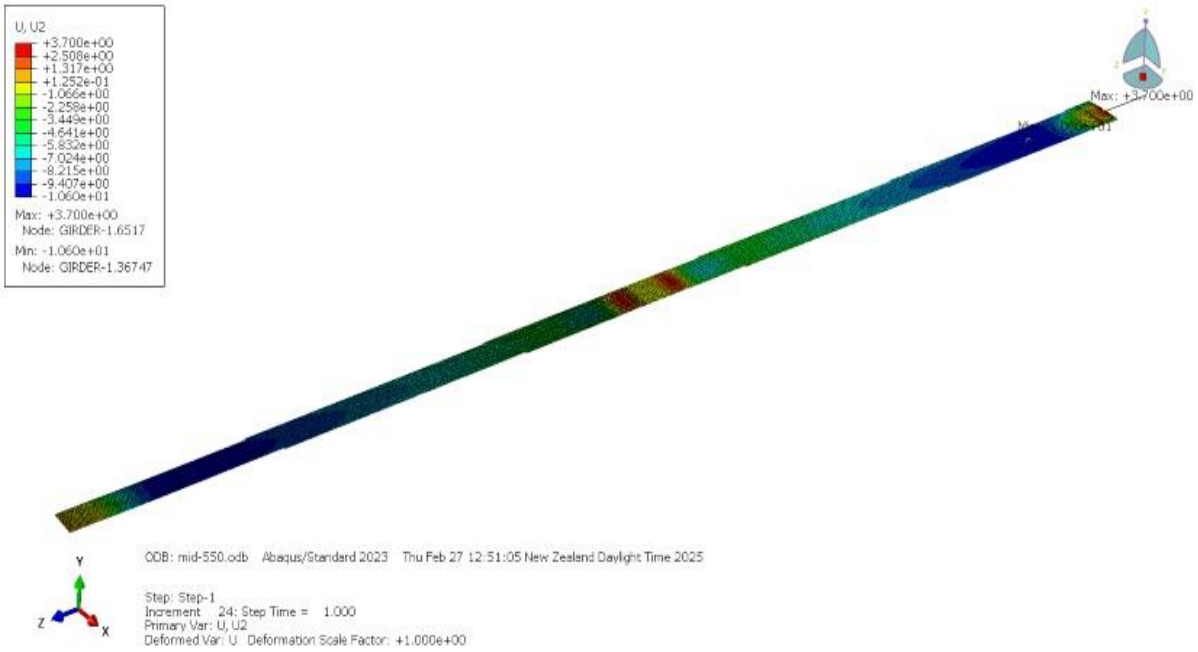

Figure 70 Shows deflection at bottom surface of tub girder.

Stress distribution analysis

The stress distribution analysis, as seen in the simulation results shown in Figure 71,72, explains the stress variation across different parts of the cold-formed steel (CFS) tub girder bridge. The study reveals a maximum von Mises stress of around 550 MPa, which is mostly concentrated at the web and bottom surface intersections near the supports and the mid-span bottom surface. Taking into consideration that the yield strength of the cold-formed steel is set at 550 MPa, the measured stress levels indicate local yielding in these areas of high stress concentration, especially at the web- bottom surface intersections near the supports and in the bottom surface due to bending tension. The webs also bear high stress near the supports; this stress concentration explains the need for the addition of stiffeners at the supports to prevent shear buckling. While most of the structure falls within tolerable stress levels, the stress accumulation at key points confirms that reinforcements are necessary to enhance structural integrity. A high stress accumulation is also observed at the deck box section intersections and top flanges, particularly where the box sections are in contact with the flange. This observation implies that the load transfer from the deck to the girder is causing localized stress concentrations, which may lead to deformation or fatigue in the long run if not properly addressed. Such reinforcement will help the bridge maintain its load-carrying capacity, hence preventing early failure under heavy loads. In conclusion, the stress distribution shows an efficient load transfer mechanism; however, including stiffener placement and localized reinforcement at areas of stress concentration, are necessary to enhance the safety of the structure.

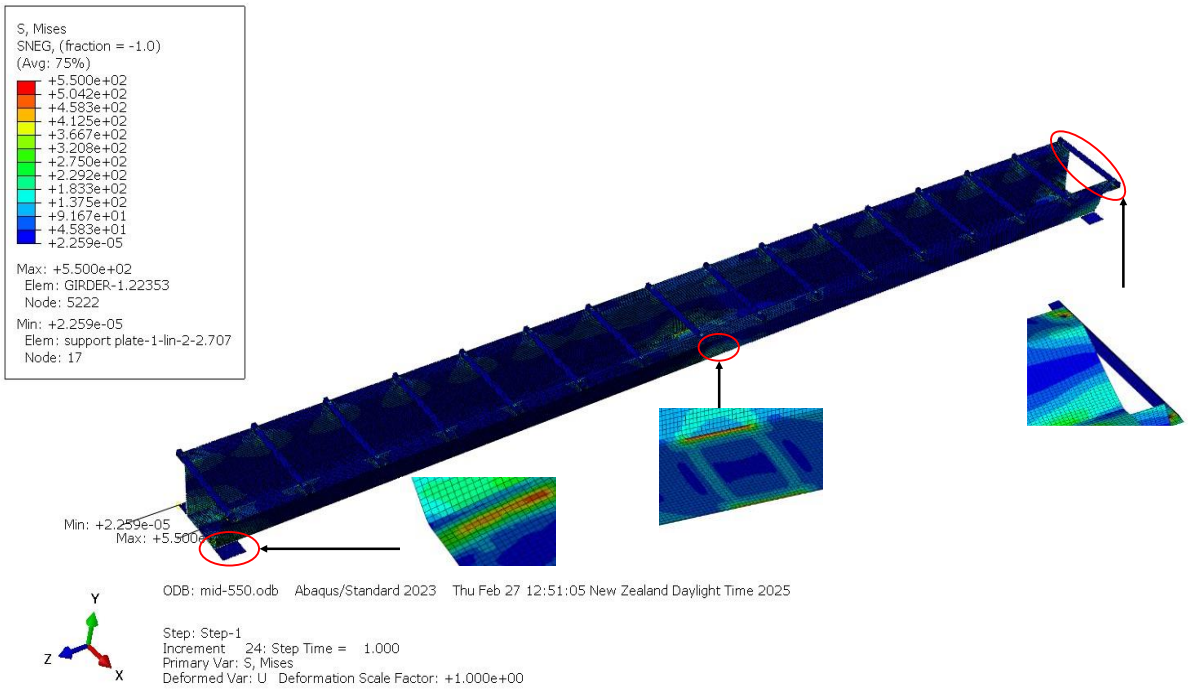

Figure 71 shows Results from the Von Mises stress analysis of CFS tub girder bridge.

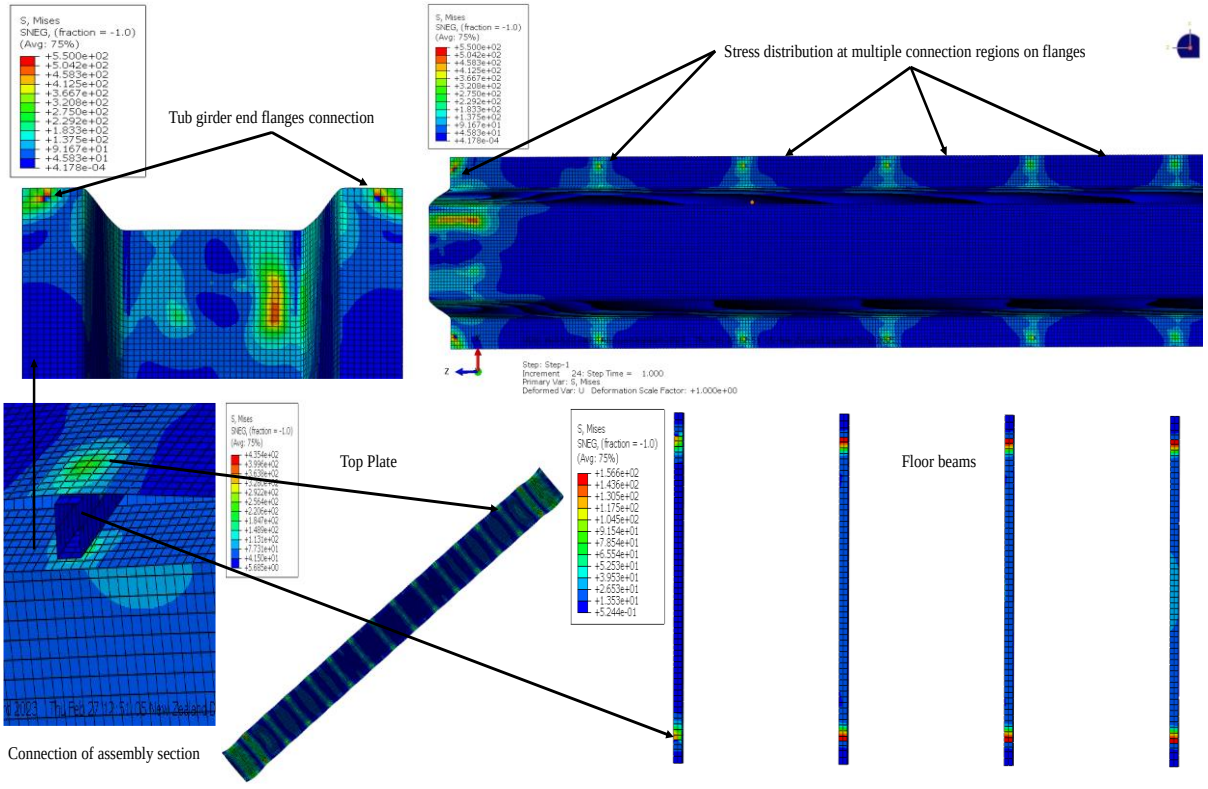

Figure 72 shows the connector region where high stress concentration was observed in different parts of assembly.

5.2 Effects of a 30 -Meter Span on Deflection and Stress in a flat foot Cold-Formed Steel Pedestrian Bridge

Introduction

Flat beam steel bridges as shown in Figure 73, 74, 75,76 form an integral part of modern infrastructure, offering good spanning capability for medium to long span bridges while keeping the structural depth minimum. These bridges generally use the concept of the orthotropic decks, where the steel deck plate is supported by the longitudinal and the transverse ribs for efficient load distribution and enhanced load-carrying capacity. The orthotropic form achieves the minimum weight for the bridge by optimizing structural efficiency through its ability to provide unique stiffness levels in orthogonal directions, thus optimizing the bridge for various load cases [65]. Additionally, advancements in the field of modular prefab structures, like the Callender-Hamilton bridge imagined by New Zealand engineer Archibald Milne Hamilton, have revolutionized the bridge building sector by providing for rapid assembly and installation, particularly under difficult circumstances or emergencies [66]. These advancements mark the improvement over the steel flat beam bridge by incorporating the latest design features and strong building processes for the demands placed by contemporary civil engineering projects.

Figure 73 shows steel flat beam bridge [67].

Figure 74 shows steel orthotropic decks [65].

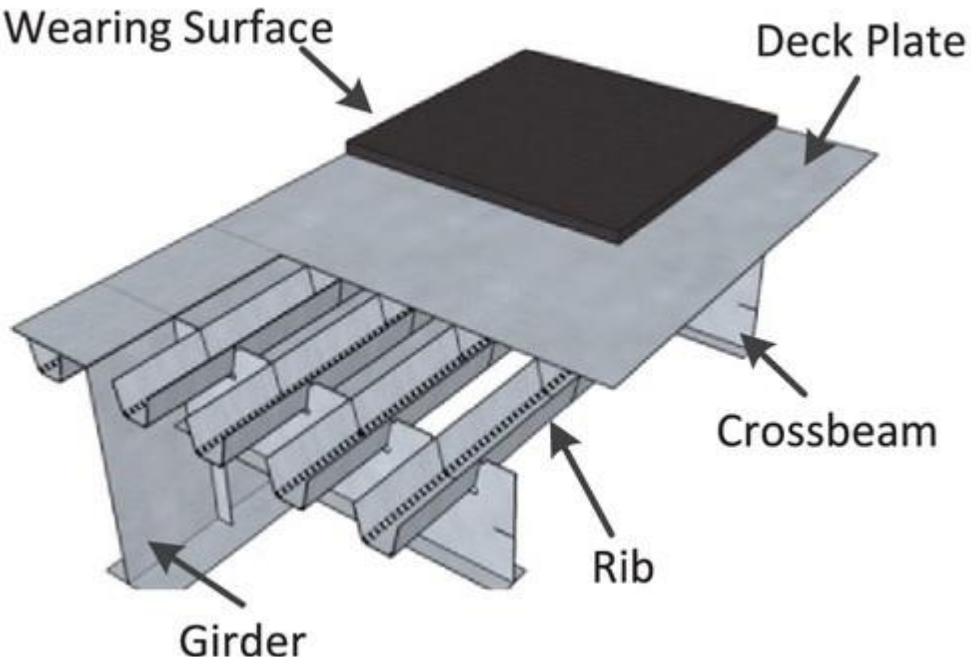

Figure 75 shows Rib-to-Deck Joint in Orthotropic Steel Bridge Deck, Photo credit ASCE[65].

Figure 76 shows flat bridge used as utility bridge [67].

Model parts

The CFS flat foot bridge parts were created in 3D modeling space, deformable shell and later extruded to specific required dimensions for different parts. The parts used in pedestrian bridge are mentioned in table-7 with dimensions and follows with Figure-77.

Table 7 shows type of parts used with length, thickness in mm and their application.

Part	Section application	Length (mm)	Thickness (mm)
FS-50020	Transverse Facing Back-to-Back (BTB)	3170	1.95
FS-63020N	Main Span	30000	1.95

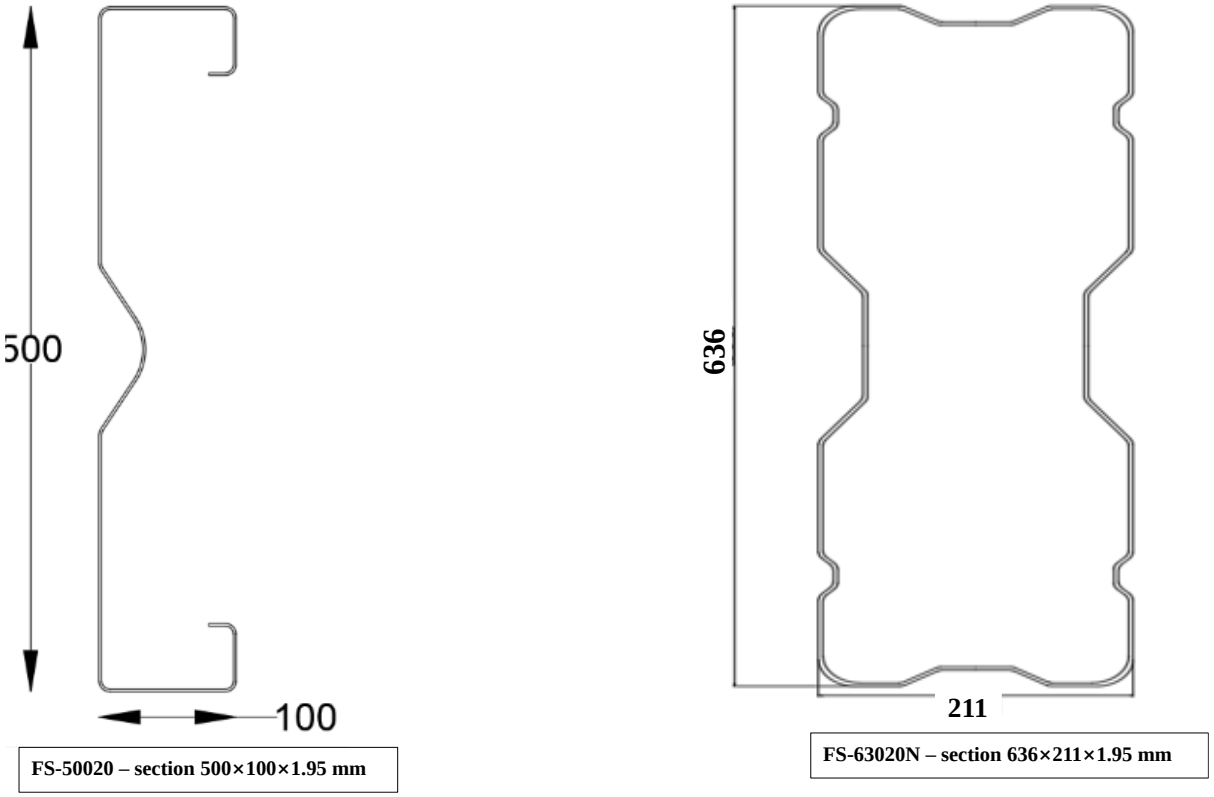

Figure 77 shows geometry and dimensions used for CFS flat foot bridge.

Material properties

The data used in the FE models corresponded to the ‘static’ values of the material properties obtained from consulting the manufacturer and section thickness is 1.95mm- mean with the yield stress of 550 MPa and the elastic behaviour was defined using a Poisson’s ratio of 0.3 and with a Young’s modulus (E) of 203 Gpa.

Assembly

The depiction is of a flat-foot bridge that is built with a simple but strong, yet efficient structural system consisting longitudinal and transverse beams as shown Figure 78. The bridge uses two parallel longitudinal nested section beams the entire length of the bridge that supplies necessary support while allowing the transfer of the load. Transverse beams that are distributed with equal distance the longitudinal elements to provide a ladder-like structure that increases rigidity while providing equal transfer of the load to the bridge deck. The nested section elements enhance torsional rigidity while reducing excessive deflection at the time of pedestrian loading. The specific design is well-suited to lightweight pedestrian bridges with a compromise between the structural efficiency of the bridge, ease of manufacture, and module component design. Additionally, the open structure allows the flexibility of decking material to include a range of decking material types such as timber plank, composite slab, or metal grating that renders the bridge adaptable to various site conditions and aesthetics.

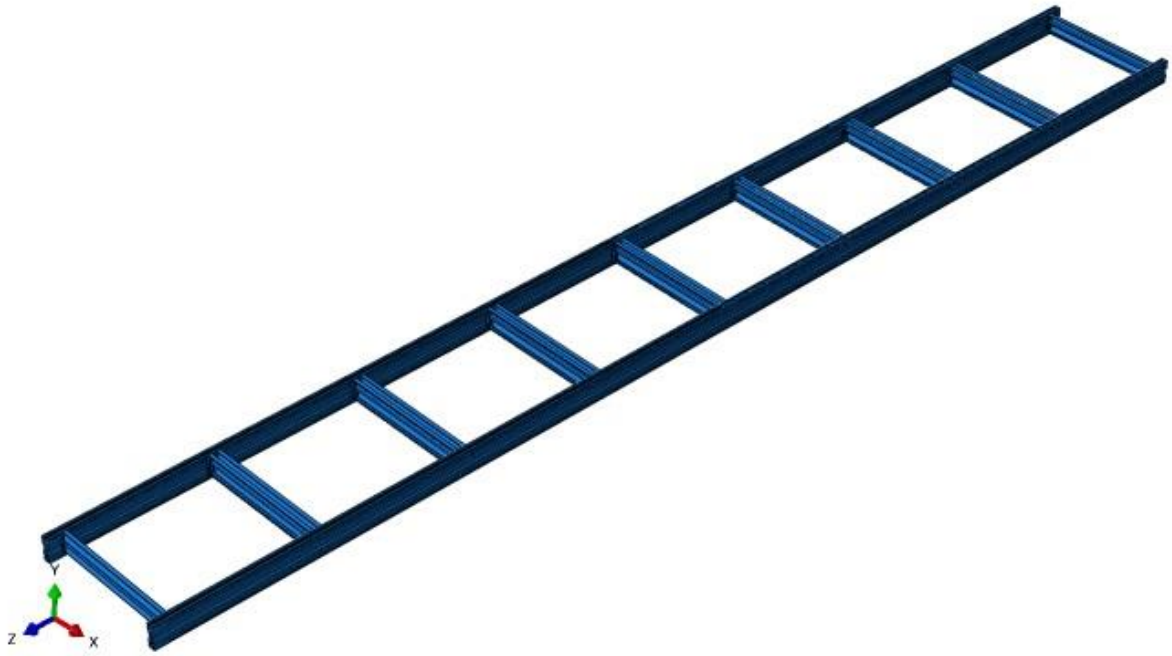

Figure 78 shows the assembly of the flat foot bridge model.

Boundary condition

The Figure 79 represent the applied boundary conditions for a cold-formed steel (CFS) pedestrian bridge having a span of 30-meter and width of 3.5-meter. The boundary conditions are defined at the both the end points of the bridge and at the mid-point (15 meters) to simulate the real-life support constraints accurately. The BC-1, at the first end, in which all displacement and rotational degrees of freedom (U1, U2, U3, UR1, UR2, UR3) are restrained to zero, reflecting a fully constrained support preventing any kind of movement and/or rotation. The BC-2 refers to the other end of the bridge, in which only the vertical displacement (U2 = 0) and two rotational degrees of freedom (UR2, UR3 = 0) are restrained, effectively modeling a pinned support to allow axial expansion and shrinkage while preventing the movement and rotation in the upward direction. The last BC-3, applied at the mid-point (15 meters), in which only the vertical displacement (U2 = 0) alone is restrained. This represents an intermediate support, such as a pier or a bearing, to avoid the extreme deflection at the middle point of the

span. All the boundary conditions in aggregate provide a real-life support system to the bridge, allowing the proper structure under loading condition along with the real-life deformations.

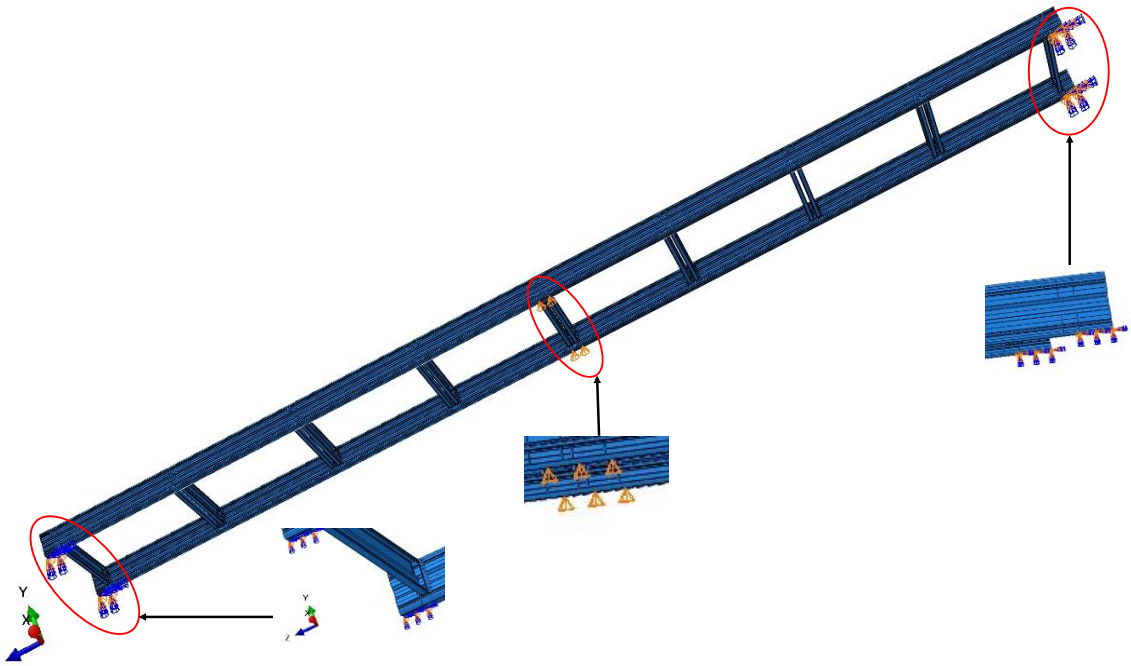

Figure 79 shows the applied boundary conditions at the bottom of Main span section on both ends and midspan.

Meshing

The Element Type belong to shell family are being selected. Shell elements are of two types: the 3-node triangular shell referred to as S3 and the 4-node quadrilateral shell referred to as the reduced-integration version of the S4R. The S4R is usually selected since it is well-suited to problems with a lot of bending dominated problems as well as being computationally efficient to calculate. Triangles (S3) are selected if the quadrilateral elements cannot easily fill the entire area, ensuring complete meshing coverage.

The 20mm is the mesh size that is being used. To maintain sufficient resolution for capturing stress variations while keeping the computational cost reasonable. A finer mesh

might provide a closer approximation, but a lot of processing is necessary. Conversely, a larger mesh might not provide very realistic results. The 20mm helps to ensure the model can observe where stress is accumulated, notably at areas of significant stress, such as at joints and areas of applied loads.

Using 20mm by 20mm element size as shown in Figure 80 to construct the mesh is the optimal means of illustrating the way stress occurs and the way the bridge made of cold-formed steel will operate. It is also cost-effective with the ability to calculate the structure thoroughly to enhance the bridge design.

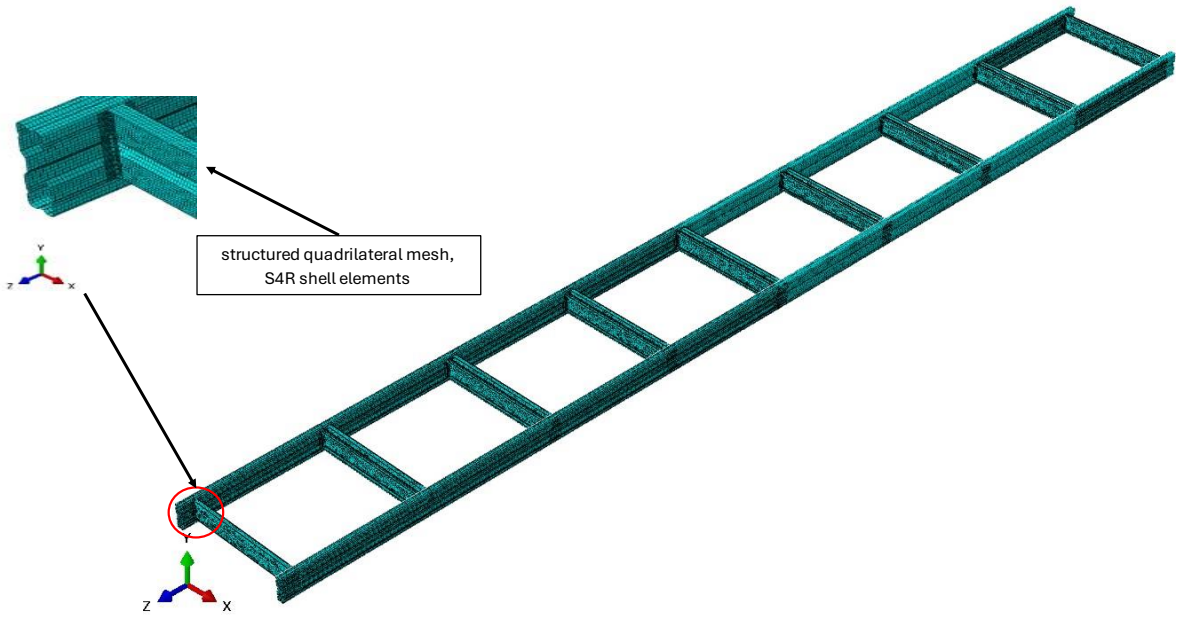

Figure 80 shows structural meshing of assembly.

Results and discussion

Deflection

The results from the finite element analysis (FEA) shown in the Figures 81,82 and 84 represent the vertical displacement (U2) in a 30-meter long and 3.5-meter-wide bridge structure

under 5kpa loading conditions. The structure is subjected to a uniformly distributed loading, essentially replicating pedestrian loading. Additionally, the boundary condition at the 15-meter point in the middle gives the structure two effective 15-meter-long spans in the overall 30-meter structure. The end points at 0 and 30 are fixed, essentially inhibiting any displacement at 0 and 30.

The results obtained from the simulation explain the pattern of vertical displacement (U2) across the bridge structure as shown in Figure 84, 85. The maximum deflection observed was -91.19 mm, occurring exactly at the center of the mid transverse member, as expected for the reaction of a simply supported structure under defined loading conditions. The outcomes from the deflection reveal the point at 7.5 and 22.5 meters at which the downward deflection is at a maximum at -58.92 mm as shown in Figure 80 and 81, consistent with expected positions based on the support at the 15-meter point. The pattern in the deflection is symmetrical, reflecting the way in which the boundary conditions and the distribution of the load are applied. The size in the deflection reduces in magnitude approaching the 0-meter, 15-meter, and 30-meter points, at which the displacement approximates zero. Based on the criterion in the span/200 [58] standard relative to the admissible maximum deflection, the admissible in this case is 75mm. Since the noted maximum value at -91.19 mm does not lies in the admissible domain, the structure cannot be deemed to be in the expected deformation limits under the applied loading. In summary, Since the recorded maximum deflection is -91.19 mm for transverse beams, which exceeds the permissible limit of 75 mm, the deformation surpasses the acceptable threshold for serviceability. This suggests that under the given loading conditions, the structure experiences excessive deflection.

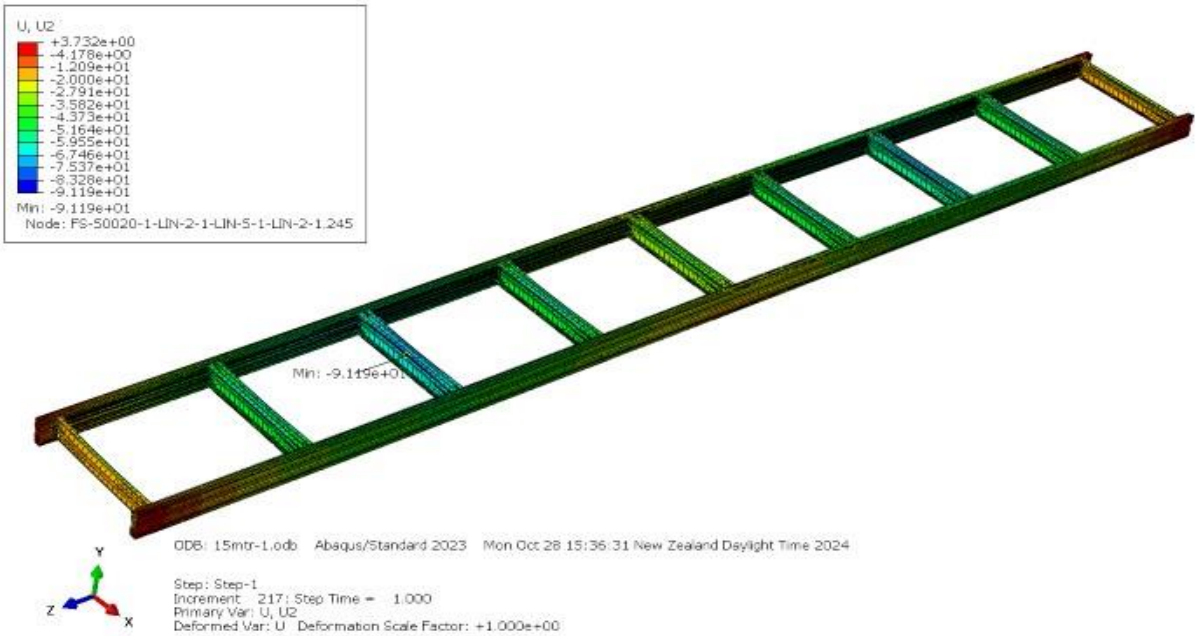

Figure 81 shows final deflection of CFS foot bridge.

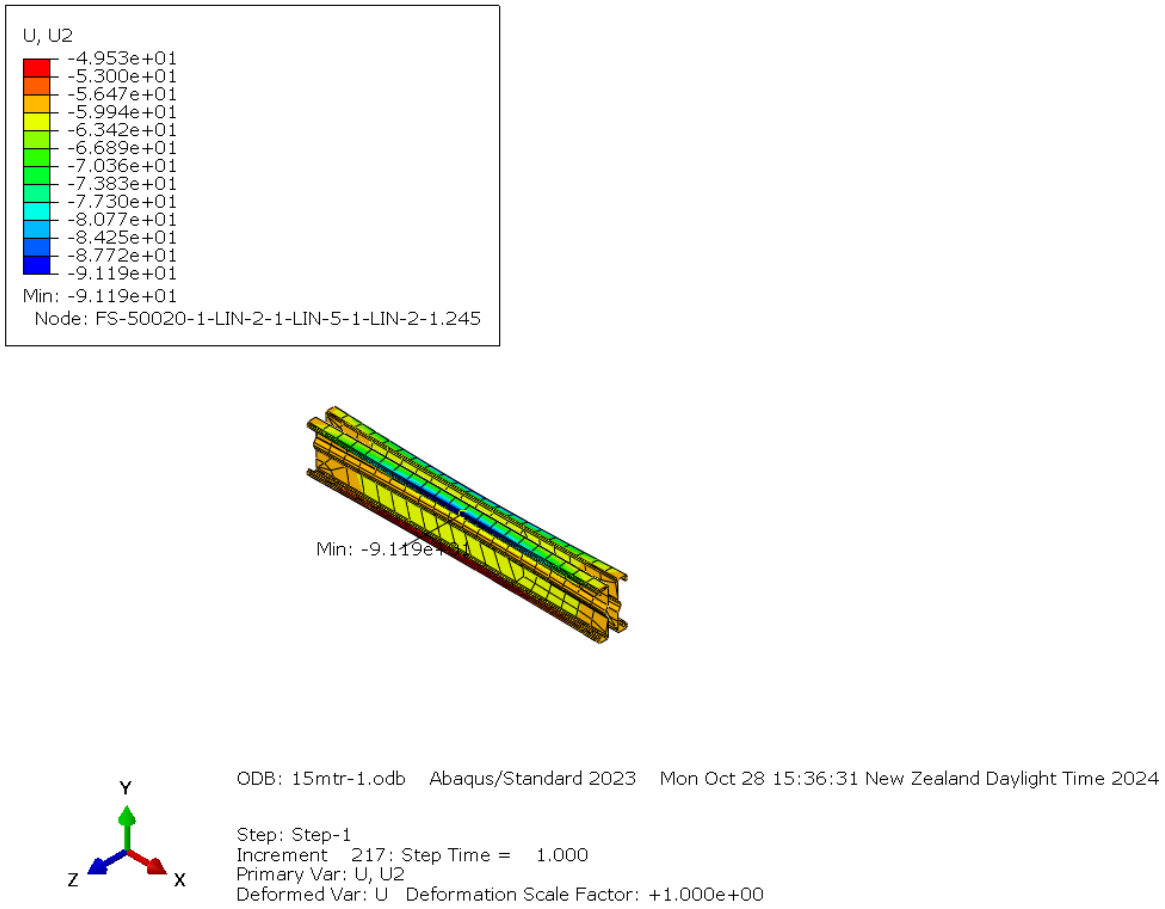

Figure 82 shows final transverse deflection of CFS foot bridge.

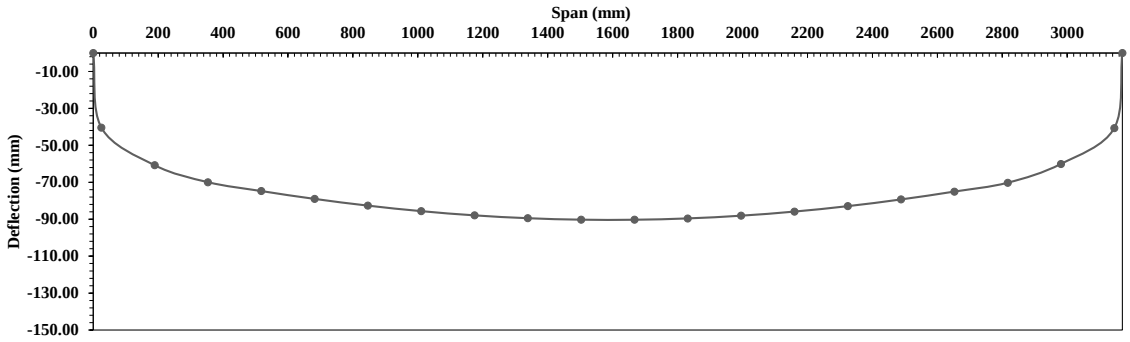

Figure 83 shows symmetrical distribution of vertical displacement along the transverse of flat foot bridge.

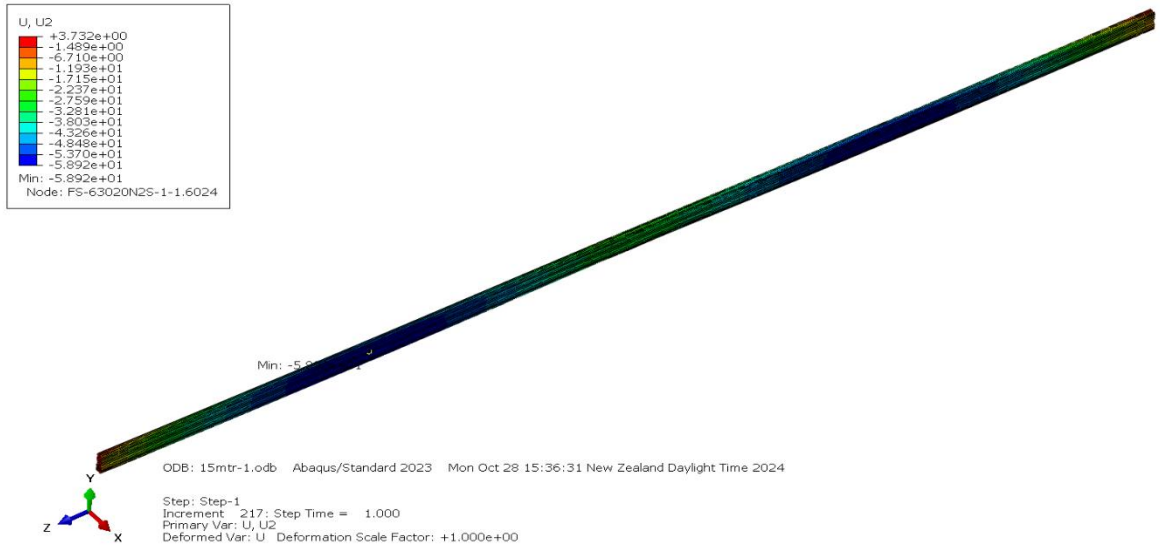

Figure 84 shows final main span beam deflection of CFS flat foot bridge.

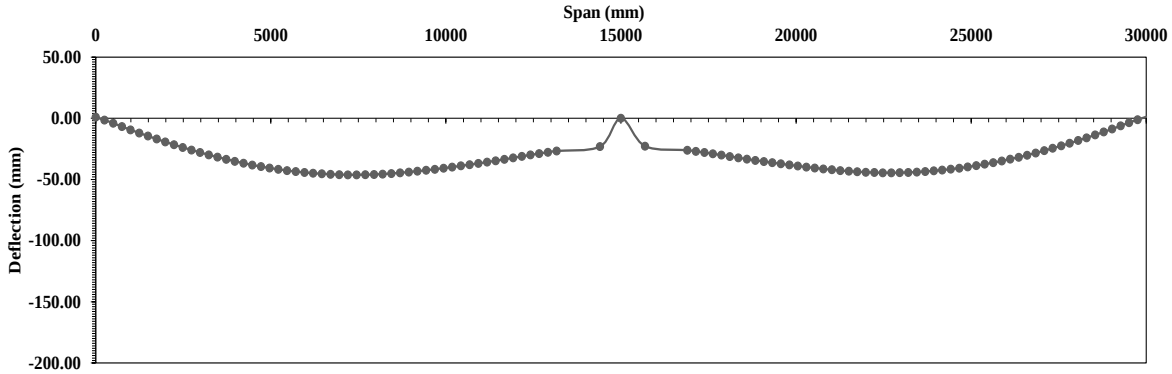

Figure 85 shows symmetrical distribution of vertical displacement along the bottom main beam of flat foot bridge.

Stress distribution analysis

The stress distribution study, as shown in Figure 86 and 87, illustrates the distribution of stress through the different elements in the CFS foot bridge. The evaluation identifies a local von Mises stress at 582.4 MPa, at the joints between the transverse and the longitudinal elements. Noting the approximated 550 MPa value in the yield point of the cold-formed steel, the stressed zones in the above location represent the area at the risk of yielding under heavy loading. However, most sections in the bridge experience significantly low stress. This finding suggests the structure's overall design is efficient in spreading the loads and reducing the accumulation of heavy stresses in the zones other than the joints. The observation suggests the structure's design, in terms of handling the structure's loads, ensures the majority of the structure's components are at reasonable stress levels in the case above, the bottom surface in the centre of the main beam, experience heavy accumulation.

Figure 86 shows Results from the Von Mises stress analysis of CFS foot bridge.

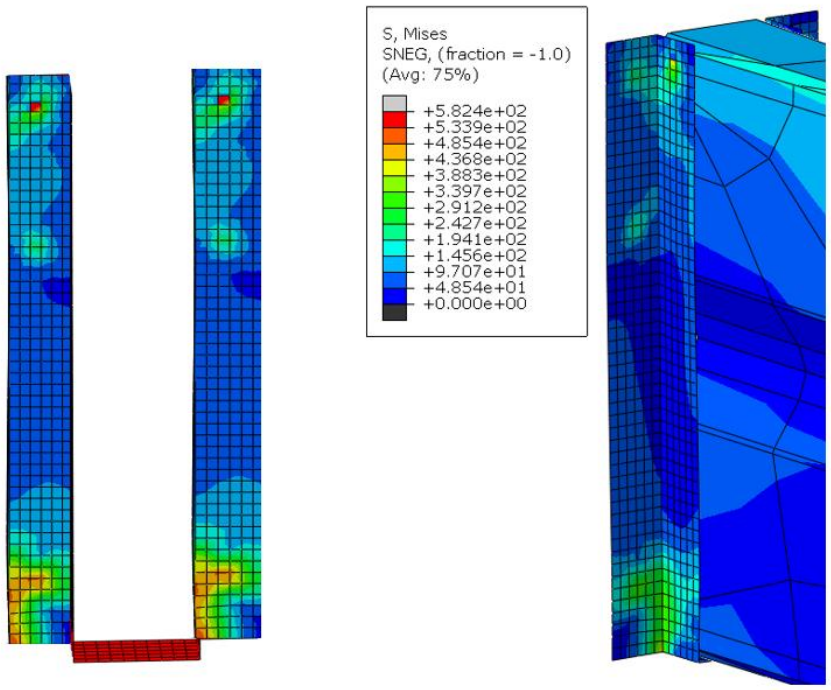

Figure 87 shows the connector region where high stress concentration was observed in different parts of assembly.

5.3 Effects of a 10 - Meter Span on Deflection and Stress in a Cold-Formed Steel box Pedestrian Bridge

Introduction

Figure 88 shows the model of CFS box bridge and its configuration in terms of its geometry. The bridge appears to have a box-section configuration with vertical and horizontal members forming a closed rectangular frame, which enhances torsional rigidity. An in-depth discussion of individual items utilized in its bridge model can be seen in Table 4, with a discussion of its use of materials and dimensions in terms of its cross-sectional shape. Overall dimensions for its bridge model include a 10-meter long, 2.5-meter wide, and 3.2-meter-high configuration, modelled for computational analysis.

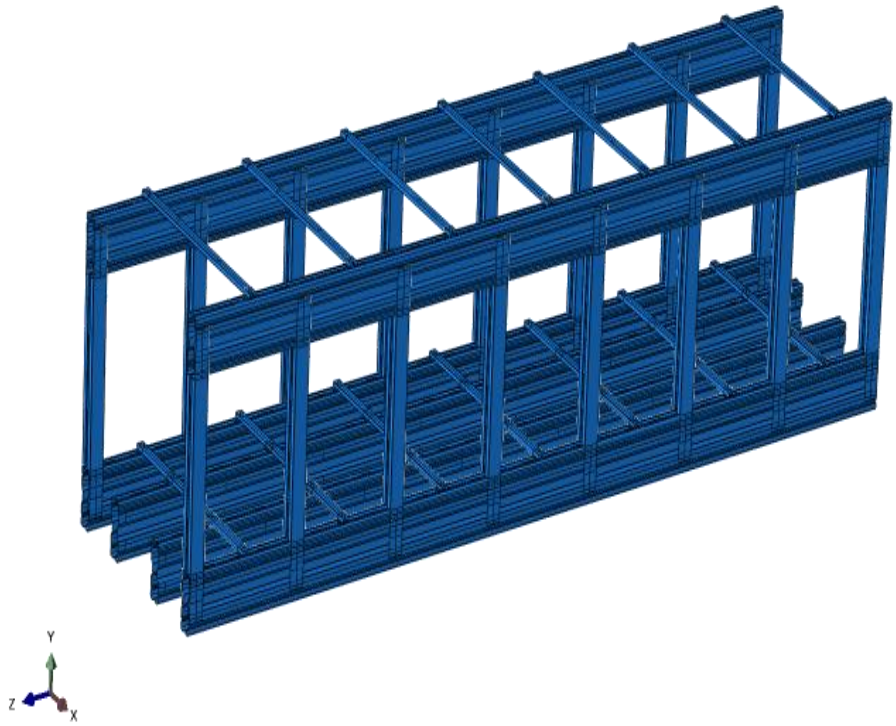

Figure 88 shows the design and geometry of the box bridge model.

Model parts

The CFS box bridge parts were created in 3D modeling space, deformable shell and later extruded to specific required dimensions for different parts. The parts used in pedestrian bridge are mentioned in table-8 with dimensions and follows with Figure-89.

Table 8 shows type of parts used with length, thickness in mm and their application.

Part	**Section application**		**Length (mm)**	**Thickness (mm)**
FS-90195	Top	Transverse	2600	3.0
FS-90195	Bottom		2600	3.0
FS-63020N	Main Span	Top chord and Bottom chord	10000	3.0
FS-63020N			10000	3.0
FS-200195	Vertical Members		3000	3.0

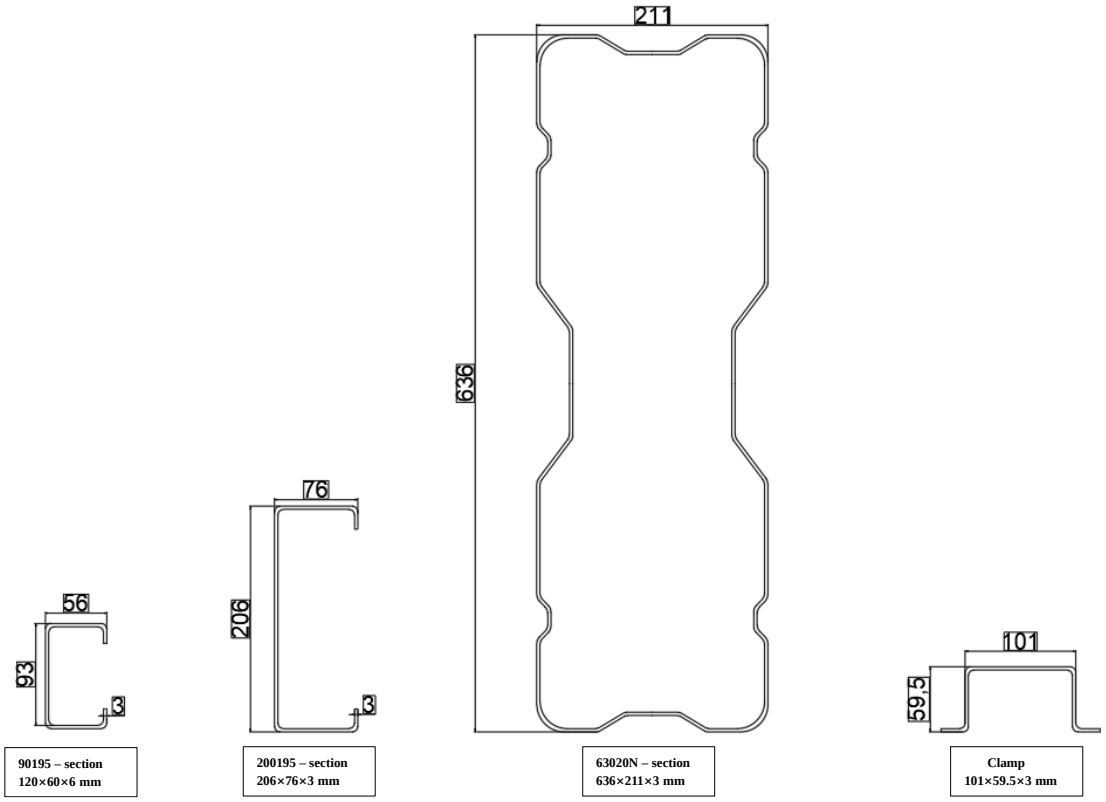

Figure 89 shows geometry and dimensions used for CFS box pedestrian bridge.

Material properties

The data used in the FE models corresponded to the ‘static’ values of the material properties obtained from consulting the manufacturer and section thickness is 3mm- mean with the yield stress of 550 MPa and the elastic behaviour was defined using a Poisson’s ratio of 0.3 and with a Young’s modulus (E) of 203 Gpa.

Assembly

The box structure composed of several interconnected structural members forming a closed rectangular frame of span 10 meters. It consists of longitudinal top and bottom chords, interconnected through vertical members, together providing a strong and stable form as shown in Figure 88. The absence of any diagonal members or truss-like structures identifies this form

as a non-truss, box-section bridge, underlining its torsional stiffness and allowing for simple loading distribution. U-clamps are utilized in addition to allow for simple interconnection between both top and bottom transverse sections and respective chords.

The presence of gusset plates is noticeably absent in this assembly and in its stead, vertical parts (sections) join directly with top and bottom chords, simplifying construction work. Transverse floor beams join firmly with bottom longitudinal parts through U-clamps, allowing loads placed onto them to disperse uniformly through the bridge's breadth. Overall, modularity in bridge form is prioritized, allowing for prefabrication of box sections at an offsite location, with rapid and efficient onsite assembly, a move that effectively conserves the form's integrity and function, and at the same time reduces construction duration and manpower requirements.

Meshing

The process for the type of elements chosen for the analysis for the cold-formed steel (CFS) pedestrian bridge includes setting the Element Shape to quadrilateral (Quad) and selecting the Structured meshing technique as shown in Figure 90. This method ensures the formation of high-quality, regularly formed mesh, contributing towards increased numerical efficiency and increased result accuracy. An element size of 20mm has been chosen for the whole assembly for attaining the balance between the efficiency of the computations and the accuracy of the resulting data. This is fine enough for the elements to pick up stress gradients in the thin-walled elements while keeping the computations affordable. The chosen element is from the Shell type, the S4R element, described as the 4-node quadrilateral shell element, together with triangular shell elements (S3). An element size of 20mm ensures the mesh remains sufficiently refined even where triangular elements are located, picking up deformations sufficiently, and avoiding over-refinement causing increased computation times.

S4R elements are best for the analysis for the thin-walled CFS sections given their ability for shear locking prevention and stress distribution improvement. Even though triangular S3 elements can be necessary for complex parts, their use must be minimal for the prevention of the occurrence of numerical inaccuracies. Additionally, the use of the structured meshing technique improves the accuracy of the distribution of the stress, thus lessening the error and raising the quality of the analysis using the finite elements.

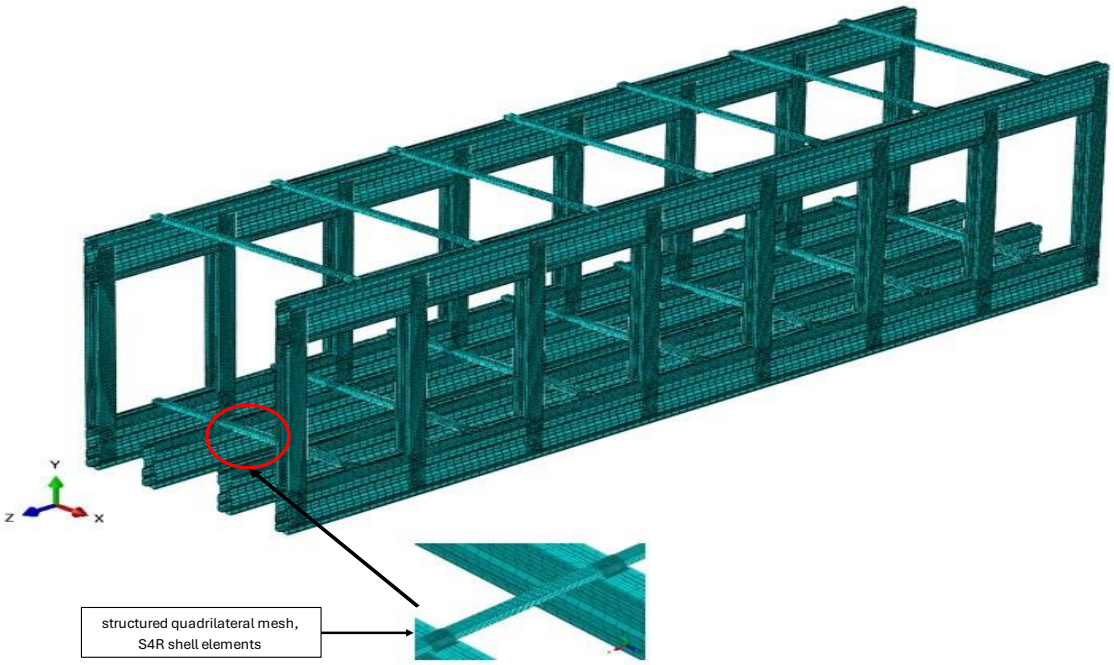

Figure 90 shows structural meshing of assembly.

Results and discussion

Deflection

The deflection analysis shown in Figure 92 represents the deformation under a uniformly distributed load of 5 kPa applied to the top surface of the transverse beams. The bridge has a span of 10000 mm and a width of 2500 mm. According to the deflection limit criteria of span/200, the maximum allowable deflection for this structure is:

Maximum allowable deflection = $\frac{\text{span}}{200} = \frac{10000}{200} = 50\text{mm}.$

Additionally Figure 92 illustrates the transverse beams under a load of 5 kPa, with deflection results displaying a regular load distribution; all maximum deformations remain within allowable limits. Therefore, the transverse beams can carry the applied load and transfer it to the major truss members with minimal deformations.

Figure 91 (Graph) represents the result of this setup, the deflection shown in graph displays a symmetrical distribution of vertical displacement along the bridge span, which is characteristic of beams or truss members under uniformly distributed loading. The deflection values are nearly zero at the fixed ends (0 mm and 10000 mm) due to the applied boundary conditions, while the maximum downward deflection of approximately -13.9 mm occurs at mid-span (around 5000 mm), where bending moments recorded are the highest.

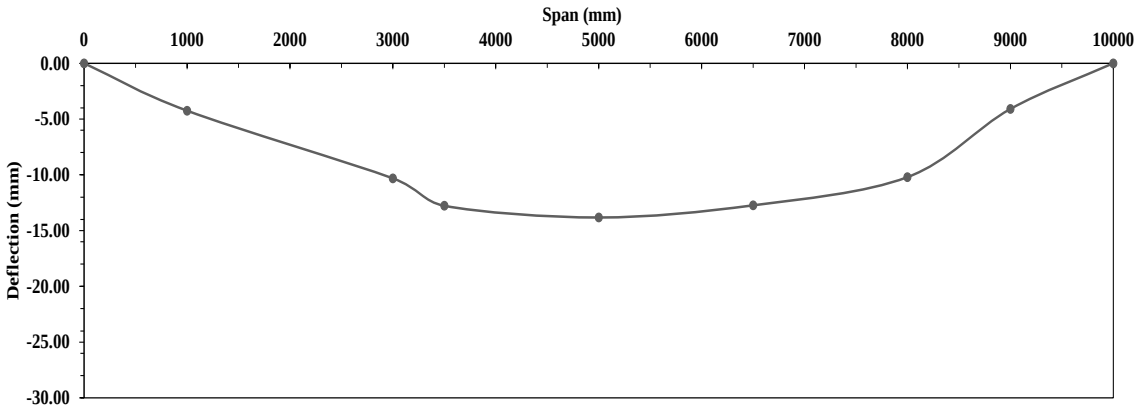

Figure 91 shows symmetrical distribution of vertical displacement along the bridge span of CFS bridge.

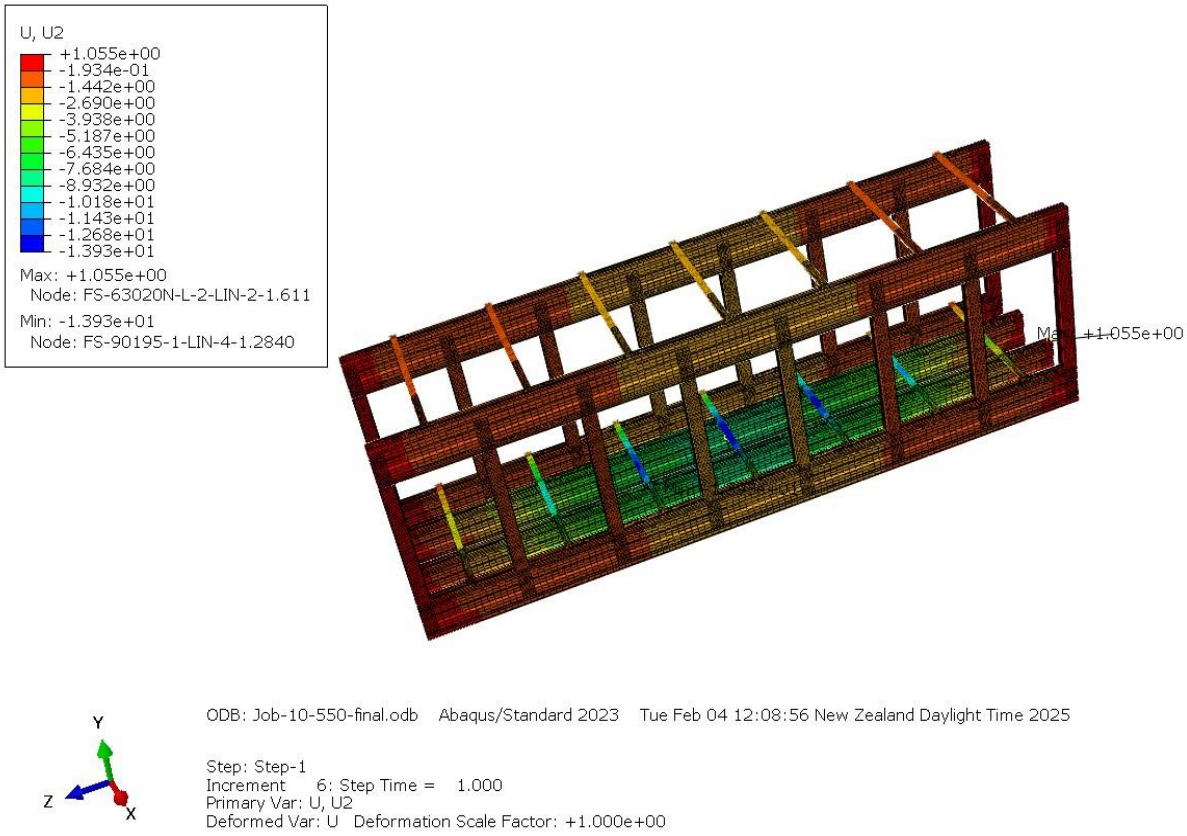

Figure 92 shows final deflection of CFS bridge.

Stress distribution analysis

Stress Distribution Study as shown in Figure 93,94 illustrate the distribution of stress throughout various parts of the CFS bridge. Maximum von Mises stress is 550 MPa as shown in Figure 93, located at intersections of the transverse and longitudinal members. Because the yield strength for the steel, when cold formed is also 550 MPa, the high stress areas will yield under heavy load. Yet most of the structure experience much less stress, as indicated by the stress distribution contour.

The clamps as shown in Figure 94 is the greatest evidence for the fact that points under tension can typically be located at the joints where forces transfer occurs. Blue spots indicate lower stress regions, suggesting that the bridge effectively distributes loads across the structure, minimizing excessive stress build-up in non-critical areas.

Recommendations for Improving Structural Performance: Strengthening Critical Members, Increase the cross-sectional size of transverse beams and longitudinal members to enhance overall stiffness and reduce stress concentrations at joints.

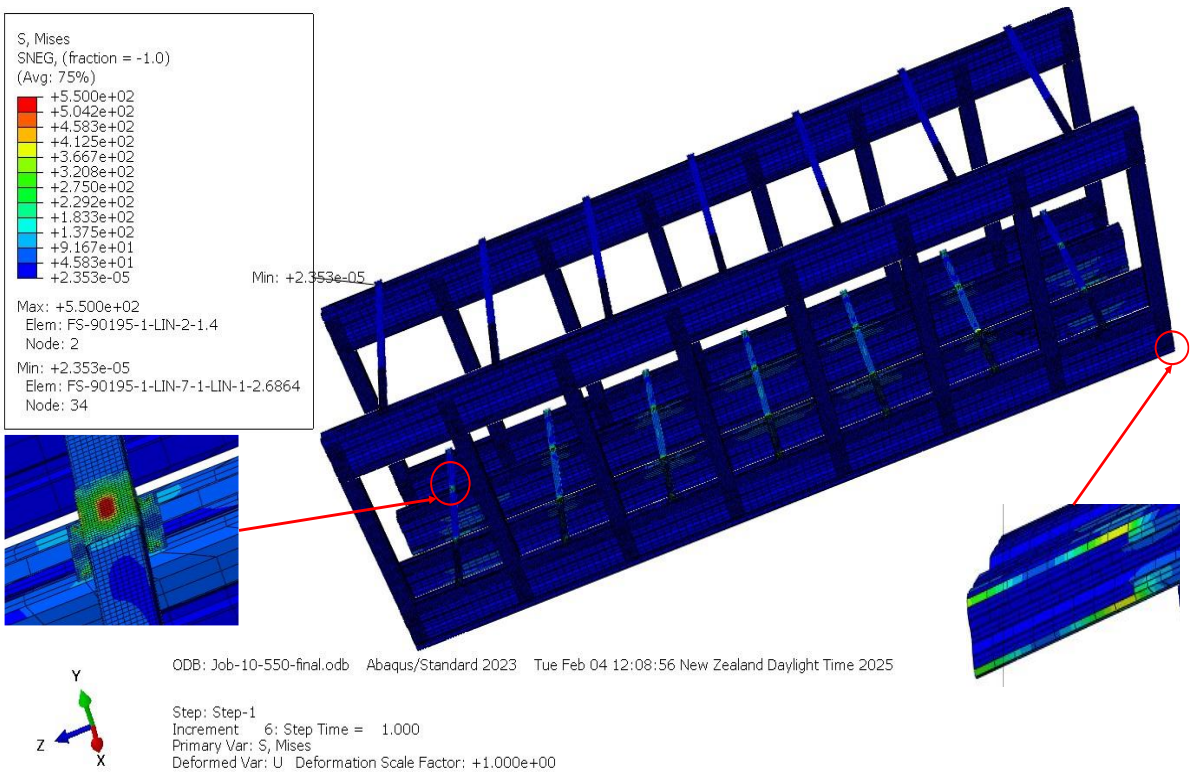

Figure 93 shows Results from the Von Mises stress analysis of CFS bridge.

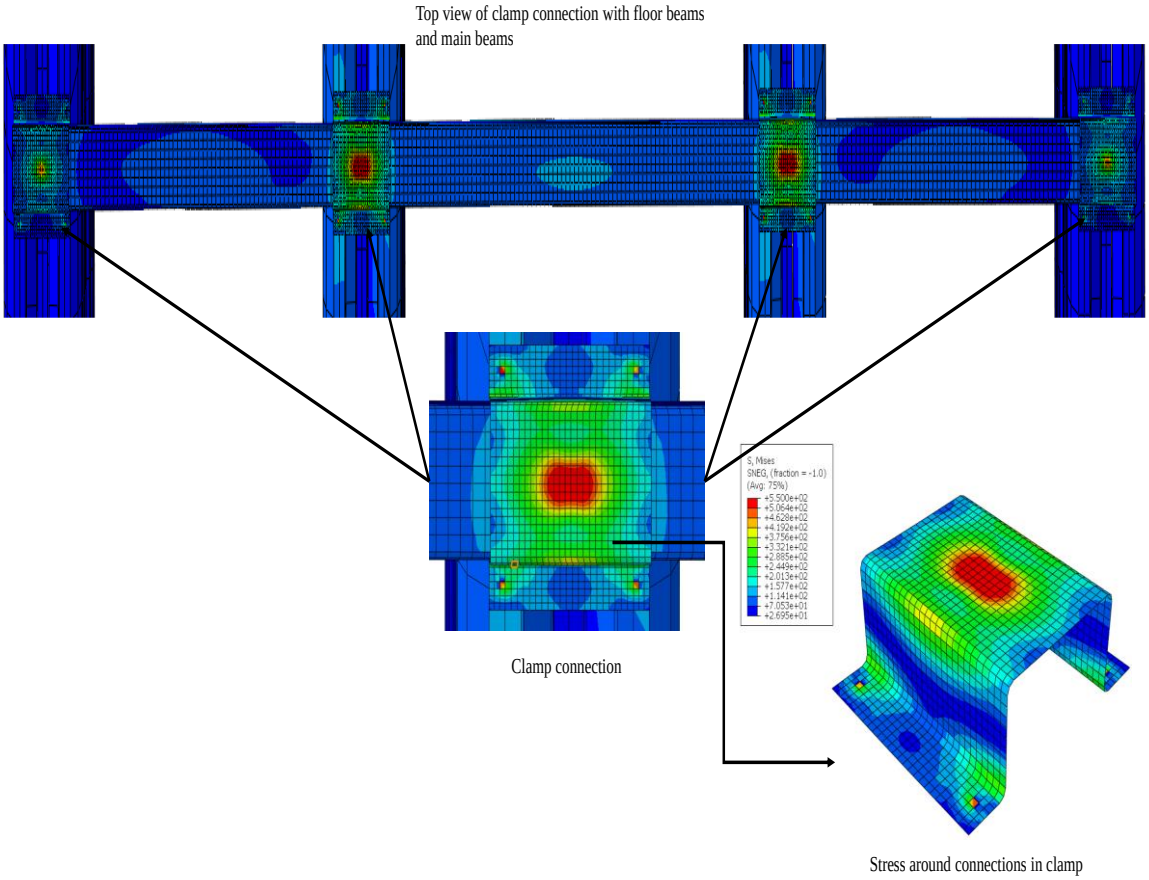

Figure 94 shows the connector region where high stress concentration was observed in different parts of assembly.

Chapter 6 – Comparative Deflection and Stress Analysis of Cold-Formed Steel Bridges: Influence of Span and Structural Form

This section has a comparative evaluation of six cold -formed steel pedestrian bridge configurations each analyzed under a uniform live load of 5 kPa [55] and evaluated against deflection and stress limits. The deflection allowed for each span follows the standard serviceability criteria of L/200 [58] and the yield strength is taken as 550 MPa, reflecting high strength -formed steel sections.

6.1 Flat Pratt Truss Bridge (Span: 6000 mm)

A Flat Pratt Truss bridge is an excellent structure in terms of its resistance to short-span conditions. The maximum 0.8 mm deflection is so much less than the allowable 30 mm that it indicates very high global stiffness. The stress at peak is 77.14 MPa, which is way below the yield limit of 550 MPa. This is a verification of the truss's good efficiency in utilizing axial forces for transferring loads and minimizing the bending effect.

However, by using 5 mm and 6 mm thick sections, the stress utilization becomes extremely low and hence we arrive at the issue of material overconsumption. That is the safety margin is indeed sufficient, but we still can call the structure overly designed for the span and the load it carries. A thinner section with the same performance could be a way of establishing that material usage can be reduced without impairing the safety or serviceability of the structure.

6.2 Panel Bridge (Span: 7200 mm)

The Panel Bridge is not qualified for serviceability criteria according to the results of both deflection and stress. A deflection of 65.88 mm is more than the limit of 36 mm for the bridge, also the stress reached 639.4 MPa, which was higher than the 550 MPa yield strength.

Hence, the bridge now can be considered weak because the reinforcement is not provided to its span. The panelized bridge configuration is not the best option because of the very high deflection and extremely high stresses at connections, which limits the span to a short distance. The design will be unfeasible, like the thick profile or the stiffeners would be necessary for structural compliance.

6.3 Box Truss Bridge (Span: 6700 mm)

The Box Truss Bridge spanning 6.7 meters presents a well-balanced structural response. The deflection of 20.3 mm in this case is not excessive yet gives more benefit as it remains in below 30 mm, also the peak stress of 535 MPa is marginally lower than the 550 MPa point. The closed box truss configuration contributes to uniform distribution of the load and is a good stiffness around any connections. If compared to the Flat Pratt Truss that is safe, the Box Truss makes better use of the material, so it is lighter in weight and still secure. This type of construction is very much recommended for short-span pedestrian bridge applications.

6.4 Tub Girder Bridge (Span: 15000 mm)

The Tub Girder Bridge delivers strong performance in deflection with a maximum of 10.60 mm against an allowable 37.5 mm, demonstrating high flexural rigidity. However, the peak stress of 550 MPa indicates full material utilization. The tub-shaped closed section efficiently resists bending and twisting explaining the low deflection, but critical stress zones particularly at the bottom flange and web-flange junctions require further attention. While safe under current loading, the section has no margin for increased demand suggesting a structurally efficient but borderline design in terms of stress.

The comparative analysis of the six cold-formed steel pedestrian bridge configurations highlights the varying performance characteristics across different span lengths and structural

layouts. While some bridges—such as the Flat Pratt Truss and Box Truss—demonstrate exceptional stiffness and low stress levels, others like the Panel Bridge and Flat Foot Bridge reveal critical deficiencies, particularly under longer spans or inadequate transverse stiffness. The Tub Girder and Box Bridge designs show promising results in terms of deflection but operate close to or at material yield, indicating limited reserve capacity. For a comprehensive overview of structural performance—including deflection limits, stress behavior, and span efficiency—refer to the summary table and accompanying graphs, which clearly illustrate how each bridge type compares under consistent loading and material conditions. These insights provide a strong foundation for selecting or refining bridge designs based on specific span requirements and structural priorities.

6.5 Flat Foot Bridge (Span: 30000 mm)

The Flat Foot Bridge is 30 meters long in total and is mid supported with two effective spans of 15 meters each. Structurally, the bridge behaves well in the main span direction with a maximum deflection of 58.92 mm which is within the acceptable limit of 75 mm. The outcome gives the impression that the primary load-carrying system is sufficiently resistant to the applied uniform loading of 5 kPa. Conversely, the transverse beams show a deflection of 91.19 mm which is very high and is therefore not within acceptable limits. In addition, the maximum stress developed in the structure is 582.4 MPa which is higher than the yield strength of 550 MPa. The results indicate that although the bridge behaves well in its main span, the transverse members or deck system lack sufficient stiffness and reinforcement leading to excessive deformation and overstressing of the clamps. The outcome gives the impression that the primary load-carrying system is sufficiently resistant to the applied uniform loading of 5 kPa. Conversely, the transverse beams show a deflection of 91.19 mm which is very high and is therefore not within acceptable limits. If full structural compliance were to be achieved, there would be a need to raise the transverse stiffness through a closer spacing of floor beams or the

addition of stiffer cross members or the use of a stiffer deck profile. The test results bring out the necessity of designing in both directions equally for the span and transverse beam, mostly in the case of open-deck pedestrian bridges.

6.6 Box Bridge (Span: 10000 mm)

Spanning 10 meters, the Box Bridge not only executes a good deflection control but also has a measured 13.9 mm compared to the 50 mm allowable limit. On the other hand, the stress approaches the 550 MPa yield strength showing the section is fully utilized. The closed geometry of the box contributes to stiffness and torsional resistance, although the appearance of the stress peaks at the problem points suggests that the bridge could gain the most benefit from the provision of more detailed joints and the existence of additional bracing to keep a long-term performance and to prevent the overstrain in the critical regions.

6.7 Summary Overview and Structural Performance Comparison

The comparative analysis of six different configurations of cold-formed steel pedestrian bridges clarifies the disparate performance characteristics linked to varying span lengths and structural types. Some configurations like the Flat Pratt Truss and Box Truss, bridge show good stiffness with low stress levels while others like the Panel Bridge and Flat Foot Bridge show evident shortcomings especially in cases where long spans or lacking transverse stiffness are involved. The Tub Girder and Box Bridge configurations produce favorable results in terms of deflection. however, these types of bridges work near or at the material yield point and hence imply a limited reserve capacity. To ensure a comprehensive assessment of structural performance that encompasses deflection limits, stress responses and span efficiency, the use of Table 9 in conjunction with the relevant Figures 95 and 96 which graphically illustrate the comparative performance of each bridge configuration under uniform loading and material conditions is suggested.

The Figure 97 and table 10 clarify the structural performance of six various configurations of cold-formed steel pedestrian bridges, evaluated in relation to their deflections-to-span ratios. The Box Bridge and the Tub Girder both display sufficient stiffness and deflection values, making them serviceable over long spans. The Flat Pratt Truss displays excessive stiffness, and thus the possibility of overdesign. In comparison, the Box Truss Bridge displays a proportionate performance acceptable for the case of smaller spans. These results provide a solid basis for the selection of bridge configurations for a particular span requirement and structural consideration. These results provide a solid basis for the selection of bridge configurations for a particular span requirement and structural consideration.

Table 9 Summary: Structural Performance of Cold-Formed Steel Bridges

Bridge Type	**Span (mm)**	**Max Deflection (mm)**	**Allowable Deflection (mm)**	**Max Stress (MPa)**	**Yield Stress (MPa)**	**Performance Summary**
Flat Pratt Truss	6000	0.8	30.0	77.14	550	Over-conservative, very stiff
Panel Bridge	7200	65.88	36.0	639.4	550	Structurally inadequate
Box Bridge	10000	13.9	50.0	550.0	550	Deflection within limit, stress at yield
Flat Foot Bridge (Main Span)	15000	58.92	75.0	582.4	550	Deflection within limit for main span, but transverse fails
Tub Girder Bridge	15000	10.6	37.5	550.0	550	Efficient, stress at yield
Box Truss Bridge	6000	20.3	30.0	535.0	550	Balanced and efficient

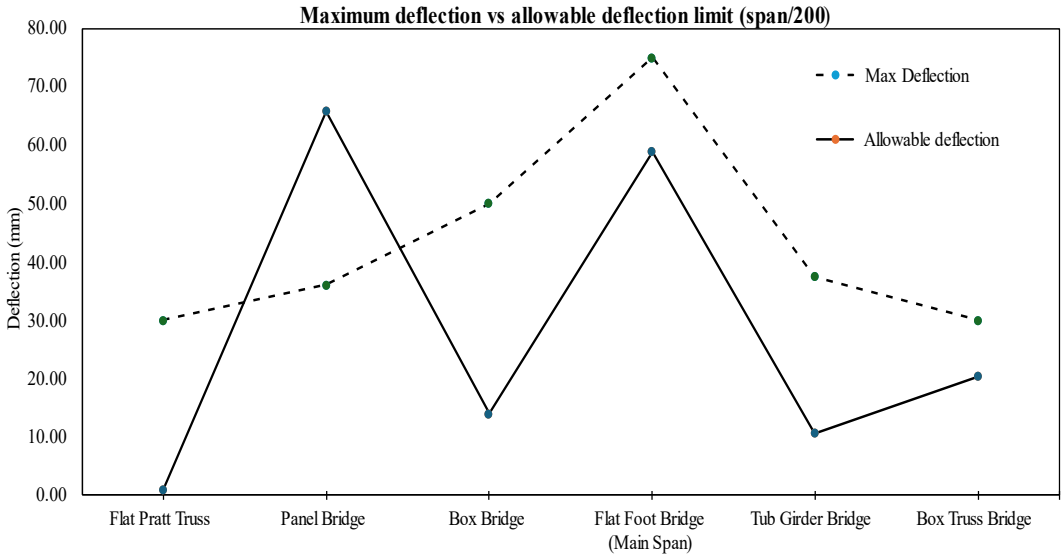

Figure 95 shows Maximum deflection vs allowable deflection limit (span/200)

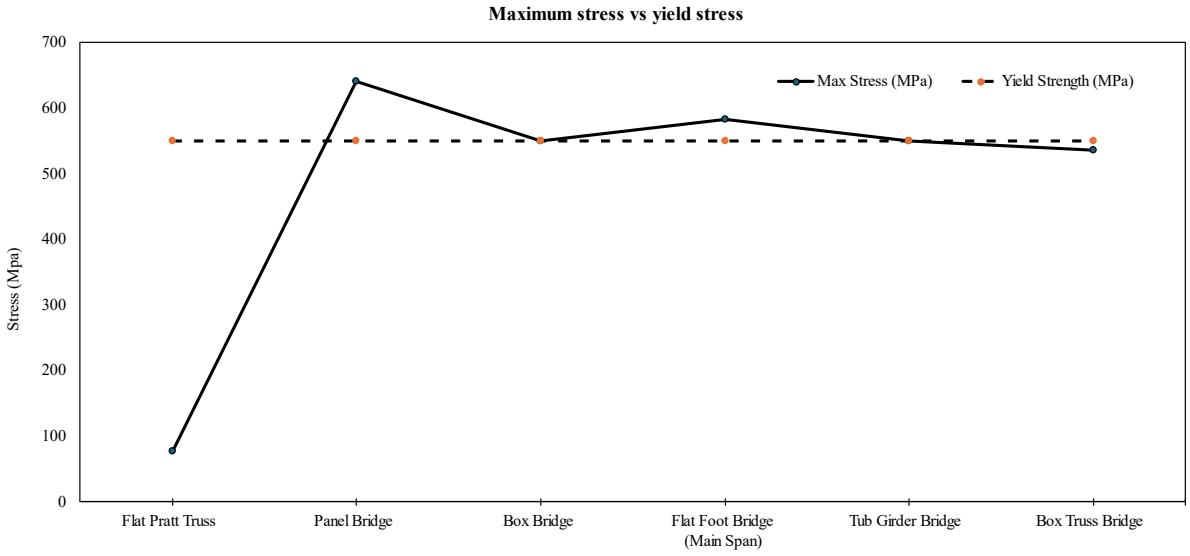

Figure 96 shows maximum stress vs yield stress.

Table 10 Maximum deflection-to-span ratio for different CFS pedestrian bridge types

Bridge Type	Ratio (Max Deflection/ Span)
Flat pratt truss	0.00013
Panel bridge	0.00915
Box bridge	0.00139
Flat foot bridge (Main Span)	0.003928
Tub girder bridge	0.0007067
Box truss bridge	0.0034

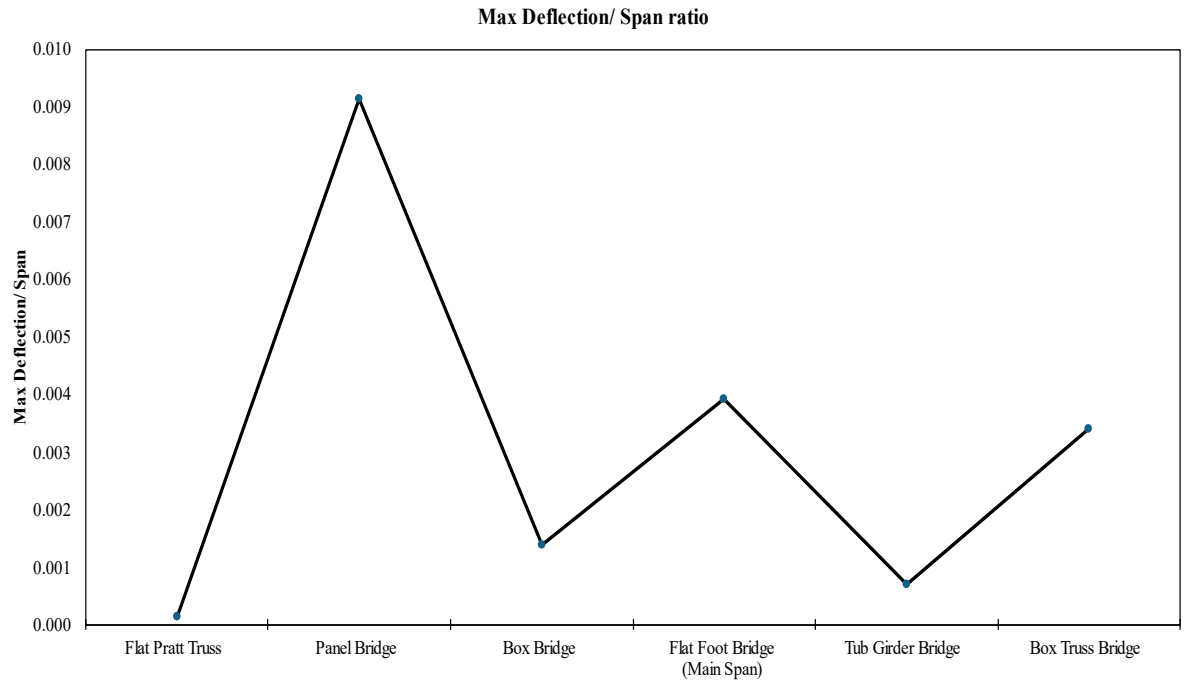

Figure 97 shows max deflection/ span ratio

6.8 Summary Overview of Connection Safety Assessment

A comprehensive finite element analysis (FEA) was conducted to assess the stress behaviour at key connection regions across all six bridge types. The Von Mises stress values obtained from each simulation were compared against the material yield strength of 550 MPa

for cold-formed steel (CFS) to determine connection safety. The following tables 11 and Figures 98,99 present a technical evaluation of each bridge's critical connection zones.

- Only Flat pratt truss and box truss bridges had safe connection designs.
- Panel bridge, flat foot, tub girder, and box bridge exhibited unsafe or marginally safe connections under the standard 5 kPa load.
- Design revisions are essential for unsafe zones — especially gusset plate and clamp areas, which are most prone to stress concentrations.
- This analysis reinforces the importance of connection detailing in cold-formed steel (CFS) bridge performance and provides a benchmark for safe stress limits in similar applications.

Table 11 Maximum von mises stress in connections by bridge type

Bridge type	**Critical connection region**	**Max stress (MPa)**	**Yield strength (MPa)**	**Safety status**
Flat pratt truss bridge	floor beam to L-angle clamp	55.46	550	Safe
Panel bridge	Clamp zone, panel gusset plate around connections region	639.4	550	Unsafe
Box truss bridge	floor beam to clamp around connections region	516.9	550	safe
Box Bridge	floor beam to main beam clamp	550	550	Marginally safe
Flat Foot Bridge	floor beam to clamp around connections region	582.4	550	Exceeds yield
Tub Girder Bridge	floor beam to flange around connection region	630	550	Unsafe

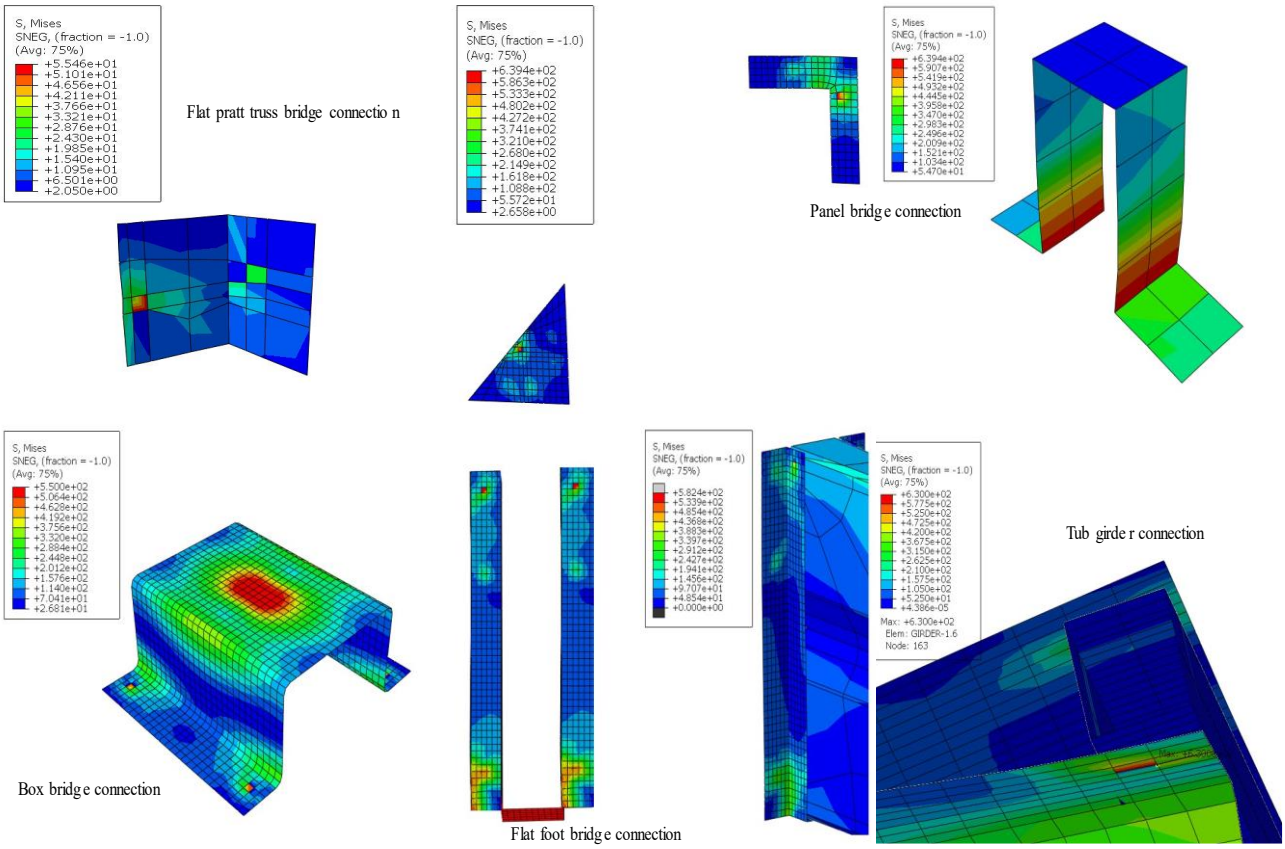

Figure 98 shows critical connection zone of each bridge.

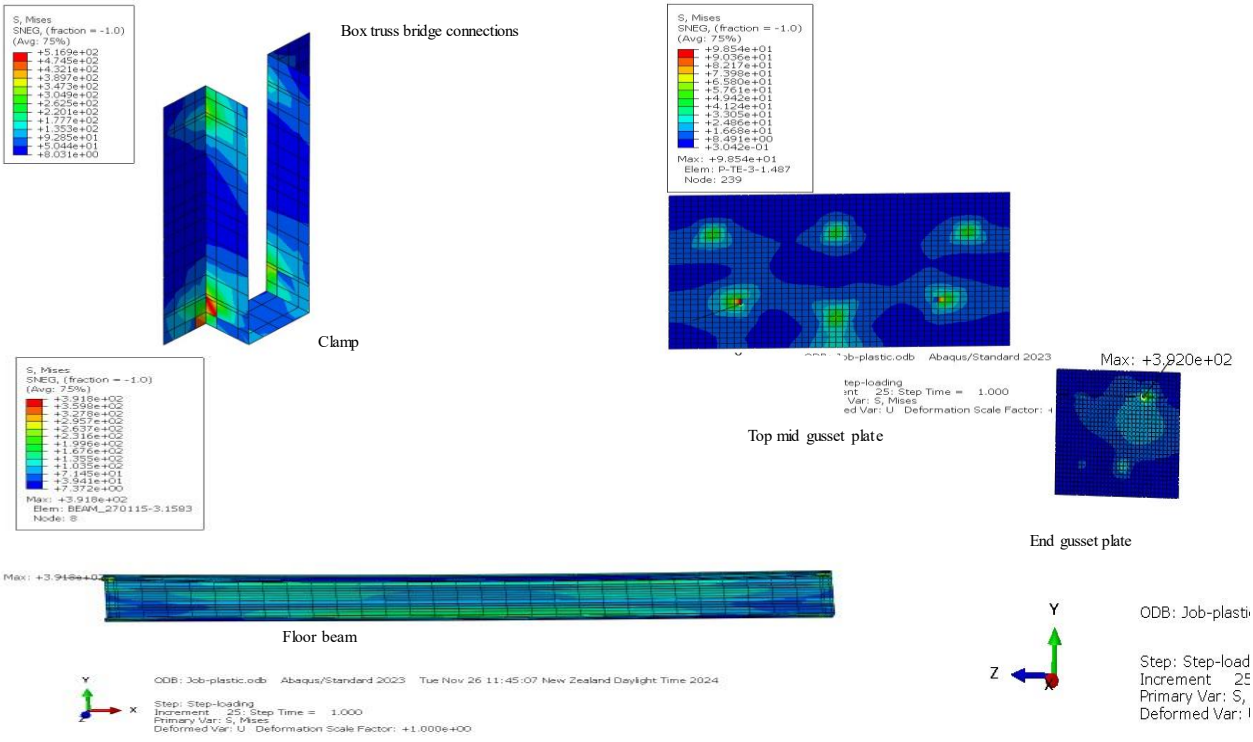

Figure 99 shows critical connection of box truss bridge

Chapter 7 – Conclusion

An analysis of different geometric arrangements of CFS pedestrian bridges shows that the box truss structure emerges as structural efficient design, satisfying deflection requirements as well as stress distribution conditions.

- The maximum deflection of the box truss bridge transverse is -20.30 mm, which is far below the acceptable span/200 limit of -33.5 mm, thus satisfying serviceability requirements.
- The deflection of the main beam (bottom chord) at mid span is -2.87 mm, further evidence of the structural efficiency and sufficient axial stiffness of the design.
- The maximum von Mises stress is 535 MPa, which is well below the yield strength limit of 550 MPa for cold-formed steel, demonstrating that the bridge can withstand applied loads without exceeding material limits.
- The stress distribution along the structure is even with no major stress concentrations that may lead to early structural failure.
- The box truss bridge design efficiently redistributes loads among its structural members, thus avoiding localized deformations and allowing for an even load path distribution.
- Compared to panel and flat bridge designs that undergo large deflections and localized stresses, the novel nested-section truss design considerably enhances rigidity and load-carrying capacity.
- The use of a truss structure greatly minimizes bending moments, with stresses being efficiently distributed throughout the structure, thus making it more durable and resistant.

- The geometric layout of the box truss bridge is critical to its superior performance the deeper truss increases the moment of inertia, resulting in lower deflections while allowing for lightweight construction at the same time.
- From a material efficiency perspective, the box truss bridge employs cold-formed steel in a way that avoids excessive overdesign while ensuring that no structural element undergoes overstress.
- Unlike the panel bridge with some components that had ultimate stresses near the yield point, and long-span footbridge that suffered deflections that exceeded allowed thresholds, the box truss bridge establishes a perfect balance between structural strength and weight effectiveness.
- Additional developments, such as the use of stiffener reinforcements to increase strength in joints and connector detailing refinements, can enhance overall performance and, in turn, ensure long-term durability under conditions of pedestrian loading.

7.1 Future scope

To validate the results for deflection and stress distribution, experimental tests of the box truss bridge under realistic loading conditions is needed to be performed. These tests will verify the predictions obtained from finite element analysis (FEA). A detailed analysis of screw connections is required. Screws are only considered based on edge spacing and center-to-center spacing in this context [68], but more detailed finite element analysis of screw detail must be conducted. With this, there will be a careful check to find out the transfer mechanism of the load, stress concentration at a local scale of screws and the potential for slip or failure at connections. In addition, analyse both the vibrational properties and fatigue life of the structure.

7.2 Contributions and Guidelines for Engineers

- Performing a comparative FEA-based evaluation of six CFS pedestrian bridge configurations using novel CFS nested sections.
- Highlighting the importance of connection modeling simplification via MPC connectors for efficient simulations without compromising global accuracy.
- Demonstrating that box truss geometry provides superior structural performance in terms of deflection, stress distribution and safe connections under a 5 kPa load.
- Introducing a benchmark deflection-to-span ratio (refer Table 10 and Figure 97) for each bridge type, aiding early-stage design decisions.
- Providing verified modeling and geometry-specific performance data, it is a beginning reference for future CFS pedestrian bridge design, being highly relevant to engineering professionals.

Appendix (Detailed manufacturing drawings for CFS box truss bridge)

This appendix includes detailed fabrication schematics of the cold-formed steel (CFS) box truss pedestrian bridge. These drawings illustrate dimensions, material and fabrication specifications required in fabricating the bridge. The data includes component views, sectional views, connection specifications and assembly instructions, which all help ensure fabrication precision. The drawings meet standard engineering practices[68][44] and all measurements are in mm. These technical representations aim to guide fabrication and help in future modifications, if required.

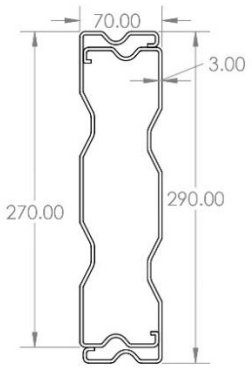

1. 270115N

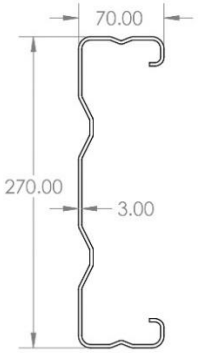

2. 270115

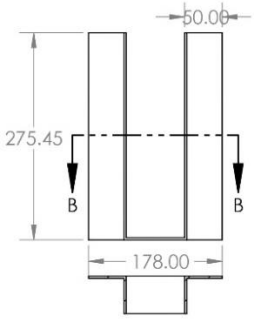

SECTION B-B
SCALE 1 : 6

3. Transverse Clamp

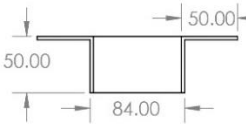

Top-View Clamp

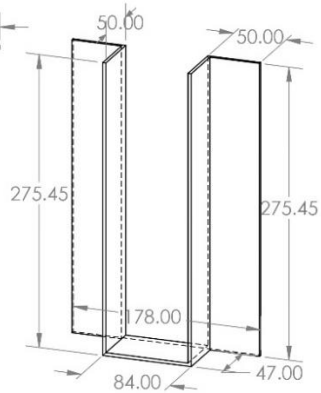

3D- View Clamp

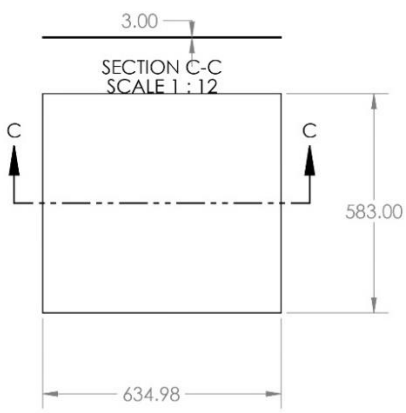

4. Outter Plates - 1

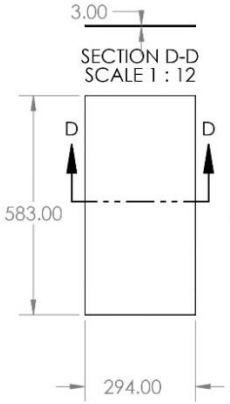

5. Outter Plates - 2

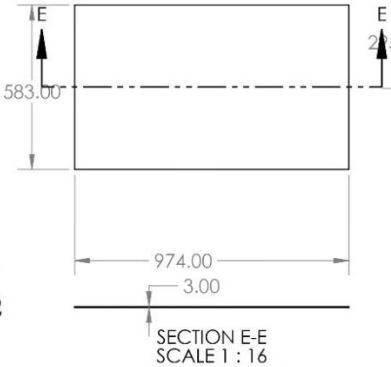

SECTION E-E
SCALE 1 : 16

6. Outter Plates - 3

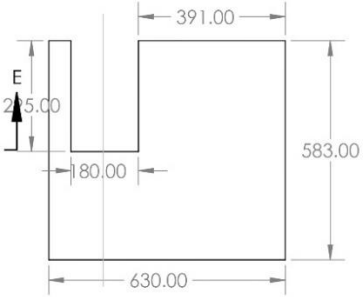

7. Inner Plates - 1

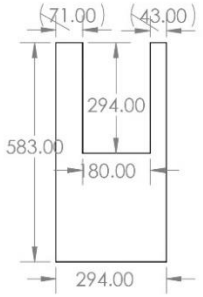

8. Inner Plates - 2

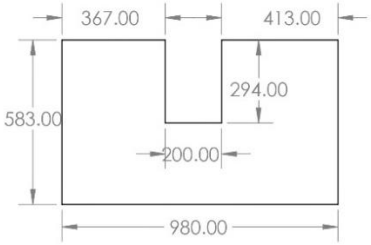

9. Inner Plates - 3

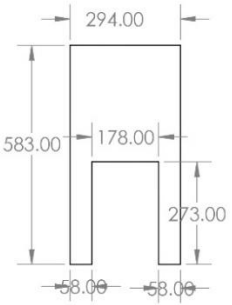

10. Inner Plates - 4

UNLESS OTHERWISE SPECIFIED: DIMENSIONS ARE IN MILLIMETERS SURFACE FINISH: TOLERANCES: LINEAR: ANGULAR:		FINISH:			DEBURR AND BREAK SHARP EDGES	DO NOT SCALE DRAWING	REVISION
	NAME	SIGNATURE	DATE			TITLE: Box Truss Bridge	
DRAWN							
CHK'D							
APPV'D							
MFG							
Q.A				MATERIAL: CFS-3mm		DWG NO. Detail drawings	A3
				WEIGHT:		SCALE:1:50	SHEET 1 OF 5

ITEM NO.	PART NUMBER	QTY (NOS).	TOTAL Length (mm)
1	270115N	04	26800
2	270115	10	30000
3	270115N (Vertical)	10	25000
4	270115 (Inclined)	08	21600
5	Transverse Clamp	20	
6	Outter- plate-1	12	
7	Outter- plate-2	06	
8	Outter- plate-3	02	
9	Inner - plate-1	12	
10	Inner - plate-2	04	
11	Inner - plate-3	02	
12	Inner - plate-4	02	

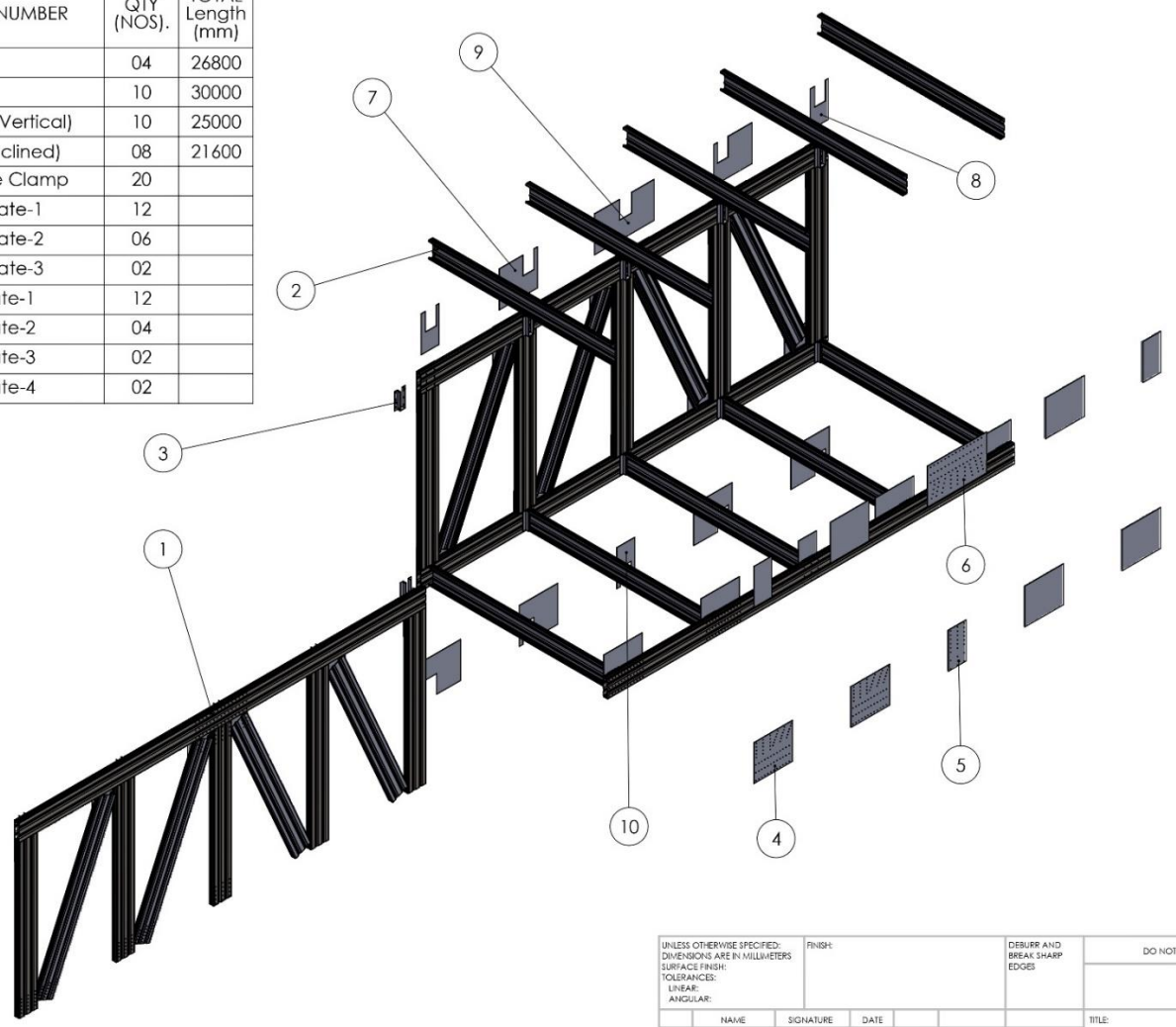

UNLESS OTHERWISE SPECIFIED:
DIMENSIONS ARE IN MILLIMETERS
SURFACE FINISH:
TOLERANCES:
LINEAR:
ANGULAR:

FINISH:

DEBURR AND BREAK SHARP EDGES

DO NOT SCALE DRAWING | REVISION

	NAME	SIGNATURE	DATE
DRAWN			
CHK'D			
APPV'D			
MFG			
Q.A			

TITLE:
Box Truss Bridge

MATERIAL:
CFS-3mm

DWG NO.
Detail drawings

A3

WEIGHT:

SCALE:1:50

SHEET 2 OF 5

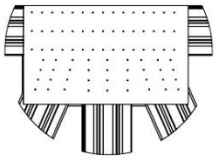

DETAIL W
SCALE 1 : 25

5.5mm Dia screw, 85 Nos with spacing 30mm.

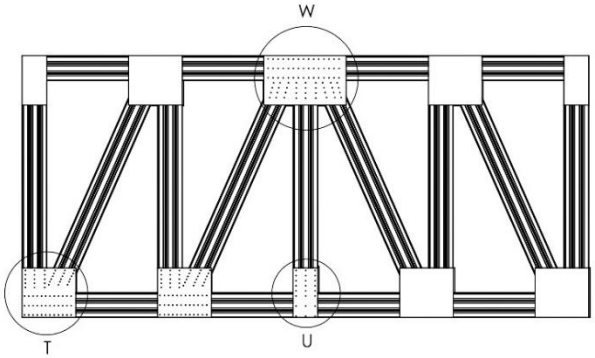

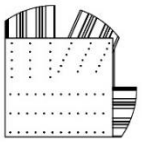

DETAIL T
SCALE 1 : 25

5.5mm Dia screw, 69 Nos with spacing 30mm.

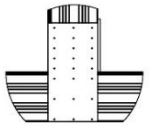

DETAIL U
SCALE 1 : 25

5.5mm Dia screw, Total 24 Nos with spacing 30mm.

UNLESS OTHERWISE SPECIFIED: DIMENSIONS ARE IN MILLIMETERS SURFACE FINISH: TOLERANCES: LINEAR: ANGULAR:			FINISH:			DEBURR AND BREAK SHARP EDGES	DO NOT SCALE DRAWING	REVISION
	NAME	SIGNATURE	DATE				TITLE: Box Truss Bridge	
DRAWN								
CHK'D								
APPV'D								
MFG								
Q.A					MATERIAL: CFS-3mm		DWG NO. Detail drawings	A3
					WEIGHT:		SCALE:1:50	SHEET 3 OF 5

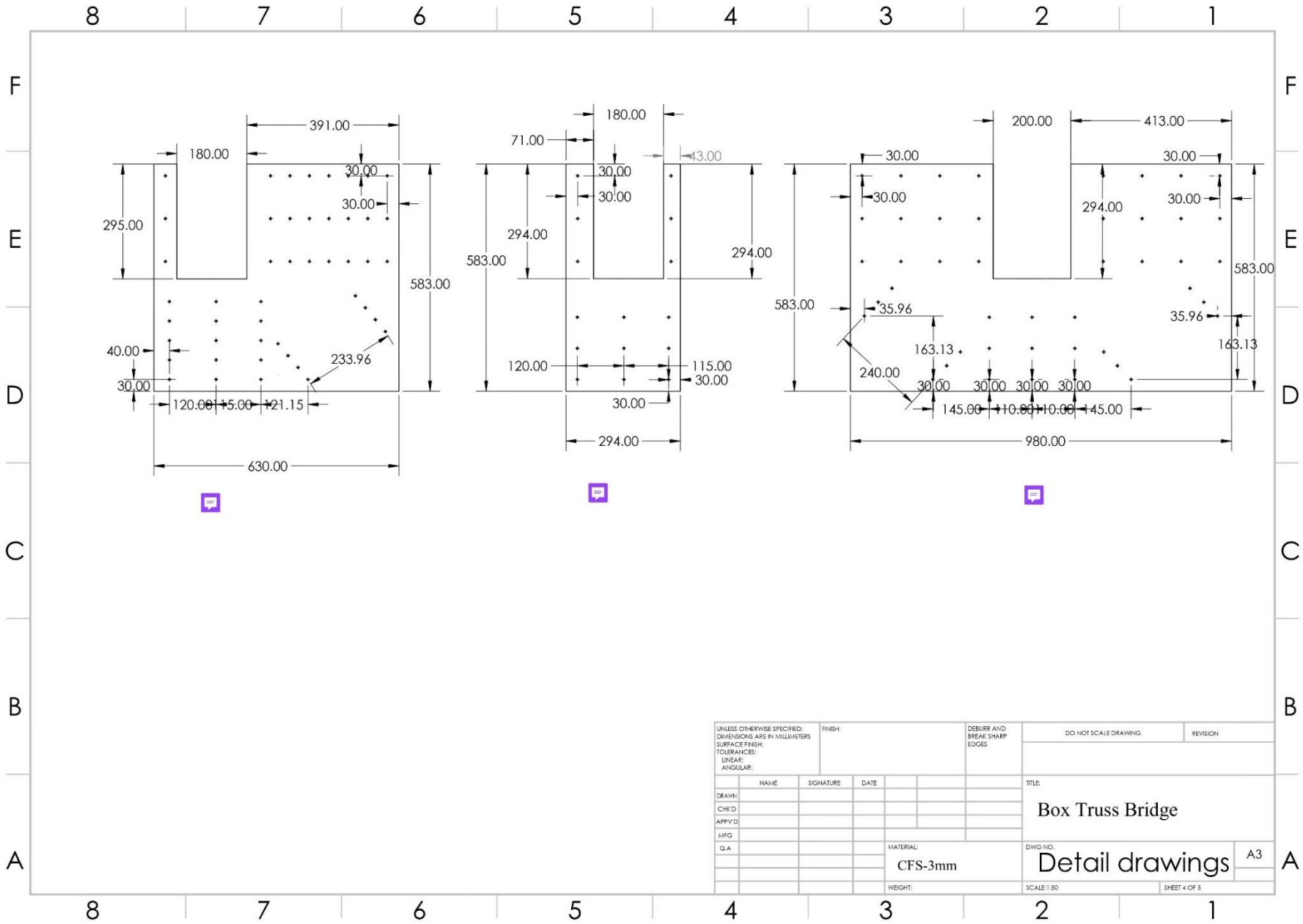
8 7 6 5 4 3 2 1
F E D C B A
391.00
180.00
30.00
30.00
295.00
583.00
40.00
233.96
30.00
120.00 15.00 21.15
630.00
180.00
71.00
43.00
30.00
30.00
294.00
583.00
294.00
120.00
115.00
30.00
30.00
294.00
200.00
413.00
30.00
30.00
30.00
30.00
294.00
583.00
583.00
35.96
35.96
163.13
163.13
240.00
30.00 30.00 30.00 30.00
145.00 110.00 110.00 145.00
980.00
UNLESS OTHERWISE SPECIFIED:
DIMENSIONS ARE IN MILLIMETERS
SURFACE FINISH:
TOLERANCES:
LINEAR:
ANGULAR:
FINISH:
DEBURR AND BREAK SHARP EDGES
DO NOT SCALE DRAWING
REVISION
NAME SIGNATURE DATE
DRAWN
CHK'D
APPV'D
MFG
Q.A
TITLE:
Box Truss Bridge
MATERIAL:
CFS-3mm
DWG NO.
Detail drawings
A3
WEIGHT:
SCALE:1:50
SHEET 4 OF 5

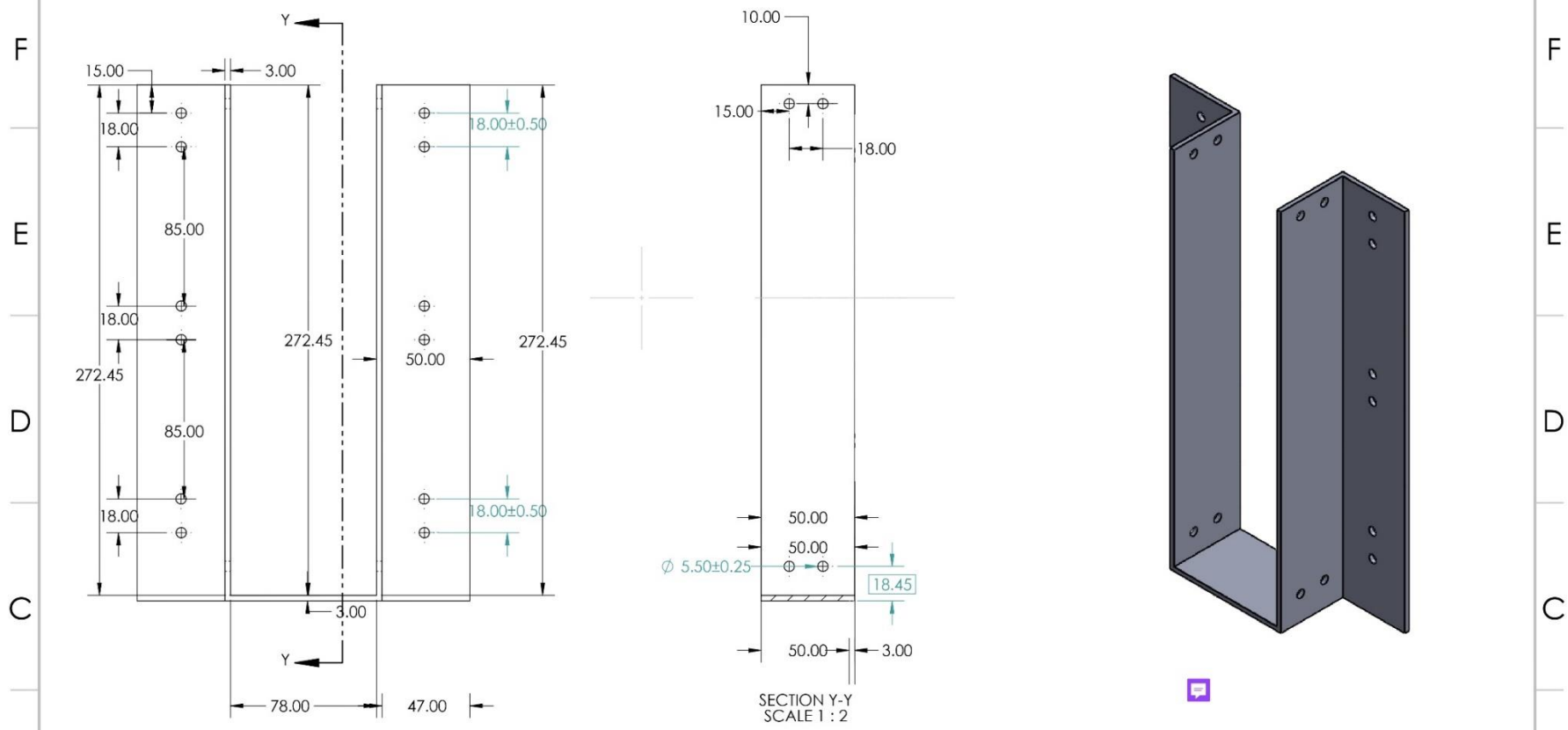

UNLESS OTHERWISE SPECIFIED: DIMENSIONS ARE IN MILLIMETERS SURFACE FINISH: TOLERANCES: LINEAR: ANGULAR:		FINISH:		DEBURR AND BREAK SHARP EDGES	DO NOT SCALE DRAWING	REVISION
	NAME	SIGNATURE	DATE		TITLE: Box Truss Bridge	
DRAWN						
CHK'D						
APPV'D						
MFG						
Q.A				MATERIAL: CFS-3mm	DWG NO. Detail drawings	A3
				WEIGHT:	SCALE:1:50	SHEET 5 OF 5

References

[1] Alessio Pipinato, *Innovative Bridge Design Handbook: Construction, Rehabilitation and Maintenance*, 2nd edition. Oxford, UK: Elsevier, 2021.

[2] Andreas Keil, *Pedestrian Bridges: Ramps, Walkways, Structures*, First. Berlin: Birkhauser Verlag , 2013.

[3] C Caprani, "Caprani, C 2018, Are Australian bridges safe, and can we do better?, The Conversation, Victoria, Australia, viewed 30 November 2020," https://theconversation.com/are-australianbridges- safe-and-can-we-do-better-101825.

[4] D. Goodman, "'Timber Bridges in Local Government – Part of the Solution not the Problem', 2017 IPWEAQ Conference, Townsville, Australia.,"

[5] T. Y. WEIWEI LIN, *BRIDGE ENGINEERING BRIDGE ENGINEERING Classifications, Design Loading, and Analysis Methods*. 2017.

[6] A. Awaludin, M. Y. M. Making, M. N. Ikhsan, and Y. Adiyuano, "Performance of a Cold Formed Steel Pedestrian Bridge under Static and Dynamic Loads," *Civil Engineering Dimension*, vol. 23, no. 2, pp. 108–114, Oct. 2021, doi: 10.9744/ced.23.2.108-114.

[7] Y. Halabi and W. Alhaddad, "Manufacturing, Applications, Analysis and Design of Cold-Formed Steel in Engineering Structures: A Review," *International Journal of Advanced Engineering Research and Science*, vol. 7, no. 2, pp. 11–34, 2020, doi: 10.22161/ijaers.72.3.

[8] R. W. Lautensleger and I. P. Andrade, "Galvanized Cold-Formed Steel Bridges for Low-Volume Roads."

[9] A. M. D. A. Jasim, L. S. Wong, A. W. Al-Zand, and S. Y. Kong, "Evaluating Axial Strength of Cold-formed C-Section Steel Columns Filled with Green High-performance Concrete," *Civil Engineering Journal*, vol. 10, pp. 271–290, Dec. 2024, doi: 10.28991/CEJ-SP2024-010-014.

[10] M. I. Zaed Ammar, D. Irawan, D. Iranata, and B. Suswanto, "Study analysis on failure mechanism of small span pedestrian cold formed truss bridge," *International Journal of Engineering Research and Technology*, vol. 13, no. 7, pp. 1757–1763, 2020, doi: 10.37624/ijert/13.7.2020.1757-1763.

[11] W.-W. Yu, "Cold-Formed Steel Structures."

[12] Ç. Dizdar, E. Baran, and C. Topkaya, "Strength and stiffness of floor trusses fabricated from cold-formed steel lipped channels," *Eng Struct*, vol. 181, pp. 437–457, Feb. 2019, doi: 10.1016/j.engstruct.2018.12.041.

[13] J. V Wood and J. L. Dawe, "Full-Scale Test Behavior of Cold-Formed Steel Roof Trusses", doi: 10.1061/ASCE0733-94452006132:4616.

[14] J. L. Dawe, Y. Liu, and J. Y. Li, “Strength and behaviour of cold-formed steel offset trusses,” *J Constr Steel Res*, vol. 66, no. 4, pp. 556–565, Apr. 2010, doi: 10.1016/j.jcsr.2009.10.015.

[15] M. Reda, T. Sharaf, A. ElSabbagh, and M. ElGhandour, “Behavior and design for component and system of cold-formed steel roof trusses,” *Thin-Walled Structures*, vol. 135, pp. 21–32, Feb. 2019, doi: 10.1016/j.tws.2018.10.038.

[16] C. Mathieson, G. C. Clifton, and J. B. P. Lim, “Novel pin-jointed connection for cold-formed steel trusses,” *J Constr Steel Res*, vol. 116, pp. 173–182, Jan. 2016, doi: 10.1016/j.jcsr.2015.08.009.

[17] P. Pouladi *et al.*, “Scholars’ Mine Scholars’ Mine Finite-Element Analysis of the Eaves Joint of Cold-Formed Steel Finite-Element Analysis of the Eaves Joint of Cold-Formed Steel Portal Frames having Single Channel-Sections Portal Frames having Single Channel-Sections Recommended Citation Recommended Citation ‘Finite-Element Analysis of the Eaves Joint of Cold-Formed Steel Portal Frames having Single Channel-Sections’ (2018). International Specialty Conference on Cold-Formed Steel Structures.”

[18] M. Zeynalian, S. Bolkhari, and P. Rafeei, “Structural performance of cold-formed steel trusses used in electric power substations,” *J Constr Steel Res*, vol. 147, pp. 53–61, Aug. 2018, doi: 10.1016/j.jcsr.2018.04.002.

[19] N. Usefi, H. Ronagh, and P. Sharafi, “Numerical modelling and design of hybrid cold-formed steel wall panels,” *Thin-Walled Structures*, vol. 157, Dec. 2020, doi: 10.1016/j.tws.2020.107084.

[20] J. Tjernlund, “ACEX30-19-16.”

[21] C. W. Roeder, M. Asce, K. E. Barth, A. M. Asce, and A. Bergman, “Effect of Live-Load Deflections on Steel Bridge Performance”, doi: 10.1061/ASCE1084-070220049:3259.

[22] S. K. Jha, A. Bambole, D. Jadhav, A. Dongre, and D. Goldar, “Optimum and efficient design of steel foot over bridges,” *Research on Engineering Structures and Materials*, 2024, doi: 10.17515/resm2024.167st0129rs.

[23] P. B. Potyrała, J. Ramón, and C. Rius, “PROJECTE O TESINA D’ESPECIALITAT Títol Use of Fibre Reinforced Polymer Composites in Bridge Construction. State of the Art in Hybrid and All-Composite Structures,” 2011.

[24] J. M. Davies, “Recent research advances in cold-formed steel structures,” 2000. [Online]. Available: www.elsevier.com/locate/jcsr

[25] V. Chandrikka, B. S. Lakshmi, M. Praveenkumar, S. Shanmugavel, and B. Sivasurya, “ANALYSIS AND DESIGN OF COLD FORMED STEEL FOOT OVER BRIDGE,” *International Research Journal of Engineering and Technology*, 2019, [Online]. Available: www.irjet.net

[26] W.-W. Yu, R. A. Laboube, and Y. Laboube, “H A I L E D B Y P R O F E S S I O N A L S A R O U N D T H E W O R L D as the definitive text on the subject, Cold-Formed Steel Cold-Formed Steel Design Cold-Formed Steel Design.”

[27] Y. Dai, K. Roy, Z. Fang, B. Chen, G. M. Raftery, and J. B. P. Lim, “Buckling resistance of axially loaded cold-formed steel built-up stiffened box sections through experimental testing and finite element analysis,” *Eng Struct*, vol. 302, Mar. 2024, doi: 10.1016/j.engstruct.2023.117379.

[28] M. Li, “Study on dynamic test of a large span steel truss pedestrian bridge,” in *Advanced Materials Research*, 2011, pp. 769–775. doi: 10.4028/www.scientific.net/AMR.255-260.769.

[29] E. Jonback and G. Yakoub, “Optimization of Steel Truss Girders in Pedestrian Bridges Using Genetic Algorithm.” [Online]. Available: www.chalmers.se

[30] B. V Hota S GangaRao, R. Ward, and V. Howser, “H. V. S. GangaRao, R. Ward , and V. How er. Value Engineering Approach lO Low-Volume Road Bridge Selection. Journal of Structural E11gi11eeri11g, ASCE, Vol. 114 , No. 9 cpl. 198 , pp. 1962-1977.”

[31] S. Kumar Nalla, “EXPERIMENTAL AND NUMERICAL INVESTIGATION OF A NOVEL COLD-FORMED STEEL LONG SPAN TRUSS,” 2023.

[32] J. P. Lawrence Martin, *Structural Design of Steelwork to EN 1993 and EN 1994*, 3rd Edition. London: CRC Press, 2007.

[33] J. L. M Hirt, *Steel bridges: conceptual and structural design of steel and steel-concrete composite bridges*. Swizerland: EPFL Press, 2013.

[34] Andreas Keil, *Pedestrian bridges: Ramps, walkways, structures*. Munich, 2013.

[35] W.-W. Yu, “Yu, W.W. ‘Cold-Formed Steel Structures’ Structural Engineering Handbook Ed. Chen Wai-Fah Boca Raton: CRC Press LLC, 1999.”

[36] P. Palma and R. Steiger, “Structural health monitoring of timber structures – Review of available methods and case studies,” Jul. 10, 2020, *Elsevier Ltd*. doi: 10.1016/j.conbuildmat.2020.118528.

[37] M. Salamak, “Typical damages and protections of concrete bridges located on areas with ground deformations. TYPICAL DAMAGES AND PROTECTIONS OF CONCRETE BRIDGES LOCATED ON AREAS WITH GROUND DEFORMATIONS.” [Online]. Available: https://www.researchgate.net/publication/256472327

[38] P. R. . Lewis, Ken. Reynolds, and Colin. Gagg, *P. R. Lewis, K. Reynold. C. Gagg, Forensic Material Engineering, New York: CRC Press, 2009.* CRC Press, 2004.

[39] “B. M. Imam, M. K. Chryssanthopoulos, A review of metallic bridge failure statistics, 5th International Conference on Bridge Maintenance, Safety and Management (IABMAS’10). Philadelphia, USA, 2010.”.

[40] E. Yamaguchi, R. Okamoto, and K. Yamada, “E. Yamaguchi, R. Okamoto, K. Yamada, Post-Member-Failure Analysis Method of Steel Truss Bridge, Procedia Engineering, 14, 2011, pp. 656-661.,” in *Procedia Engineering*, 2011, pp. 656–661. doi: 10.1016/j.proeng.2011.07.083.

[41] A. Manda and S. Nakamura, “A. Manda, S. Nakamura, Progressive Collapse Analysis of Steel Truss Bridges, Proceedings of the School Engineering, Tokai University, Series E 35, 2010, pp. 27-34.,” 2010.

[42] R. Pinho, C. Casarotti, and S. Antoniou, “A comparison of single-run pushover analysis techniques for seismic assessment of bridges,” *Earthq Eng Struct Dyn*, vol. 36, no. 10, pp. 1347–1362, 2007, doi: 10.1002/eqe.684.

[43] “Abaqus/CAE User’s Guide ABAQUS 2016.”

[44] *Bridge manual : manual number: SP/M/02*. NZ Transport Agency, 2013.

[45] W. Wang, K. Roy, H. Rezaeian, Z. Fang, and J. B. P. Lim, “Moment capacity of cold-formed steel trusses with Howick Rivet Connectors: Tests, modelling and design,” *Eng Struct*, vol. 322, Jan. 2025, doi: 10.1016/j.engstruct.2024.119171.

[46] L. Chen and Y. C. Wang, “Efficient modelling of large deflection behaviour of restrained steel structures with realistic endplate beam/column connections in fire,” *Eng Struct*, vol. 43, pp. 194–209, Oct. 2012, doi: 10.1016/j.engstruct.2012.05.030.

[47] K. F. Chung and K. H. Ip, “Finite element investigation on the structural behaviour of cold-formed steel bolted connections,” 2001. [Online]. Available: www.elsevier.com/locate/engstruct

[48] T. Anapayan and M. Mahendran, “Numerical modelling and design of LiteSteel Beams subject to lateral buckling,” *J Constr Steel Res*, vol. 70, pp. 51–64, Mar. 2012, doi: 10.1016/j.jcsr.2011.08.016.

[49] J. H. Zhang and B. Young, “Numerical investigation and design of cold-formed steel built-up open section columns with longitudinal stiffeners,” *Thin-Walled Structures*, vol. 89, pp. 178–191, 2015, doi: 10.1016/j.tws.2014.12.011.

[50] A. Bagheri Sabbagh, M. Petkovski, K. Pilakoutas, and R. Mirghaderi, “Cyclic behaviour of bolted cold-formed steel moment connections: FE modelling including slip,” *J Constr Steel Res*, vol. 80, pp. 100–108, Jan. 2013, doi: 10.1016/j.jcsr.2012.09.010.

[51] J. Becque and K. J. R. Rasmussen, “Numerical Investigation of the Interaction of Local and Overall Buckling of Stainless Steel I-Columns”, doi: 10.1061/ASCEST.1943-541X.0000052.

[52] Z. Li, S. Ádány, and B. W. Schafer, “Modal identification for shell finite element models of thin-walled members in nonlinear collapse analysis,” *Thin-Walled Structures*, vol. 67, pp. 15–24, 2013, doi: 10.1016/j.tws.2013.01.019.

[53] J. Xu, X. Chen, J. Li, and Z. Li, “Mechanical characteristics and comfort evaluation under pedestrian vertical excitation of a thin-walled cold-formed steel footbridge,” in *IOP Conference Series: Materials Science and Engineering*, IOP Publishing Ltd, Jan. 2021. doi: 10.1088/1757-899X/1028/1/012008.

[54] D. Bačinskas *et al.*, “Structural Analysis of GFRP Truss Bridge Model,” in *Procedia Engineering*, Elsevier Ltd, 2017, pp. 68–74. doi: 10.1016/j.proeng.2017.02.018.

[55] *Bridge manual : manual number: SP/M/02*. NZ Transport Agency, 2013.

[56] Moodie Outdoor Products, “installation of a pedestrian bridge for Parramatta City Council at 3rd Settlement Reserve by Moodie Outdoor products.”

[57] G. W. Li, Z. X. Wu, D. H. Wen, J. F. Shao, and C. X. Hu, “Experimental investigation on the cold-forming effect of high strength cold-formed steel sections,” *Structures*, vol. 58, Dec. 2023, doi: 10.1016/j.istruc.2023.105615.

[58] “36. SNZ-HB-86302004 span”.

[59] M. Embaby and M. H. El Naggar, “Experimental and numerical investigation for steel shear panels of modular bridge,” *J Constr Steel Res*, vol. 219, Aug. 2024, doi: 10.1016/j.jcsr.2024.108743.

[60] “TRILATERAL DESIGN AND TEST CODE FOR MILITARY BRIDGING AND GAP-CROSSING EQUIPMENT AGREED TO BY: GERMANY UNITED KINGDOM UNITED STATES OF AMERICA PUBLISHED IN THE UNITED STATES,” 2019.

[61] Y. Dai, K. Roy, Z. Fang, G. M. Raftery, and J. B. P. Lim, “Web crippling resistance of cold-formed steel built-up box sections through experimental testing, numerical simulation and deep learning,” *Thin-Walled Structures*, vol. 192, Nov. 2023, doi: 10.1016/j.tws.2023.111190.

[62] Canam-Bridges, “Canam-Bridges Long Span Standard Truss Bridge A division of Canam Group.”

[63] J. Manuel *et al.*, “CONSTRUCTION ENGINEERING OF STEEL TUB-GIRDER BRIDGE SYSTEMS FOR SKEW EFFECTS A Dissertation Presented to The Academic Faculty,” 2012.

[64] “U-BEAM ™ Bridge System AN AASHTO 2021 FOCUS TECHNOLOGY GALVANIZED STEEL PRESS-BRAKE-FORMED TUB GIRDERS PRESENTERS Jeff Simkins National Bridge Sales Manager.”

[65] “59.design-manual-for-orthotropic-steel-plate-deck-bridges”.

[66] N. M. A. B. WM Baker, “Callender-Hamilton Truss Bridges: The New Zealand History,” Auckland: 4th Australasian Engineering Heritage Conference, Nov. 2014.

[67] U. road runner bridge, “Prefabricated Steel Bridge Kits,” https://roadrunnerbridge.com/steel-utility-bridges.html.

[68] “ASNZS-4600-2018”.